**TECHNISCHE
UNIVERSITÄT
WIEN**
Vienna University of Technology

DIPLOMARBEIT

Investigation of the influence of thoron on radon monitors and development of innovative measurement techniques

zur erlangung des akademischen Grades

Diplom-Ingenieurin

im Rahmen des Studiums

Technische Physik

eingereicht von

Katharina Newrkla

Matrikelnummer 01027339

ausgeführt am Atominstitut
der Fakultät für Physik der Technischen Universität Wien

Betreuung
Betreuer: Univ.-Prof. DI Dr. Franz Josef Maringer
Mitwirkung: DI Hannah Wiedner
in Kooperation mit dem Labor Radioaktivität im Bundesamt für Eich- und Vermessungswesen

Wien, 15.03.2018

_____   _____
Unterschrift Verfasserin   Unterschrift Betreuer

Kurzfassung

Inhalation von Radon ist nach dem Rauchen die zweithäufigste Ursache für Lungenkrebs. In der neuen EU-Strahlenschutzrichtlinie 2013/59/Euratom, deren Umsetzung in österreichisches Recht derzeit am Laufen ist, sind nationale Maßnahmen zum Schutz der Bevölkerung gegen eine erhöhte Radon-Exposition vorgeschrieben. Eines der Ziele des derzeit laufenden europäischen Forschungsprojekts MetroRADON ist die qualitätsgesicherte metrologische Rückführbarkeit von Radonmessgeräten und Detektoren zur effektiven Überprüfung der Einhaltung eines Grenzwertes für die Radon-Konzentration in Innenräumen im Rahmen des Strahlenschutzes.

Das Ziel dieser Diplomarbeit ist die Untersuchung, der Vergleich und die Weiterentwicklung innovativer Messmethoden für die Aktivitätskonzentrationen von Radon (Rn-222) und Thoron (Rn-220). Dazu wurden Messungen der Aktivitätskonzentrationen in der Bodenluft und in Innenräumen im Wald- und Mühlviertel und im Radioaktivitätslabor des Bundeamts für Eich- und Vermessungswesen (BEV) in Seibersdorf durchgeführt. Ergänzend zu den Radon- und Thoronmessungen in der Luft wurde die Gammadosisleistung an den Messorten detektiert, der Radongehalt in Wasserproben mittels einer Ionisationskammer gemessen und die Aktivitätskonzentrationen von Radionukliden der Uran-Radium- und Thoriumzerfallsreihe in Bodenproben mittels Low-level-Gammaspektrometrie bestimmt.

Die Bodenluftmessungen wurden im oberösterreichischen Mühlviertel und niederösterreichischen Waldviertel mit AlphaGUARD Radonmessgeräten durchgeführt. Das Hauptziel dieser Messungen war die Untersuchung des Einflusses von Thoron auf die gemessenen Radon-Aktivitätskonzentrationen. Die Messungen, welche das Thoron nicht berücksichtigen, überschätzten die Radon-Aktivitätskonzentration um bis zu 38 % in der Anwesenheit hoher Thoron-Aktivitätskonzentrationen. In zukünftigen

Projekten soll mit Hilfe einer im Rahmen dieser Diplomarbeit entwickelten Thoronquelle im Labor der Einfluss von Thoron auf Radonmessungen unter kontrollierten Bedingungen genauer untersucht werden.

Im Zuge des Vergleiches unterschiedlicher Messmethoden wurden auch die Messunsicherheiten und damit die Genauigkeit und Präzision der Messmethoden untersucht. Die Ergebnisse dieser Arbeit dienen als wissenschaftliche Basis für die praktische Anwendung von Radon- und Thoronmessungen und als Startpunkt für weitere Untersuchungen im Rahmen des MetroRADON Projekts.

Abstract

Inhalation of radon is, behind smoking, the second largest cause of lung cancer. The new EU council directive 2013/59/Euratom, the implementation of which into Austrian law is currently ongoing, stipulates national action plans for the protection of the population from excessive radon exposure. One of the objectives of the currently ongoing European research project MetroRADON is the quality-assured metrological traceability of radon detectors and measuring instruments in order to effectively monitor the indoor radon concentration in the context of radiation protection.

The aim of this diploma thesis is the investigation, comparison and development of innovative techniques for the measurement of the activity concentrations of radon (Rn-222) and thoron (Rn-220). For this purpose, measurements of their activity concentration in soil air and indoors are taken in the Austrian Wald- and Mühlviertel and in the radioactivity laboratory of the Federal Office for Metrology and Surveying (BEV) in Seibersdorf. Additionally, gamma dose rate measurements are carried out, the radon content in water samples is determined using an ionization chamber and the activity concentrations of radionuclides of the uranium and thorium decay chains in soil samples is measured using low-level gamma spectrometry.

The soil air measurements were carried out in parts of Upper and Lower Austria using AlphaGUARD radon monitors. The main objective of these measurements was to study the influence of thoron on the measured radon activity concentrations. It was found that measuring instruments that do not account for thoron overestimated the radon activity concentrations by up to $38\,\%$ in the presence of high thoron activity concentrations. In future research the influence of thoron on radon measurements is to be investigated in greater detail using a thoron source developed in the laboratory.

In the course of the comparison of different measurement techniques, the measure-

ment uncertainties and with that, the accuracy and precision of the measurement techniques are also investigated. The results of this thesis serve as a scientific basis for the practical applications of radon and thoron measurements and as a starting point for further investigations in the scope of the MetroRADON project.

Contents

8. Conclusion 103

Bibliography 105

Appendices 117

1. Introduction

Radon (Rn-222) is a radioactive noble gas that occurs naturally in soil and water as a product of the uranium-238 decay chain. In 1998, it was classified as a human lung carcinogen based on data from epidemiological studies of underground miners exposed to high radon activity concentrations (ICRP 2010). It is considered to be the second largest cause of lung cancer (Zeeb and Shannoun 2009). Evidence has shown that even long-term average radon activity concentration levels below $200\,\mathrm{Bq/m^3}$, are associated with a risk of lung cancer (Darby et al. 2005).

Over one third of the natural radiation dose received by the general population in Austria is due to the inhalation of radon and radon progeny (Ditto et al. 2013). The Austrian Radon Project (ÖNRAP) was started in 1992 in order to investigate the radon activity concentrations in Austrian homes and identify areas of high radon exposure (Friedmann, H. et al. 2007). The result was a radon potential map of Austria[1], which determines the radon potential class of each municipality.

Thoron (Rn-220) has a half-life of less than one minute and is a product of the thorium-232 decay chain. In several findings, an influence of thoron on radon activity concentration measurements has been observed (Michielsen and Bondiguel 2015; Tokonami 2010). As it can introduce bias in radon risk estimates, it is important to investigate this influence and develop methods to reduce it.

---

[1]`https://geogis.ages.at/GEOGIS_RADON.html`

1.1. MetroRADON

Although the Austrian committee for radiation protection has published reference levels for indoor radon activity concentrations, they are not legally binding. However, this is about to change, as the European Council Directive 2013/59/Euratom (EU-BSS), which lays down basic safety standards for protection against the dangers arising from exposure to ionising radiation, is currently being implemented into Austrian law. To meet the challenges of the implementation of the EU-BSS in Europe, the joint research project MetroRADON[2] was initiated with the cooperation of 17 European national metrology and research institutes. The objectives of the MetroRADON project are (*MetroRADON* 2018):

1. To develop novel procedures for the traceable calibration of radon measurement instruments at low activity concentrations

2. To investigate the influence of thoron and its progeny on radon measurements

3. To compare and optimise existing radon measurement procedures in different European countries

4. To develop methodologies for the identification of radon priority areas

5. To validate the traceability of European radon calibration facilities and publish recommendations on metrologically sound calibration and measurement procedures

---

[2]`http://metroradon.eu/`

1.2. Scope and aim

As part of the MetroRADON project, the aim of this thesis is to investigate radon measurement techniques as well as determine the influence of thoron on radon activity concentration measurements by AlphaGUARDs. For this purpose, soil gas measurements were carried out in areas with high uranium and thorium content in the soil. Additionally, the soil gas permeability, the activity concentrations of radionuclides of the uranium and thorium decay chains in soil samples and above-ground gamma dose rates were determined. Furthermore, radon activity concentrations were measured in indoor air and in water samples.

Different radon and thoron measuring instruments were tested, compared and calibrated in the radioactivity laboratory of the Federal Office for Metrology and Surveying (BEV). In order to facilitate further investigations of the influence of thoron on radon measurements, a new thoron source was developed.

Part I of this thesis describes the fundamentals of radioactivity, relevant measurement techniques and the properties of radon and thoron. The experimental procedures and results are discussed in part II.

1.3. Acknowledgements

Part I.

Fundamentals

2. Radioactivity

Radioactivity is the property of unstable atomic nuclei to spontaneously emit ionizing radiation. These unstable atomic nuclei are called radionuclides or radioisotopes.

This chapter contains an overview of the mathematical description and different types of radioactive decay, an introduction to dosimetry and naturally occurring radioactive materials (particularly with regard to radon and thoron) and finally a section on the detection and measurement of radioactivity.

2.1. Mathematics of radioactive decay

It is impossible to determine when a single radionuclide will decay. The probability of decay is constant over time and does not depend on any external influences. However, the statistical behaviour of a large number of atoms can be described mathematically.

2.1.1. One-decay process

For a radioactive substance with number of atoms N, the rate of change $\frac{\mathrm{d}N}{\mathrm{d}t}$ due to radioactive decay is given by the following equation,

$$\frac{\mathrm{d}N}{\mathrm{d}t} = -\lambda N \tag{2.1}$$

where λ is the decay constant. The decay constant λ is connected to two other important quantities related to radioactive decay. The mean lifetime τ is the average lifetime of a radionuclide before decay and is given by

$$\tau = \frac{1}{\lambda} \tag{2.2}$$

The half-life $T_{1/2}$ is the time taken for half of the radionuclides in a sample to decay and is given by

$$T_{1/2} = \frac{\ln 2}{\lambda} = \tau \ln 2 \tag{2.3}$$

The solution to equation 2.1 is given by

$$N(t) = N_0 e^{-\lambda t} = N_0 e^{-t/\tau} \tag{2.4}$$

where N_0 is the number of radionuclides at time $t = 0$. A plot of equation 2.4 is given in figure 2.1.

Equations 2.1 and 2.4 can also be written in terms of the activity A of a sample:

$$\frac{\mathrm{d}A}{\mathrm{d}t} = -\lambda A \tag{2.5}$$

and

$$A(t) = A_0 e^{-\lambda t} = A_0 e^{-t/\tau} \tag{2.6}$$

The activity is given by $A = \lambda N$. It is the number of decays per unit time and is measured in Becquerel (Bq). One Becquerel is defined as one decay per second. Often the activity concentration (activity per unit volume) c_A in $\mathrm{Bq/m^3}$ or the specific activity (activity per unit mass) a in $\mathrm{Bq/kg}$ is given instead of the total activity A.
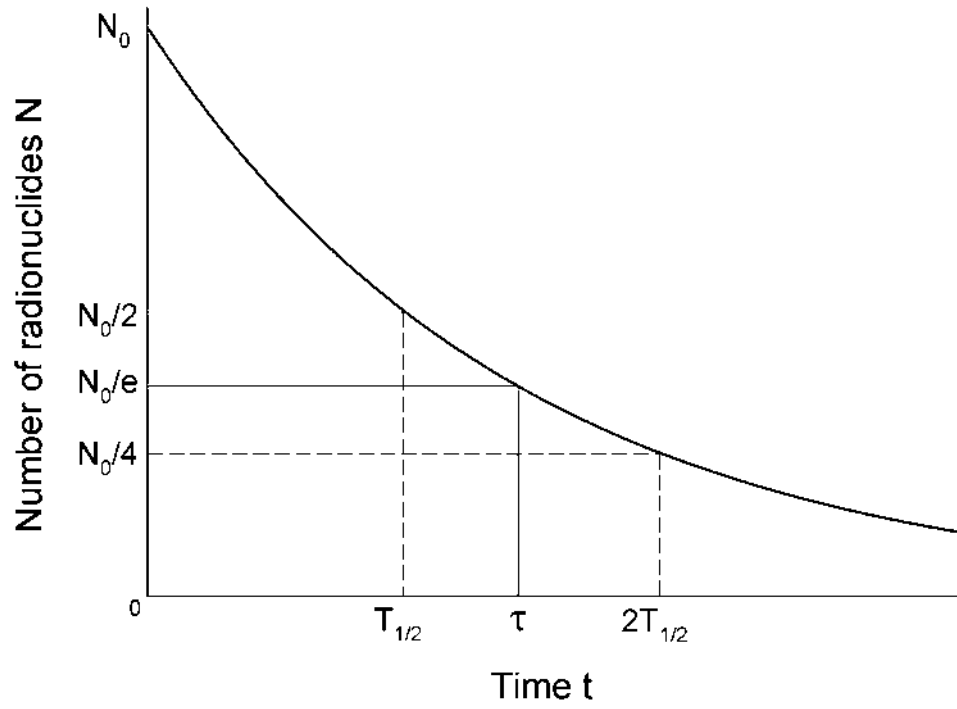
Figure 2.1.: Plot of exponential decay showing the half-life $T_{1/2}$ and mean lifetime τ.

2.1.2. Chain-decay processes

If the daughter nuclide of a decay process is radioactive itself, the previous equations cannot be applied. The decay process

$$A \longrightarrow B \longrightarrow C \tag{2.7}$$

yields the following equations for the number of atoms N_B of nuclide B:

$$\frac{\mathrm{d}N_B(t)}{\mathrm{d}t} = -\lambda_B N_B(t) + \lambda_A N_A(t) = -\lambda_B N_B(t) + \lambda_A N_A(0)e^{-\lambda_A t} \tag{2.8}$$

$$N_B(t) = \frac{N_A(0)\lambda_A}{\lambda_B - \lambda_A}(e^{-\lambda_A t} - e^{-\lambda_B t}) \qquad (2.9)$$

For a chain of any number of decays, the number of atoms of the nth nuclide in the decay chain is given by Bateman's equations (Cetnar 2006):

$$N_n(t) = \frac{N_1(0)}{\lambda_1} \sum_{i=1}^{n} \lambda_i c_i e^{-\lambda_i t} \qquad (2.10)$$

with

$$c_i = \prod_{j=1, i \neq j}^{n} \frac{\lambda_j}{\lambda_j - \lambda_i} \qquad (2.11)$$

Secular equilibrium

If the half-life of the parent nuclide A is much longer than the half-life of the daughter nuclide B $(T_{1/2}(A) >> T_{1/2}(B))$, equation 2.9 can be approximated to

$$N_B(t) = \frac{N_A(0)\lambda_A}{\lambda_B}(1 - e^{-\lambda_B t}) \qquad (2.12)$$

Due to the very long half-life of nuclide A, its activity is considered constant over the observation period. After long enough time t (about 5-6 half-lives of the daughter nuclide B), secular equilibrium is established where $N_B = \frac{\lambda_A}{\lambda_B}N_A$ and therefore $A_A \approx A_B$.

Figure 2.2 shows the activities of radionuclides A and B over time, as well as the total activity. It shows that when secular equilibrium is reached, the activity of the daughter nuclide B is given by the activity of the parent nuclide A.
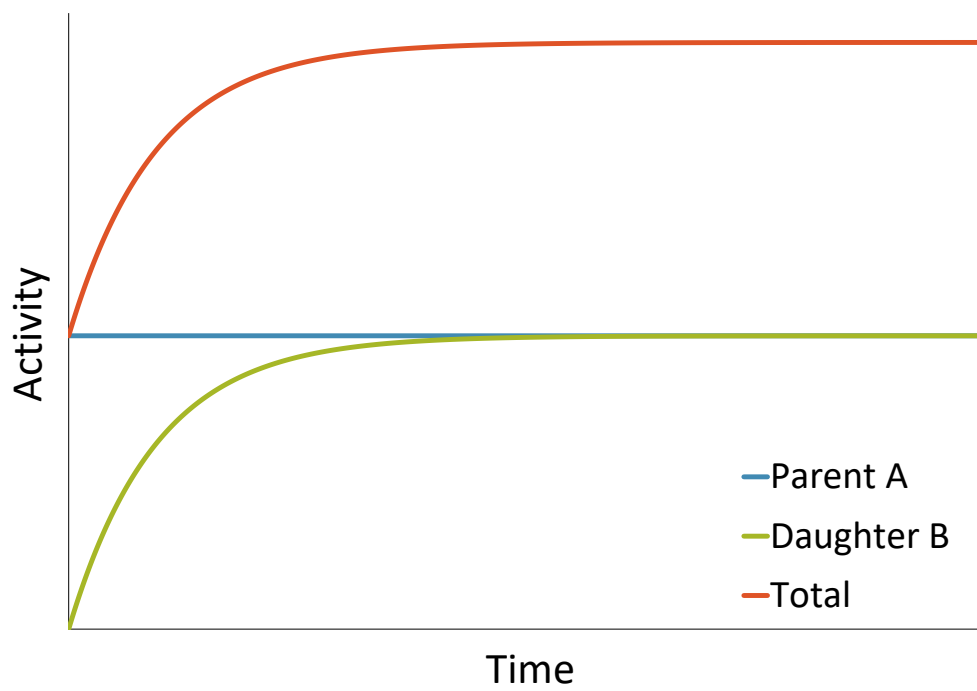
Figure 2.2.: Activities of radionuclides A and B over time, where $T_{1/2}(A) \gg T_{1/2}(B)$. Secular equilibrium is established after a few half-lives of the daughter nuclide B.

2.2. Types of radioactive decay

The main types of radioactive decay are alpha (α), beta (β) and gamma (γ) decay. Other types of decay include neutron emission, proton emission and fission. Figure 2.3 shows which type of decay each nuclide undergoes.

2.2.1. Alpha decay

During alpha decay, a radionuclide (mass number A, atomic number Z) emits an alpha particle and transforms into a daughter nuclide with mass number $A - 4$ and atomic number $Z - 2$. Alpha decay usually occurs in the heaviest radionuclides. An exception is beryllium-8, which decays into two alpha particles. An alpha particle consists of two protons and two neutrons and is identical to a helium-4 nucleus. The energy of the emitted alpha particle is typically in the range of 4–10 MeV. According to the Geiger-Nuttall law (equation 2.13), radionuclides with a shorter half-life emit alpha particles of higher energy (Geiger and Nuttall 1911).

$$\ln \lambda = -a_1 \frac{Z}{\sqrt{E}} + a_2 \tag{2.13}$$

λ ... decay constant

Z ... atomic number

E ... total kinetic energy

a_1, a_2 ... parameter constants

Alpha particles are highly ionizing, but have a low penetration depth. They can be stopped by a few centimetres of air, a piece of paper or a thin layer of skin. Alpha emitters therefore cause most damage when inhaled or ingested.

16
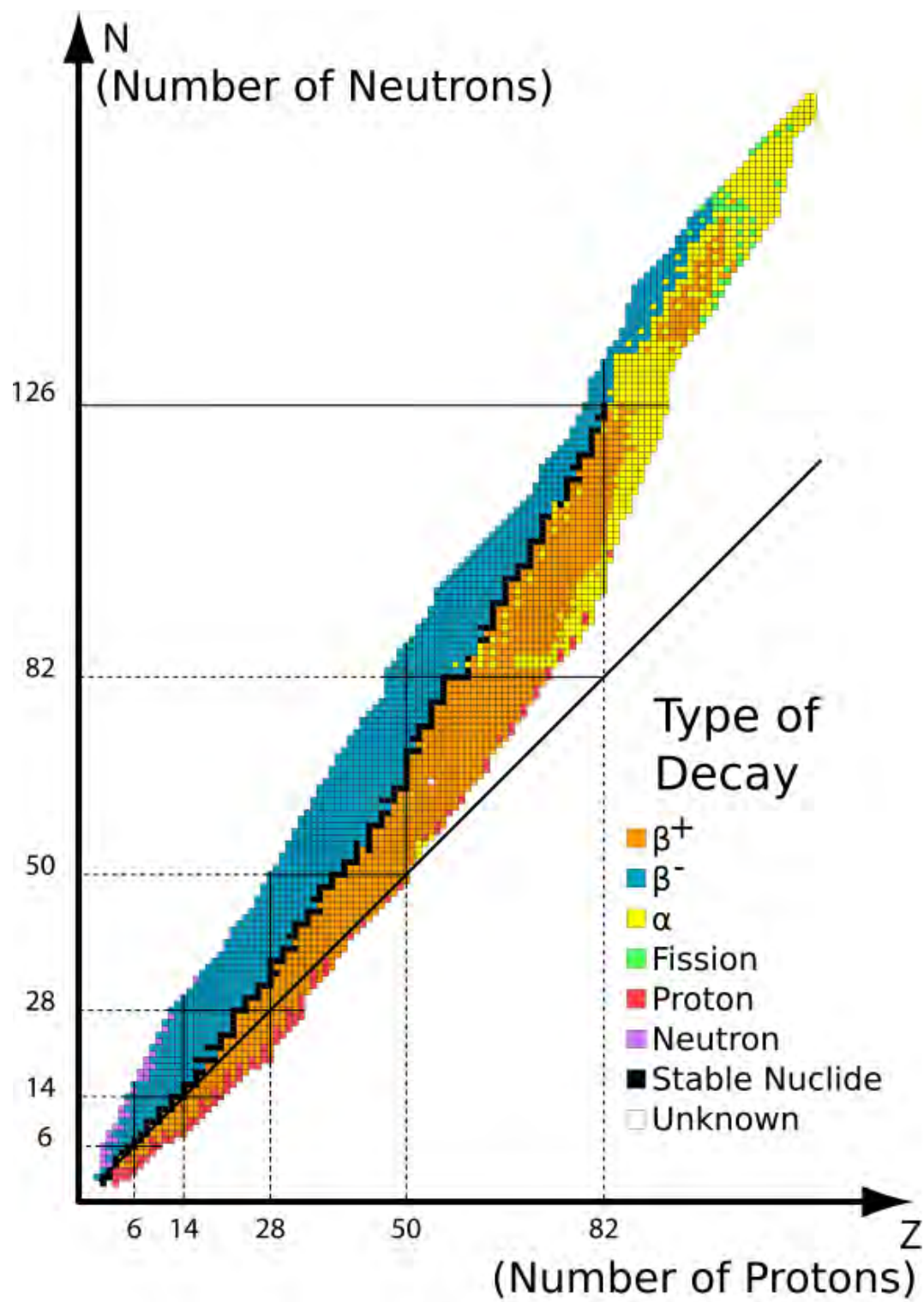
Figure 2.3.: Table of nuclides (Sjlegg 2009).

2.2.2. Beta decay

The two most important types of beta decay are β^- decay and β^+ decay. In β^- decay, a neutron transforms into a proton by the emission of an electron and an electron antineutrino. The atomic number of the daughter nuclide increases by one. In β^+ decay, a proton transforms into a neutron by the emission of a positron and an electron neutrino. The atomic number of the daughter nuclide decreases by one. Figure 2.3 shows that isotopes with more neutrons than the stable nuclide decay by the emission of an electron (β^- decay), while isotopes with fewer neutrons than the stable nuclide decay by the emission of a positron (β^+ decay). The energy spectrum of the emitted beta particles (electrons or positrons) is continuous, since the total energy of the decay process is divided between the beta particle, the (anti)neutrino and the recoiling nucleus. The total energy released during beta decay is usually between a few keV and a few MeV. Beta radiation has a penetration depth of a few meters in air and a few millimetres in human tissue. It can be stopped by a few centimetres of plastic or a few millimetres of metal.

2.2.3. Gamma decay

Gamma decay usually accompanies other types of decay. The daughter nuclide produced during alpha or beta decay is left in an excited state and can decay to a lower energy state by the emission of gamma radiation. Gamma radiation is electromagnetic radiation with energies typically between a few keV and 10 MeV. The difference between X-rays and gamma rays is that X-rays are produced by electrons while gamma rays are produced by the nucleus.

Gamma radiation interacts with matter via the photoelectric effect, Compton scattering and pair production. The photoelectric effect describes the absorption of a
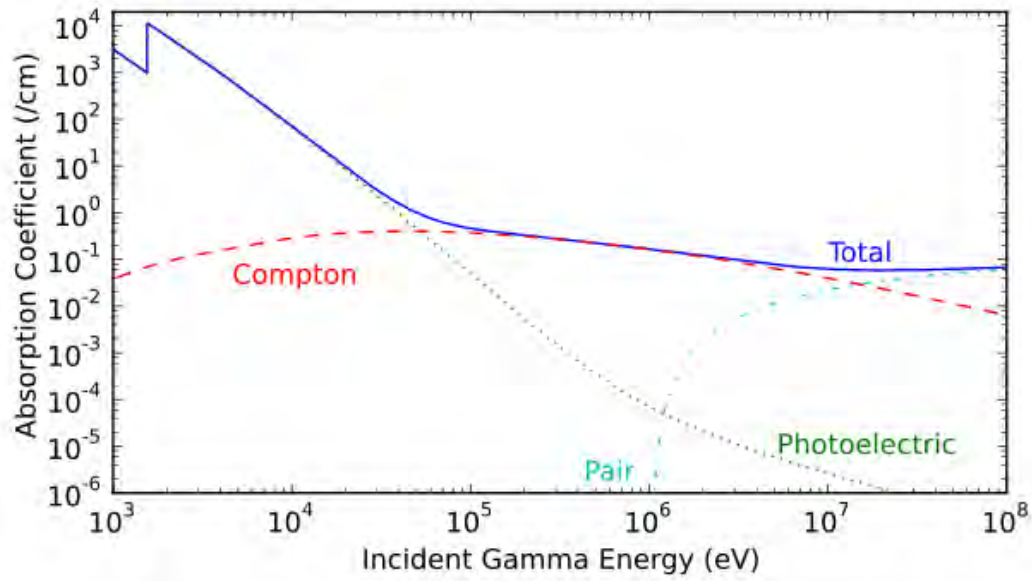
Figure 2.4.: Absorption coefficient of aluminium (Hykes 2011).

gamma photon by an atomic electron and the following ejection of that electron from the atom. Compton scattering is the inelastic scattering of a photon by an atomic electron. The electron is ejected from the atom and the gamma photon is deflected and its energy is reduced. Pair production is the conversion of gamma ray energy into the mass of an electron-positron pair in the presence of the electric field of a nucleus. The minimum energy needed for pair production is 1.02 MeV (twice the rest mass of an electron). As a result of these interactions, the intensity I of gamma radiation decreases exponentially as it passes through a distance x of material:

$$I = I_0 e^{-\mu x} \tag{2.14}$$

μ is called the absorption coefficient or attenuation coefficient. Figure 2.4 shows the absorption coefficient of aluminium and the contributions by the photoelectric effect, Compton scattering and pair production.

The intensity of 100 keV gamma radiation is reduced by half by 35 m of air, 4.15 cm of water, 1.59 cm of aluminium or 0.12 mm of lead (*Interaction of Gamma Radiation with Matter* 2017). These numbers increase with higher gamma radiation energies. Gamma radiation can pass through the human body. However, it is less ionizing than alpha or beta radiation.

2.3. Dosimetry

Dosimetry is the measurement of the dosage of ionizing radiation. Because the effects of ionizing radiation are dependent on the type of radiation and the type of material being irradiated, different measures of radiation dose are defined that take these aspects into consideration.

2.3.1. Absorbed dose

The absorbed dose D is the mean energy ϵ deposited by ionizing radiation on a unit mass m of material. It is measured in Gray (Gy).

$$D = \frac{\mathrm{d}\epsilon}{\mathrm{d}m} \tag{2.15}$$

$$[D] = \mathrm{Gy} = \mathrm{J/kg} \tag{2.16}$$

The absorbed dose is a physical quantity that does not take into consideration the effect of different types of radiation on the human body.

2.3.2. Equivalent dose

Multiplying the absorbed dose D by a radiation weighting factor w_R yields the equivalent dose H_T. It is measured in Sievert (Sv).

$$H_T = \sum_R w_R D_{T,R} \qquad (2.17)$$

$$[H_T] = \text{Sv} = \text{J/kg} \qquad (2.18)$$

The weighting factor w_R represents the relative biological effectiveness of the different types of radiation. Its values are given in table 2.1.

Radiation type	Radiation weighting factor w_R
Photons	1
Electrons and muons	1
Protons and charged pions	2
Alpha particles, fission fragments, heavy ions	20
Neutrons	Between 2.5 and 20.7, depending on neutron energy.

Table 2.1.: Radiation weighting factors (ICRP 2007).

2.3.3. Effective dose

The effective dose E also takes into consideration the sensitivities of different organs to ionizing radiation. It is calculated by multiplying the equivalent dose to each organ by a tissue weighting factor w_T. It is also measured in Sievert (Sv).

$$E = \sum_T w_T H_T \qquad\qquad (2.19)$$

$$[E] = \text{Sv} = \text{J/kg} \qquad\qquad (2.20)$$

The weighting factor w_T represents the sensitivity of different tissues of the human body to radiation. Its values are given in table 2.2.

Tissue	Tissue weighting factor w_T
Red bone-marrow, colon, lung, stomach, breast	0.12
Gonads	0.08
Bladder, oesophagus, liver, thyroid	0.04
Bone surface, brain, salivary glands, skin	0.01
Remainder of body	0.12

Table 2.2.: Tissue weighting factors (ICRP 2007).

3. Detection and measurement of radioactivity

This chapter presents an overview of the most important measurement techniques and instruments related to the measurement of radon and thoron. Measuring instruments can either be active or passive. Active measuring instruments are electronic devices that require a power source during measurement. They can be used to determine the temporal fluctuations in the measured activity concentration. Passive devices no not require a power source during measurement. At the end of the measurement period, the integrated exposure is determined. Electret ion chambers, charcoal detectors and solid state nuclear track detectors are examples of passive measuring instruments and are commonly used for indoor radon activity concentration measurements.

3.1. Gas-filled detector

Gas-filled detectors consist of a gas-filled chamber and two electrodes. As ionizing particles pass through the chamber, they ionize the gas, creating electron-ion pairs. An electric field is applied, causing the electrons and ions to drift towards the electrodes, where they cause an electric pulse. There are three main types of gas-filled detectors, differing in the amount of voltage applied to the chamber (figure 3.1).
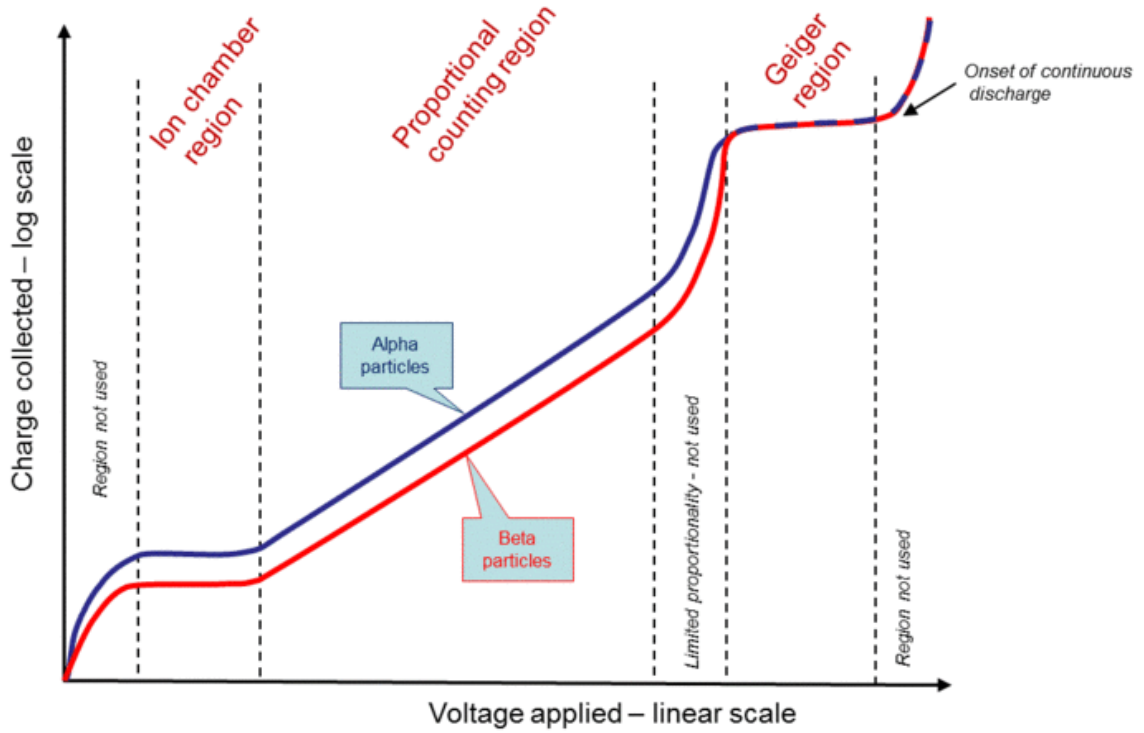
Figure 3.1.: Regions of a gas filled chamber (Sim 2012).

Ionization chambers operate at low electric field strengths sufficient to make sure that all charges are collected at the electrodes. They generate small output signals proportional to the energy of the incident ionizing particle and independent of the applied voltage.

Proportional counters operate at higher electric field strengths than ionization chambers, so that the free electrons have enough energy to ionize more gas atoms. This process is called gas amplification. The number of secondary electrons is proportional to the number of primary electron/ion pairs created by the incident particle. The output signal is therefore bigger than that of an ionization chamber, but still proportional to the energy of the ionizing particle.

Geiger counters operate at even higher electric field strengths, resulting in secondary avalanches triggered by photons emitted by excited ions. Gas amplification reaches

saturation and the output signal is no longer proportional to the incident particle's energy. Geiger counters can therefore only detect the presence of radiation, but not its type or energy.

3.2. Semiconductor detector

In semiconductor detectors, ionizing radiation produces free electrons and holes. An applied electric field causes the electrons and holes to travel to the electrodes, resulting in a measurable electric pulse. The number of electron-hole pairs is proportional to the energy of the incident radiation (Knoll 1999). Semiconductor detectors can measure photons with energies ranging from $<1\,\mathrm{eV}$ to about $10\,\mathrm{MeV}$ and charged particles with energies in the range of keV to MeV (Kukk 2011).

3.3. Scintillation detector

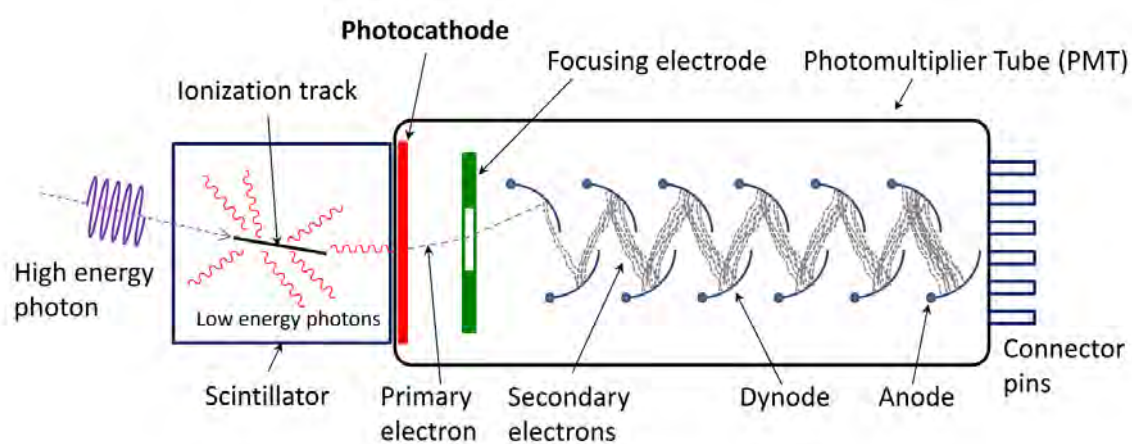**Figure 3.2.:** Schematic view of a scintillation detector (Qwerty123uiop 2013).

A scintillator is a material that emits light following the absorption of ionizing radiation. The molecules of the scintillator are excited to a higher energy state by the

incoming radiation and then relax back to their original state by the emission of light. A scintillation detector (figure 3.2) consists of a scintillator coupled to a device that converts light into an electrical current, such as a photodiode or a photomultiplier.

3.4. Electret ion chamber

An electret is a dielectric material, usually Teflon, with a quasi-permanent electric charge that produces an electrostatic field. It is fabricated by being heated while exposed to an electric field (L'Annunziata 2012). An electret ion chamber consists of an electret disc mounted inside an electrically conducting chamber. The electret disc collects the ions produced by the ionizing radiation, which reduces its charge. The charge reduction is related to the total ionization during the period of exposure (Kotrappa 2002). Electret ion chambers don't require a power source, since the electric field in the chamber is created by the electret itself. This makes them a good choice for long-term measurements of indoor radon- and thoron activity concentrations. However, they only provide an average value over the time period of exposure.

3.5. Charcoal detector

Activated charcoal can be used as a low-cost method for short-term measurements of indoor radon activity concentration. The charcoal is placed in an open container and the radon in the air adsorbs onto it. The rate of adsorption is affected by temperature, moving air streams and humidity (Alvarez 1990). After 2 to 7 days (van Velzen et al. 2010), the container is sealed air-tight and transferred to the laboratory for analysis. The radon activity concentration in the charcoal is measured by the detection of

gamma rays produced by radon progeny using either a gamma ray spectrometer or a liquid scintillation detector.

3.6. Solid state nuclear track detector

Solid state nuclear track detectors are made of insulating materials, such as inorganic crystals, glasses and plastics. When ionizing radiation passes through them, they damage the material and leave behind a latent track of about 50 Å in diameter (Kalsi, Ramaswami and Manchanda 2005). The latent tracks can be made visible by etching with sodium hydroxide or hydrofluoric acid. When used as radon detectors, the density of the tracks on the detector material is a measure of the integrated radon activity concentration over the time period of exposure.

3.7. Gamma spectrometry

The energies of gamma photons are characteristic for the nuclides by which they are emitted. When photons interact with matter, secondary electrons are created by the photoelectric effect, Compton scattering and pair production (see section 2.2.3). By measuring the energy spectrum of these secondary electrons, the identity and activity concentrations of the gamma-emitting radionuclides in a sample can be determined.

The most common detectors used in gamma spectrometry scintillation detectors and semiconductor detectors. Two important characteristics of a gamma detector are its resolution and its efficiency. The detector resolution is given by the full width half maximum (FWHM)[1] at a specific energy. It determines the minimum distance at which two peaks can still be separated from one another. The detector efficiency is

---

[1]FWHM is the width of an energy peak at half its maximum value.

the fraction of gamma photons emitted by the sample that interact with the detector to produce a count. It generally increases with the size of the detector.

4. Radon and thoron

Naturally Occurring Radioactive Material (NORM) refers to naturally-occurring ra-
dionuclides found in the environment as well as airborne radionuclides produced by
cosmic radiation interacting with the earth's atmosphere. A large fraction of the
radiation dose received by the general population is due to natural radiation.
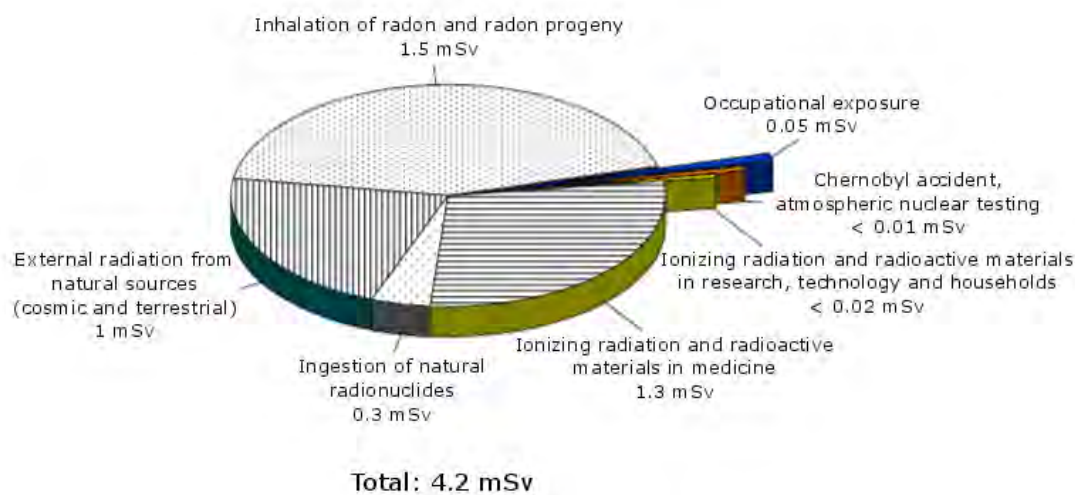
Figure 4.1.: Austrian average annual radiation dose (effective dose per person per
year). Translated from Ditto et al. 2013.

The average annual effective dose per person in Austria is 4.2 mSv, the majority of
which comes from natural sources of radiation and medical exposures (Ditto et al.
2013). More than half of the exposure from natural sources of radiation is due to the
inhalation of radon and its progeny.

4.1. Properties of radon

In this work, radon refers to the isotope ^{222}Rn. Table 4.1 lists some important properties of radon.

Atomic number	86
Mass number	222
Half-life	$3.8232 \pm 0.0008\,\mathrm{d}$
Decay mode	α
Decay energy	$5590.3 \pm 0.3\,\mathrm{keV}$
Decay product	^{218}Po

Table 4.1.: Properties of radon (Bé, Chisté, Dulieu, Browne, Chechev, Kuzmenko, Kondev et al. 2008).

Radon is a colourless, odourless and tasteless radioactive noble gas. It occurs naturally in soil and water as a product of the uranium-238 decay chain (figure 4.2).

In the open air, radon emanating from the ground is diluted quickly and the radon activity concentration is very low. In closed rooms, however, radon can accumulate, potentially leading to high radon activity concentrations. A link between high radon activity concentrations and an increased risk of lung cancer has been well established (ICRP 2010; Darby et al. 2005; Pawel and Puskin 2003; Lagarde et al. 2001). The main risk is due to short-lived radon progeny, such as ^{218}Po and ^{214}Po. They can attach to particles in the air and accumulate in the respiratory system when inhaled. There the emitted alpha particles can damage cells and thereby cause cancer.
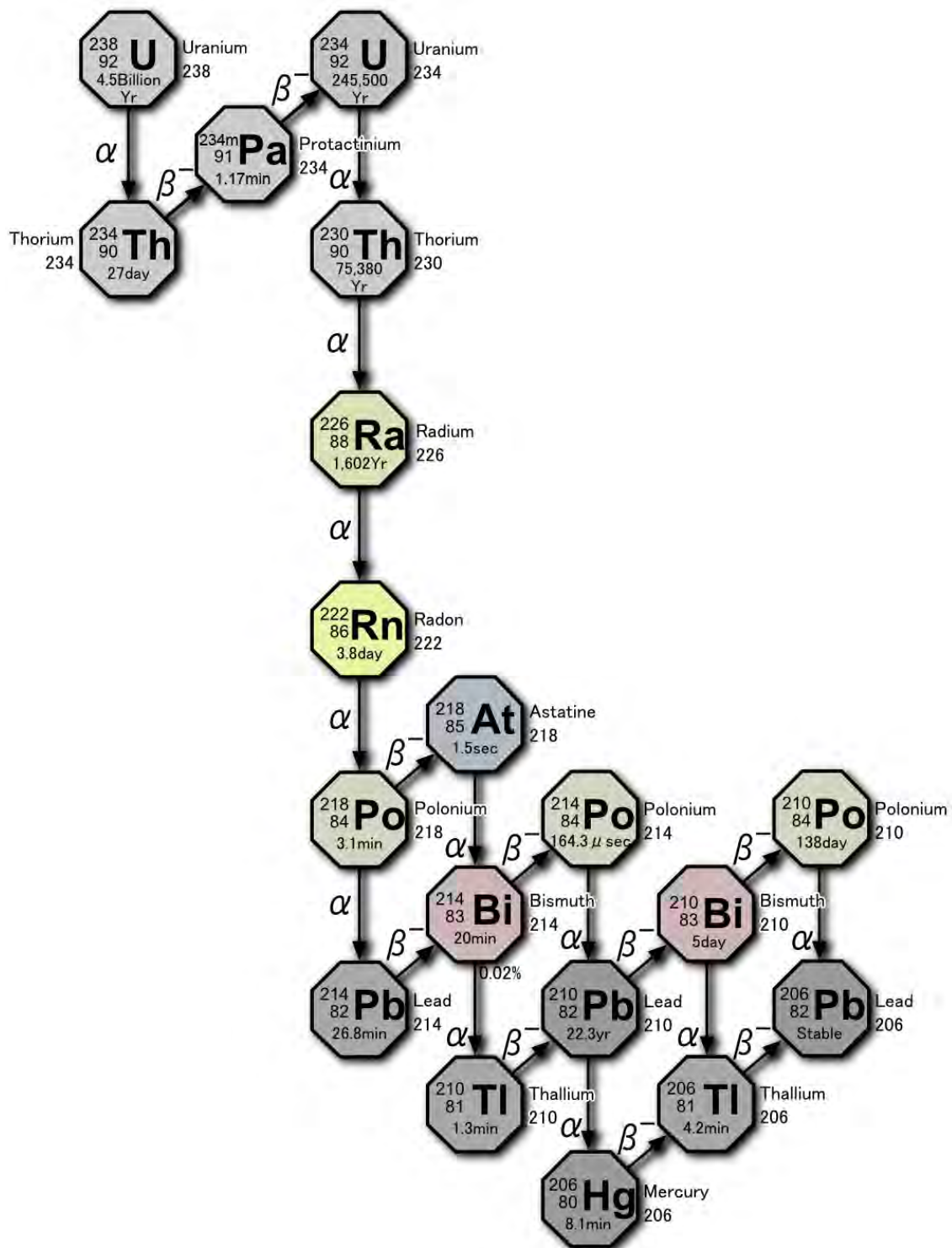
Figure 4.2.: Uranium decay chain (Tosaka 2008b).

4.2. Properties of thoron

Thoron is the historical name given to the isotope ^{220}Rn because it is a product of the thorium decay chain (figure 4.3). Table 4.2 lists some of its properties.

Atomic number	86
Mass number	220
Half-life	$55.8 \pm 0.3\,\text{s}$
Decay mode	α
Decay energy	$6404.67 \pm 0.10\,\text{keV}$
Decay product	^{216}Po

Table 4.2.: Properties of thoron (Bé, Chisté, Dulieu, Browne, Chechev, Kuzmenko, Helmer et al. 2004).

The average annual effective dose due to thoron is much smaller than that due to radon (UNSCEAR 2008). Therefore, its influence has often been neglected in studies of radon exposure. However, under certain circumstances - such as the presence of thorium in the ground or in building materials - thoron exposure can contribute significantly to the radiation dose (Cinelli et al. 2015; Gierl et al. 2014; Steinhäusler 1996). Furthermore, the presence of thoron can affect the readings obtained by radon detectors (Michielsen and Bondiguel 2015; Tokonami 2010).
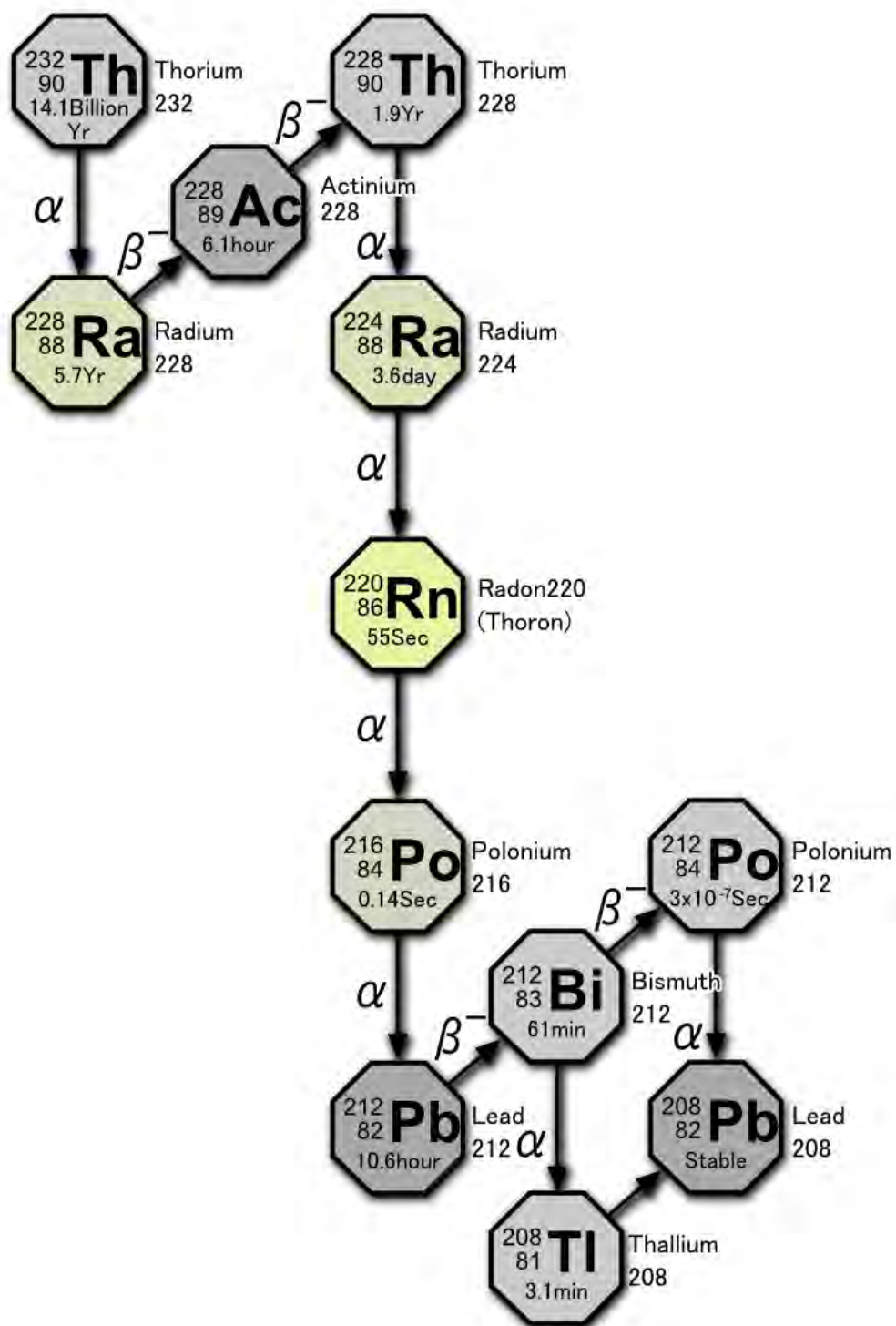
Figure 4.3.: Thorium decay chain (Tosaka 2008a).

4.3. Depth distribution in soil gas

The radon activity concentration in the soil is constant at great depths and decreases exponentially towards the surface. The distribution and the depth at which the radon activity concentration is constant depends on the diffusion length l. The diffusion length determines the distance from the source at which the concentration is reduced by a factor $1/e$.

The radon activity concentration at a depth z beneath the surface is given by

$$c_z = c_{\text{const}} \left(1 - e^{-z/l}\right) \tag{4.1}$$

c_z ... Radon activity concentration at depth z beneath the surface

c_{const} ... Constant radon activity concentration at great depth

Figure 4.4 shows a plot of the radon distribution in soils with different diffusion lengths.

The diffusion length of radon in the soil depends on the type of soil. Moist clays and loams have diffusion lengths between $20\,\text{cm}$ and $155\,\text{cm}$ and dry sands and gravels have diffusions lengths between $155\,\text{cm}$ and $195\,\text{cm}$ (Kemski, R and Siehl 1996).

The distribution of thoron activity concentration in soil gas "has no obvious regularity" (Wang et al. 2016). Diffusion lengths of thoron in soils are about two orders of magnitude lower than those of radon. Moist clays and loams have diffusion lengths between $0.3\,\text{cm}$ and $0.9\,\text{cm}$ and dry sands and gravels have diffusions lengths between $0.9\,\text{cm}$ and $2.5\,\text{cm}$ (Kemski, R and Siehl 1996). This means that, according to equation 4.1, the thoron activity concentration already reaches its maximum value just a few cm below the surface.
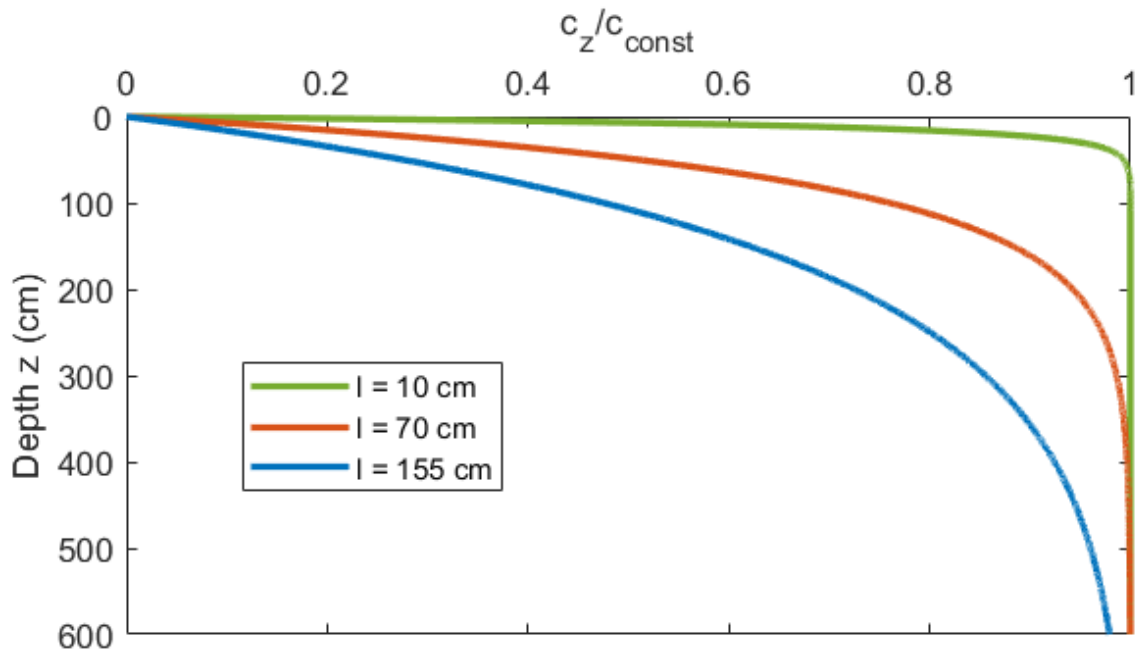
Figure 4.4.: Depth distribution of radon activity concentration in the soil at different diffusion lengths.

4.4. Indoor radon and thoron

4.4.1. Sources

The main sources of radon and thoron in houses are soil gas and building materials. Additionally, in areas where "the water source is an underground aquifer in granite or other radium-bearing rock", radon dissolved in tap water can be released into the air and contribute significantly to the indoor radon activity concentration (Bruno 1983).

Radon and thoron from the soil can enter buildings either through cracks and gaps or by diffusion through the foundation. This is facilitated by the stack effect in the lowest level of the building: the rising warm air reduces the air pressure, drawing in the soil air from below. This effect is stronger in the winter months due to the increased temperature difference between the outside air and the heated indoor air.

Radium and thorium in building materials can also contribute to the indoor radon and thoron activity concentrations. Concrete, stone and brick contain significant amounts of radium and are widely used in construction, which make them a primary source of radon among building materials (Bruno 1983). Particularly high Th-232 activity concentrations can be found in building materials made from recycled waste materials, such as fly ash or slag (Gierl et al. 2014; Steinhäusler 1996). Due to the short half-life of thoron, its indoor activity concentration decreases exponentially with increasing distance from the source (Steinhäusler 1996). Therefore, the thoron activity concentration is higher close to the walls than in the centre of the room.

4.4.2. Reference levels

"A reference level represents the maximum accepted average annual radon concentration in a residential dwelling" (Zeeb and Shannoun 2009). The Austrian reference levels for indoor radon activity concentrations are $400\,\mathrm{Bq/m^3}$ for existing buildings and $200\,\mathrm{Bq/m^3}$ for new ones.

Methods to stay within the reference levels are based on either preventing radon from entering the house in the first place by sealing floors and walls and avoiding the passage of radon from the basement into living rooms, or by increasing the air exchange rate by improving ventilation in order to reduce the accumulation of indoor radon activity concentration (WHO 2016).

4.5. Radon potential

The radon potential is a way to determine the average radon risk in an area. It can be defined using either indoor measurements of radon activity concentration or the radon activity concentration and permeability of soil gas. In any case, the radon potential is only a statistical statement and cannot predict the radon activity concentration in individual homes. The Austrian Radon Project (Friedmann, H. et al. 2007) used indoor radon measurements to create a radon potential map of Austria. The radon activity concentration and permeability of soil gas were used to determine the radon potential in Germany (Kemski, Siehl et al. 2001) and Canada (Chen and Ford 2017).

4.5.1. The Austrian Radon Project

Between 1992 and 2001, the radon activity concentration in around 20 000 randomly selected homes was measured using solid state nuclear track detectors, electret detectors and charcoal detectors. The radon potential was defined as the expected radon activity concentration in a standard situation averaged over one year (Friedmann, H. et al. 2007). Figure 4.5 shows the mean radon potential for each municipality.

4.5.2. Radon potential from soil gas measurements

In addition to soil gas radon activity concentration, soil permeability is an important factor in determining the radon potential of an area, as a high permeability can lead to increased migration of radon from soil gas into houses.

In a German research project by Kemski, Siehl et al., an empirical ranking classification (figure 4.6) was used to define a geogenic radon potential. It divides the radon
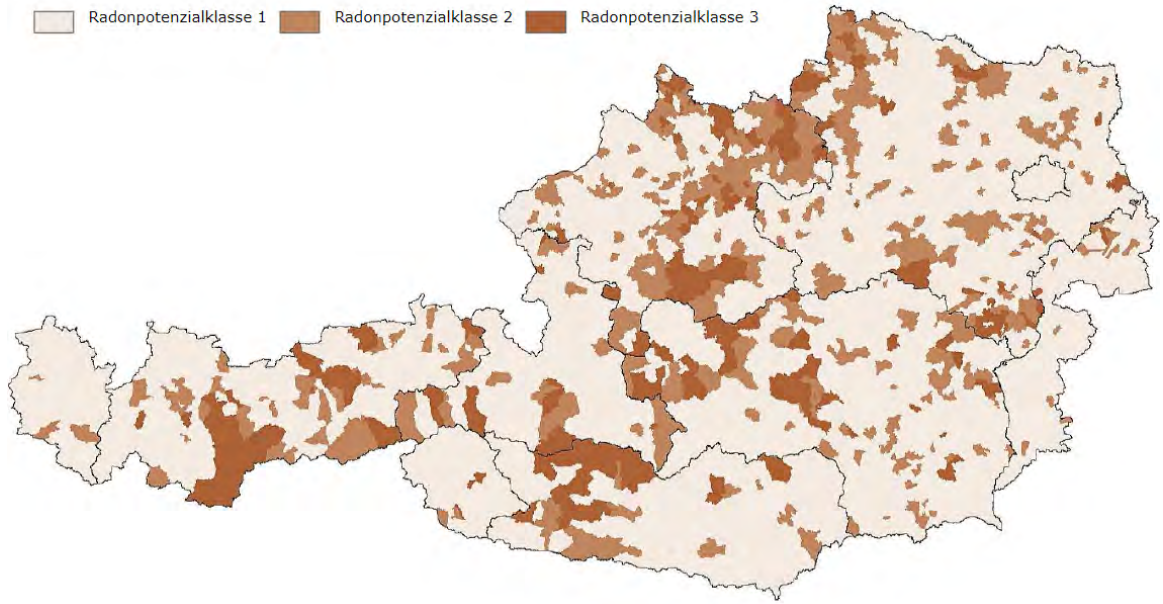
Figure 4.5.: Radon potential map of Austria (Bundesministerium für Nachhaltigkeit und Tourismus 2018). The radon potential is divided into three classes: 1: 1–200 Bq/m³, 2: 201–400 Bq/m³, 3: over 400 Bq/m³.

activity concentration and the gas permeability into three classes each, to obtain a radon potential class between 1 and 6.

A more recent Canadian study by Chen and Ford used equation 4.2 to calculate a soil radon potential (SRP) index.

$$ \text{SRP} = \frac{C - C_0}{\log P_0 - \log P} \tag{4.2} $$

C ... Soil gas radon activity concentration (kBq/m³)

$C_0 = 1\,\text{kBq/m}^3$

P ... Soil permeability (m²)

$P_0 = 1 \times 10^{-10}\,\text{m}^2$

A strong correlation was found between indoor radon potential (defined as the percentage of homes with a radon activity concentration above 200 Bq/m³) and soil radon
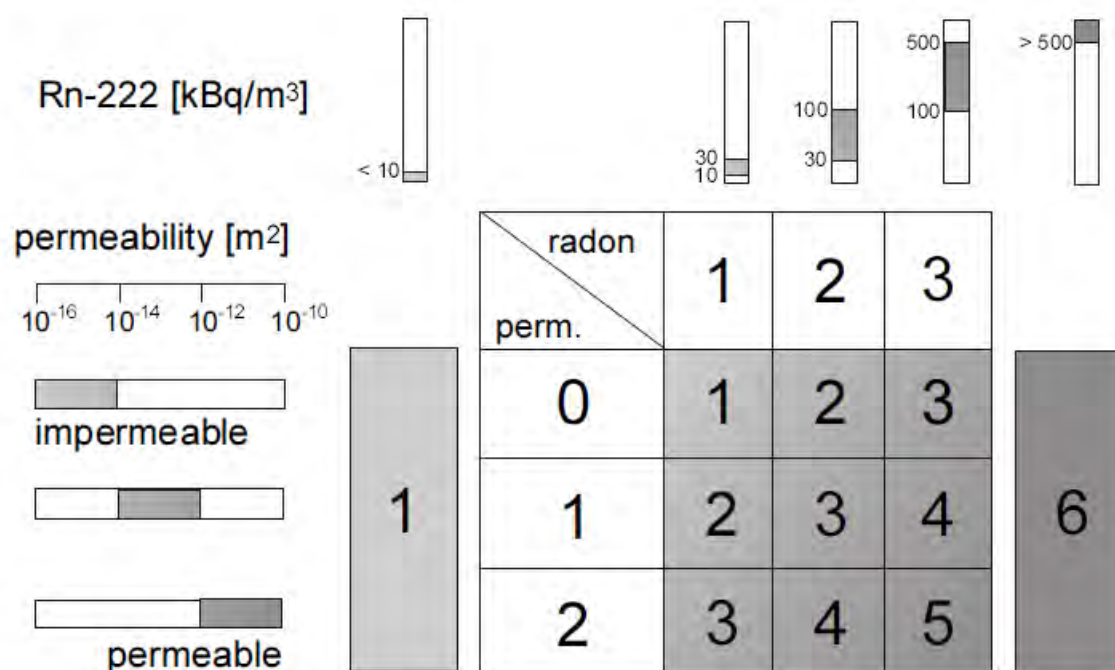
Figure 4.6.: Classification of geogenic radon potential by ranking of radon concentration in soil gas and gas permeability (Kemski, Siehl et al. 2001).

potential (SRP). This shows that a combination of the radon activity concentration in soil gas and the soil permeability can be a good indicator of the possible indoor radon activity concentration.

Part II.

Experimental procedures and results

5. Radon and thoron measurements in the laboratory

The measurements described in this chapter were carried out in the radioactivity laboratory of the Federal Office for Metrology and Surveying (BEV)[1] in Seibersdorf. The BEV is the national metrology institute of Austria. Its responsibilities include the maintenance and development of national standards and the certification, verification and calibration of measuring instruments ("Maß- und Eichgesetz" 1950).

5.1. Measuring instruments

To measure the activity concentrations of radon and thoron, a Thoron-Scout by SARAD (serial number RSCT-00022), two Corentium Pro detectors by Airthings and four AlphaGUARDs by Saphymo were used. Table 5.1 shows the names, models and serial numbers of all the AlphaGUARDs used.

The AG BEV belongs to the Federal Office for Metrology and Surveying (BEV) and is the national standard for radon measurements. The other AlphaGUARDs were provided by the Austrian Agency for Health and Food Safety (AGES)[2] in Linz.

---

[1] http://www.bev.gv.at
[2] https://www.ages.at

Name	Model	Serial number
AG BEV	PQ2000 PRO RnTn	EF 1338
AG 2	PQ2000 PRO	EF 1621
AG 6	PQ2000 PRO RnTn	EF 1625
AG 8	PQ2000 PRO	EF 1872

Table 5.1.: AlphaGUARD models and serial numbers.

5.1.1. AlphaGUARD

The AlphaGUARD (figure 5.1) uses a pulse ionization chamber "for the continuous determination of the radon- and radon progeny concentration in air" (Saphymo GmBH 2014). Figure 5.2 shows the setup of the ionization chamber.

Figure 5.1.: Photograph of the AlphaGUARD (Saphymo GmBH 2014).

Depending on the model, the AlphaGUARD comes with different measurement modes. The AlphaGUARD PQ2000 PRO comes with a diffusion mode and a flow-through mode (flow mode), while the AlphaGUARD PQ2000 PRO RnTn disposes of an additional radon/thoron operation mode (RnTn mode). In diffusion mode, a glass fiber filter allows only radon to pass through, preventing radon progeny from entering the ionization chamber. In the flow-through and radon/thoron modes, a flow-through

44
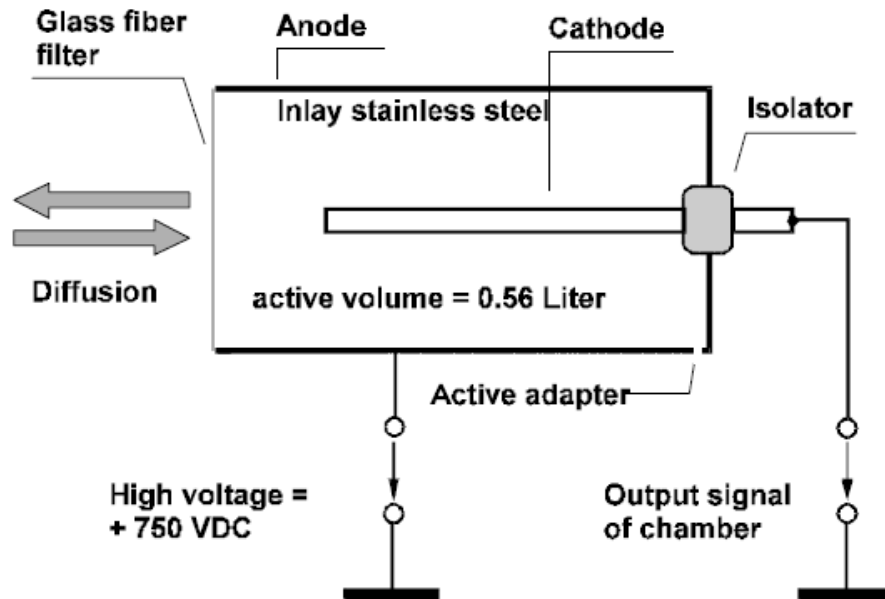
Figure 5.2.: Diagram of the AlphaGUARD ionization chamber (Saphymo GmBH 2014).

adapter is mounted in front of the glass fiber filter and radon (and/or thoron) is pumped into the ionization chamber at a rate of $1\,\mathrm{L/min}$. In radon/thoron mode, gas is only pumped into the ionization chamber for the first three minutes of a 10-minute measuring cycle in order to differentiate between radon and thoron by the difference in their half-lives. The pump is controlled by the AlphaGUARD via a remote control cable.

5.1.2. Thoron-Scout

The Thoron-Scout (figure 5.3) determines the activity concentrations of radon and thoron in air by measuring the alpha activity of their short lived decay products using a semiconductor detector. The air to be measured enters the highly permeable measurement chamber by diffusion.

Figure 5.3.: Photograph of the Thoron-Scout (SARAD GmBH 2015).

Rn-222 decays into Po-218, which is an alpha emitter with a half-life of 3.05 min. An electrostatic field causes the positively charged Po-218 ions to collect on the surface of a semiconductor detector. The number of collected Po-218 ions is proportional to the concentration of Rn-222 in the measurement chamber. An equilibrium between Rn-222 and Po-218 is reached after approximately 15 min, which is therefore the minimum response time of the Thoron-Scout to a change in the radon activity concentration. After Po-218, the decay chain continues with Pb-214, Bi-214 and Po-214. Since Po-214 is also an alpha emitter, it is also seen by the detector. It is possible to differentiate between Po-218 and Po-214 via alpha spectroscopy because of their different emission energies. However, due to the half lives of Pb-214 (26.8 min) and Bi-214 (19.9 min), an equilibrium between Po-218 and Po-214 is only reached after approximately 3 h. The Thoron-Scout offers a "fast-mode" and a "slow-mode" for the calculation of radon concentration. The "fast-mode" uses only Po-218 while the "slow-mode" uses both Po-218 and Po-214 to determine the radon activity concentration in the chamber. The "fast-mode" therefore has a faster response time while the "slow-mode" has a

higher sensitivity.

The activity concentration of Rn-220 is measured by its decay product Po-216. Po-216 has a half-life of 0.145 s, which means that an equilibrium between Rn-220 and Po-216 is reached virtually immediately. (SARAD GmBH 2015)

5.1.3. Corentium Pro

The Corentium Pro is a radon monitor designed to measure the radon activity concentration in indoor air in homes and workplaces. It uses four silicon photodiodes as radon detectors. The air enters the detectors via a passive diffusion chamber with a diffusion time constant of 25 min. Refer to the appendix for more information.

5.2. The emanation- and calibration container

Figure 5.4.: Photograph of the emanation and calibration container.

The emanation- and calibration container (figure 5.4) is an air-tight container of stainless steel with a nominal volume of 210.5 L. The removable lid is equipped with two gas valves with ball taps to allow controlled gas exchange (Genitron Instruments GmbH 1995).

The tightness of the container can be tested by filling it with radon and measuring its activity concentration over several days. Figure 5.5 shows the radon activity concentration in the container over almost two weeks.
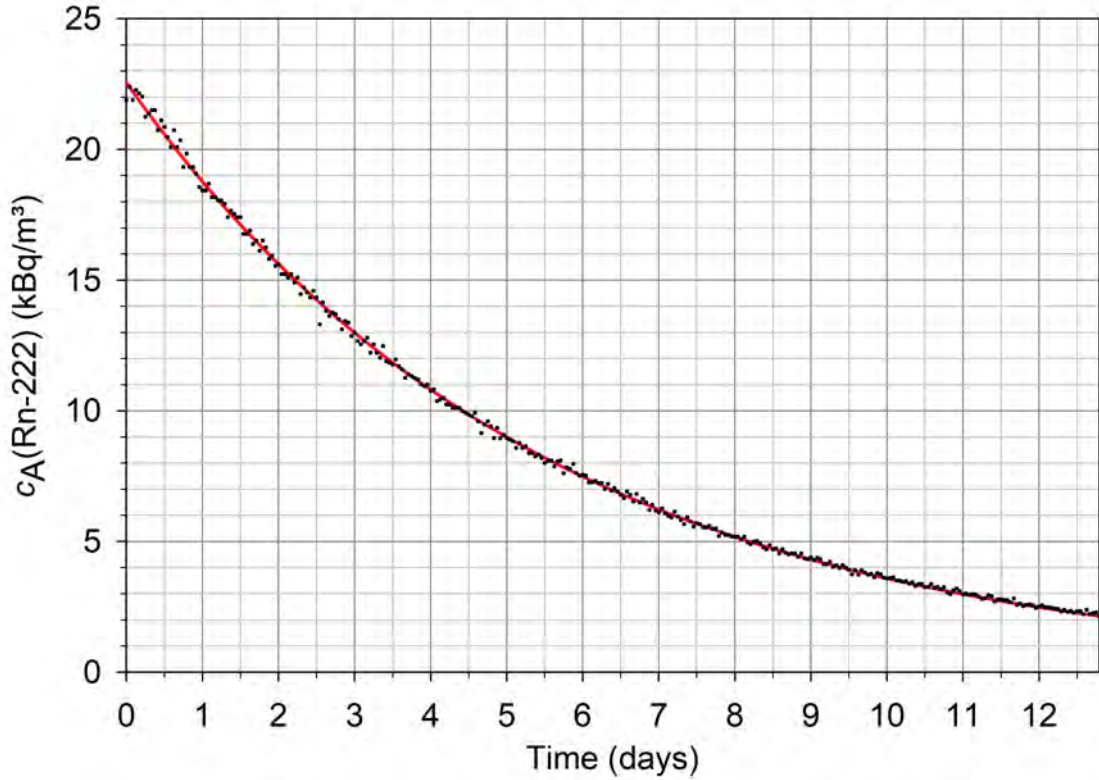
Figure 5.5.: Radon activity concentration in the emanation- and calibration container over time, measured with the AG BEV in diffusion mode. The red line shows a nonlinear regression fit through the data (refer to the appendix for the full regression report).

A nonlinear regression using SigmaPlot software yields a value of $\lambda = 0.1839 \pm 0.0003\,\mathrm{d^{-1}}$ for the decay constant, which leads to a half-life of $T_{1/2} = 3.769 \pm 0.006\,\mathrm{d}$. This is a deviation of only about 1.4 % from the literature value of $3.8232 \pm 0.0008\,\mathrm{d}$ (see

48

section 4.1). The uncertainty of the calculated half-life is likely underestimated, as it is the uncertainty associated with the nonlinear regression, but does not consider the uncertainties of the radon measurements. Another way to calculate the half-life is by using two data points, in this case at $t = 0$ and $t = 12\,\mathrm{d}$, and inserting them into the exponential decay law (equation 2.6) to obtain a value for λ. This method yields a half-life of $T_{1/2} = 3.8 \pm 0.1\,\mathrm{d}$. In this case the uncertainty is due to the uncertainty of the radon measurements. Both calculated values are close to the literature value of the half-life of radon, leading to the conclusion that the container is airtight and there is no radon loss over the observed time period.

5.3. Radon source

The radon source RADOTTO 1 (figure 5.6) is made of five 1-l-gas-washing bottles filled with standard Ra-226 solutions of different activities (Maringer and Ramer 1999).

Figure 5.6.: Photograph of the radon source RADOTTO 1.

Table 5.2 shows the activities of the Ra-226 solutions in each bottle of the radon source.

Bottle	Ra-226 Activity (Bq)
1	21130 $\pm$ 1060
2	10790 $\pm$ 540
3	5296 $\pm$ 265
4	2548 $\pm$ 127
5	1432 $\pm$ 72

Table 5.2.: Ra-226 activities of the radon source RADOTTO 1 (Maringer and Ramer 1999).

Ra-226 decays into Rn-222 with a half-life of 1600 years (Bé, Chisté, Dulieu, Browne, Chechev, Kuzmenko, Helmer et al. 2004). When the gas-washing bottles are closed, a secular equilibrium develops between the radium solution and the radon gas. By pumping air through the bottles, radon can be pumped into, for example, the emanation- and calibration container. A second, empty gas-washing bottle is placed in front of the first one for safety, so that no liquids enter the pump or measuring instrument. If all the radon gas is pumped out of one of the bottles, it takes about 3 weeks (5-6 half-lives of radon) to reach equilibrium again (see section 2.1).

5.4. Thoron source

Similar to the radon source, a thoron source was developed in order to study the effect of thoron on radon measurements or to calibrate thoron measuring instruments. The basis of the thoron source is natural monazite sand containing isotopes of the thorium decay chain Th-232, Ra-228 and Th-228 (see the appendix for the gamma spectrometry results).

Placing an open container with the monazite sand into the emanation- and calibration
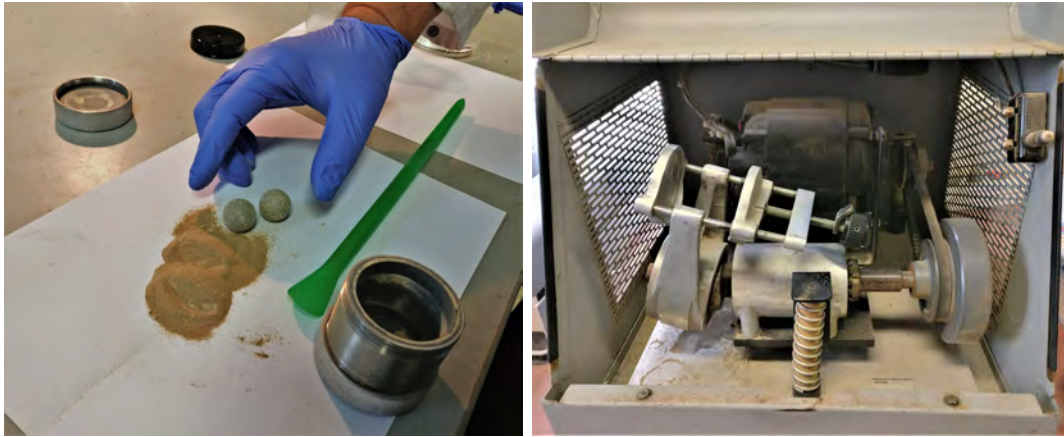
Figure 5.7.: Grinding the monazite sand. The sand is placed in a small can with two grinding balls (left). A machine (right) then shakes and vibrates the can, causing the balls to grind the sand.

container together with the measuring instruments for six hours yielded values for the average thoron activity concentration of $220 \pm 61 \, \text{Bq/m}^3$ and $153 \pm 22 \, \text{Bq/m}^3$ as measured with the AG BEV and Thoron-Scout, respectively. Due to the short half-life of thoron, much of it decays in the pore space of the sand before reaching the surface. Therefore "only a thin layer of the top surface contributes to the thoron exhalation to the environment" (Kanse et al. 2016). This means that not the total amount of monazite sand, but rather its surface area is the important factor which influences the thoron activity concentration reached in the emanation- and calibration container.

In order to increase the thoron exhalation rate, the monazite sand was ground down and placed in water. Figure 5.7 shows the process of grinding the monazite sand. A can containing the sand and two grinding balls is shaken for a few minutes at a high frequency using a motor.

To make the thoron source, 119.45 g of dry, ground-down monazite sand was mixed with 300.23 g of water in a 0.5-l-gas-washing bottle (figure 5.8). A glass fiber filter is installed at the bottom of the gas-washing bottle.

To measure the activity of the thoron source, it was connected directly to the meas-

Figure 5.8.: Photograph of the thoron source.

uring instrument AG BEV. The experimental setup is shown in figure 5.9. The radon/thoron operation mode of the AlphaGUARD has a cycle of 3 min pumping and 7 min resting to differentiate between radon and thoron. The 7 min of resting time correspond to more than seven half-lives of thoron, which is enough to ensure that the thoron source is always in secular equilibrium.
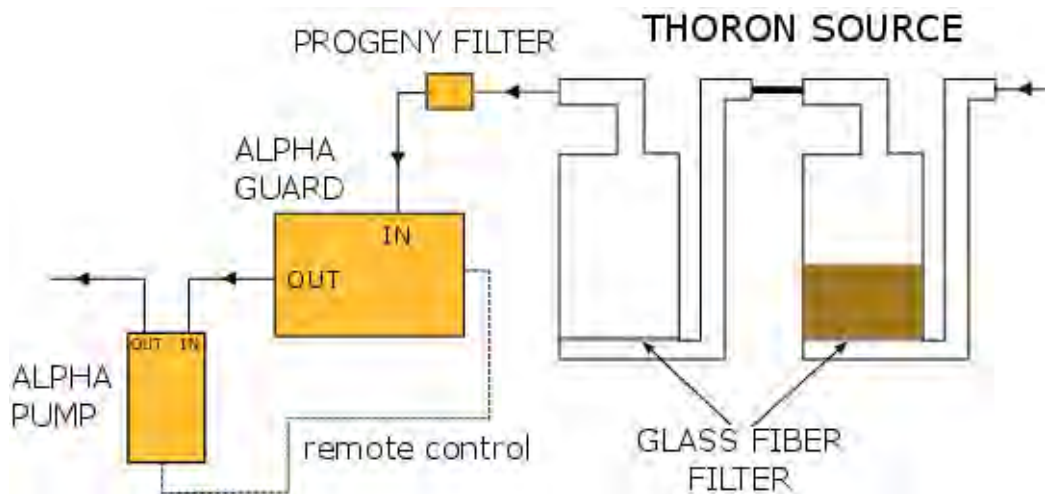
Figure 5.9.: Setup to measure the activity of the thoron source.

The measurement of the thoron source was carried out over two separate days for about six hours each and yielded an average thoron activity concentration of $c_A = 17.2 \pm 0.6 \, \text{kBq/m}^3$.

The thoron source can be used to study the influence of thoron on radon activity concentration measurements in a laboratory setting as well as for the calibration of radon/thoron measuring instruments.

A proposed setup to determine the influence of thoron on radon activity concentration measurements is shown in figure 5.10. First radon is filled into the emanation- and calibration container until the desired activity concentration is reached. A closed circuit is established between the emanation- and calibration container, the thoron source and two AlphaGUARDs. The first AlphaGUARD is in radon/thoron operation mode and controls the pump so that it is on for 3 min and then rests for 7 min. The second AlphaGUARD is in flow mode and only measures the radon activity concentration. A third measuring instrument set to diffusion mode can be placed inside the emanation- and calibration container for additional measurement of the radon activity concentration.
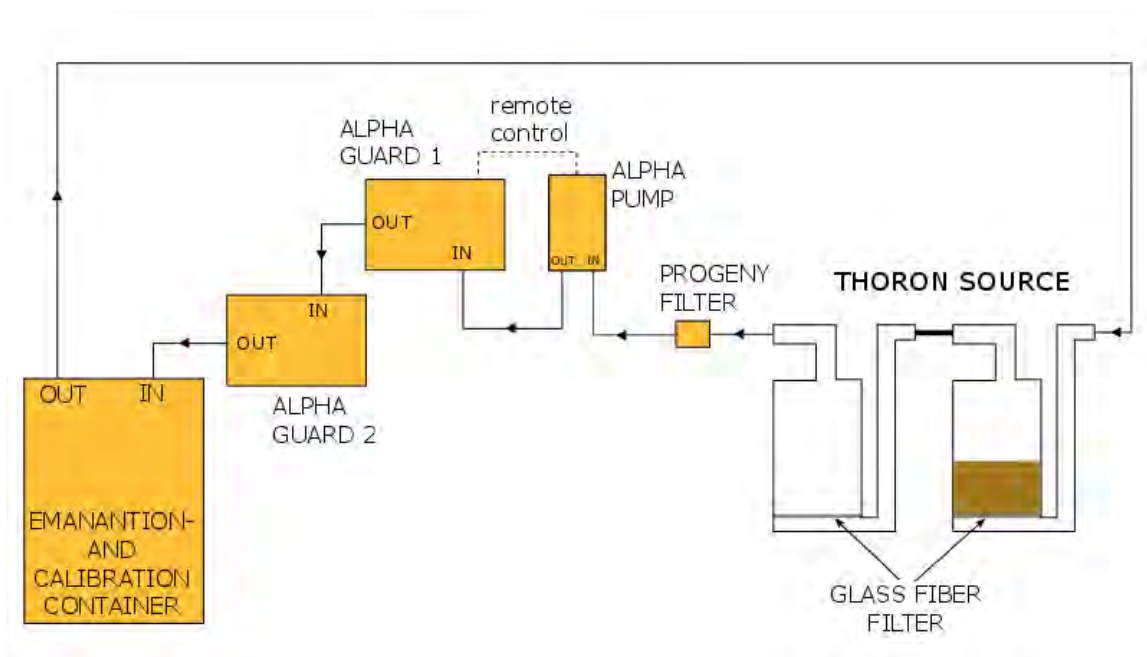
Figure 5.10.: Proposed setup to determine the influence of thoron on radon activity concentration measurements.

A similar setup can be used to calibrate thoron measuring instruments. It is shown in figure 5.11. First radon is filled into the emanation- and calibration container until the desired activity concentration is reached. Two measuring instruments, one to be calibrated and an already calibrated one are connected in parallel to the thoron source. The calibration procedure is then the same as for radon detectors and is described in section 5.5.
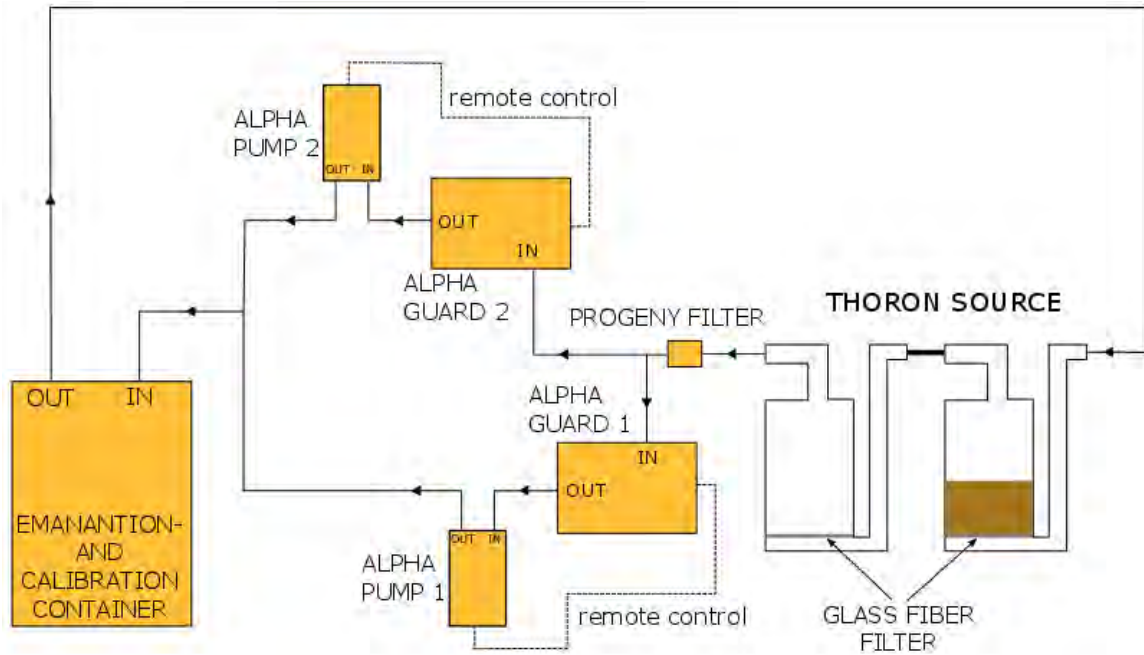
Figure 5.11.: Proposed setup for the calibration of thoron measuring instruments.

5.5. Calibration of measuring instruments

"Calibration is a comparison of measuring equipment against a standard instrument of higher accuracy" (Cable 2005). It is an important part of quality assurance. Calibration of radon measuring instruments in Austria is carried out in the Federal Office of Metrology and Surveying (BEV).

5.5.1. Corentium Pro calibration

Two Corentium Pro detectors were calibrated using the AlphaGUARD AG BEV. Measurements were carried out with all three measuring instruments inside the emanation- and calibration container and the AG BEV in 10-min flow mode. First, the blank values of the measuring instruments were determined. The emanation- and calibration container was filled with fresh air and measurements were carried out for two and a half weeks. Figure 5.12 shows the radon activity concentration in the emanation- and calibration container as measured by the AG BEV. The orange line in the diagram is a regression fit through the data points. The red line represents the exponential decay law (equation 2.4) using the theoretical value for the half-life of radon. The value of A_0 was calculated from the average radon activity concentration over the first 24 hours.

The blank value was calculated by subtracting the average value of the 'red line' from the average measured radon activity concentration over the last three days. This process was applied to all three measuring instruments. The calculated blank values are given in table 5.3. The high uncertainties are due to the high relative uncertainties of radon measurements at such low activity concentrations. The blank values were subtracted from all measurements before the calibration factors were determined.
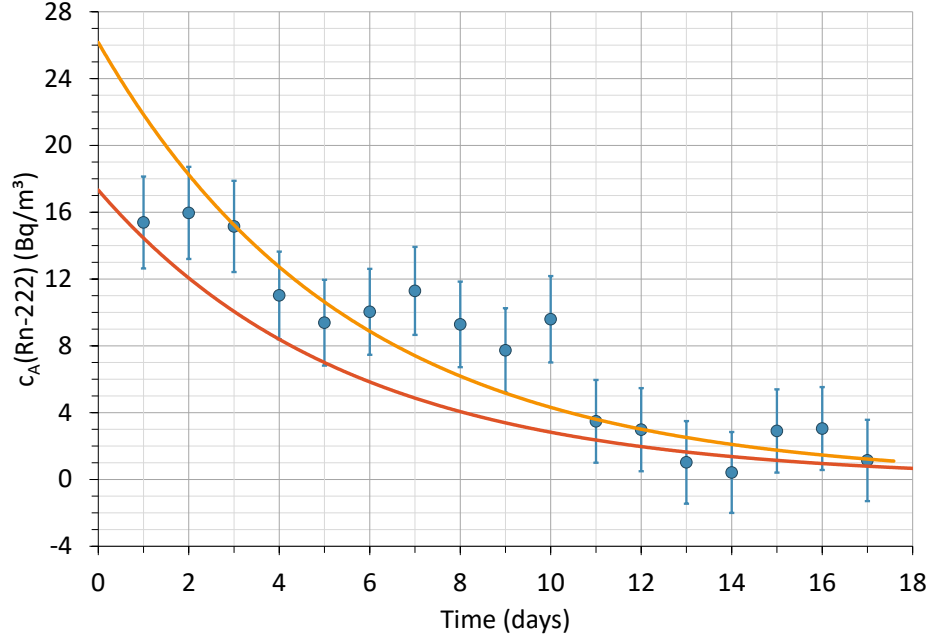
Figure 5.12.: Determination of the blank value of the AG BEV (21/12/2017-08/01/2018). The orange line in the diagram is a regression fit through the data points. The red line represents the exponential decay law using the theoretical value for the half-life of radon. The value of A_0 was calculated from the average radon activity concentration over the first 24 hours.

Calibration factors for the Corentium Pro radon detectors were calculated at radon activity concentrations of around $100\,\mathrm{Bq/m^3}$, $500\,\mathrm{Bq/m^3}$ and $3000\,\mathrm{Bq/m^3}$. This was done by calculating the mean radon activity concentration measured by the AG BEV over 24 hours and comparing this value to the mean radon concentration measured by the Corentium Pro detectors during the same time period.

$$k_f = \frac{k_f^{\mathrm{AGBEV}} c_A(\mathrm{Rn\text{-}222})_{\mathrm{AGBEV}}}{c_A(\mathrm{Rn\text{-}222})_{\mathrm{CorentiumPro}}} \tag{5.1}$$

k_f ... Calibration factor

k_f^{AGBEV} ... Calibration factor of the AG BEV (from previous calibration)

$c_A(\mathrm{Rn\text{-}222})$ ... Mean radon activity concentration over 24 hours $(\mathrm{Bq/m^3})$.

56

Measuring instrument	Blank value (Bq/m^3)
AG BEV	0.7 ± 1.4
Corentium Pro 1	3.4 ± 4.8
Corentium Pro 2	2.1 ± 4.3

Table 5.3.: Blank values of radon measuring instruments.

The calculated calibration factors for the Corentium Pro 1 and 2 are given in tables 5.4 and 5.5, respectively. The uncertainties are calculated by the propagation of the uncertainties given by the measuring instruments.

c_A(**Rn-222**)$_{\mathbf{AGBEV}}$ (Bq/m^3)	c_A(**Rn-222**)$_{\mathbf{CorentiumPro}}$ (Bq/m^3)	Calibration factor k_f	Percentage uncertainty ($k = 2$)
100 ± 6	106 ± 14	0.94	29.3 %
513 ± 13	496 ± 29	1.03	12.7 %
3088 ± 67	3183 ± 84	0.97	6.8 %

Table 5.4.: Calibration factors of the Corentium Pro 1.

c_A(**Rn-222**)$_{\mathbf{AGBEV}}$ (Bq/m^3)	c_A(**Rn-222**)$_{\mathbf{CorentiumPro}}$ (Bq/m^3)	Calibration factor k_f	Percentage uncertainty ($k = 2$)
100 ± 6	102 ± 14	0.97	29.4 %
513 ± 13	491 ± 29	1.05	12.8 %
3088 ± 67	3332 ± 87	0.93	6.8 %

Table 5.5.: Calibration factors of the Corentium Pro 2.

5.5.2. Comparison of AlphaGUARDs for in-situ measurements

As part of the quality assurance of the in-situ soil gas measurements (chapter 6), a comparison of the measuring instruments was carried out beforehand. All four AlphaGUARDs (AG BEV, AG 2, AG 6, AG8) were placed in the emanation- and calibration container and set to 60 min diffusion mode. Measurements were carried out for almost two weeks at an initial radon activity concentration of about $22\,\mathrm{kBq/m^3}$. The deviation of radon activity concentration measurements of measuring instrument X (AG 2, AG 6 and AG 8) from the AG BEV were calculated as follows:

$$c_A(\text{Rn-222}) \text{ deviation} = \frac{c_A(\text{Rn-222})_X - c_A(\text{Rn-222})_{BEV}}{c_A(\text{Rn-222})_{BEV}} \tag{5.2}$$

Figure 5.13 shows the results of comparing the individual radon activity concentration measurements of the AG BEV to the other AlphaGUARDs.

The average uncertainty of individual radon activity concentration values over the measurement period is $5.5\,\%$ for the AG BEV, $7.8\,\%$ for the AG 2, $7.5\,\%$ for the AG 6 and $7.4\,\%$ for the AG 8. This means that the deviations between the different AlphaGUARDs are within the measurement uncertainties and therefore no adjustments are necessary.
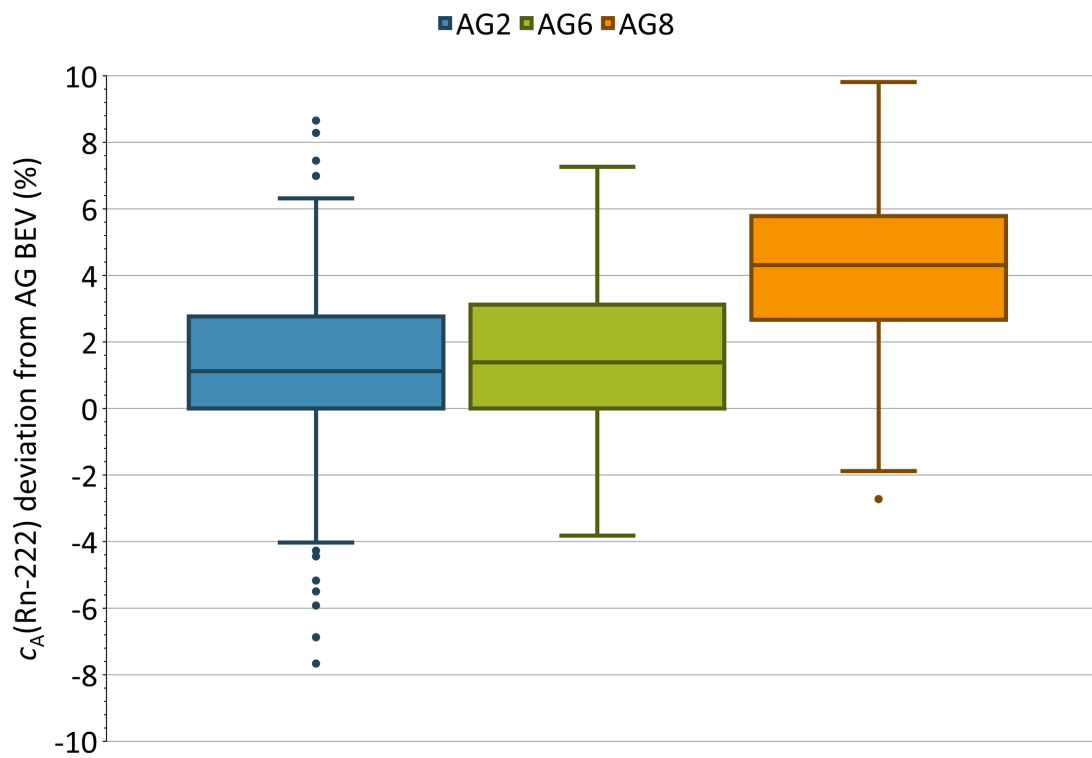
Figure 5.13.: Box plot diagram of the deviation in radon activity concentration between different AlphaGUARDs in diffusion mode.

6. Soil gas measurements in Lower and Upper Austria

The Waldviertel in Lower Austria and the Mühlviertel in Upper Austria are part of a geological zone called the Granite and Gneiss Plateau situated in the north of Austria. Due to the abundance of granite, the ground in this area has a high uranium content compared to other geological zones. Measurements of the activity concentrations of radon and thoron in soil gas were taken at eight different locations within this region. The measuring instruments used are described in section 5.1. One of the main goals of these measurements was to determine the influence of the presence of thoron on the measured values of the radon activity concentration. They were therefore taken at locations in which the soil gas was assumed to have high thoron activity concentrations based on a map of thorium concentration from the Geological Survey of Austria (figure 6.1).

Table 6.1 shows the GPS coordinates of the locations at which the soil air measurements were taken and figure 6.2 shows these locations on a map.
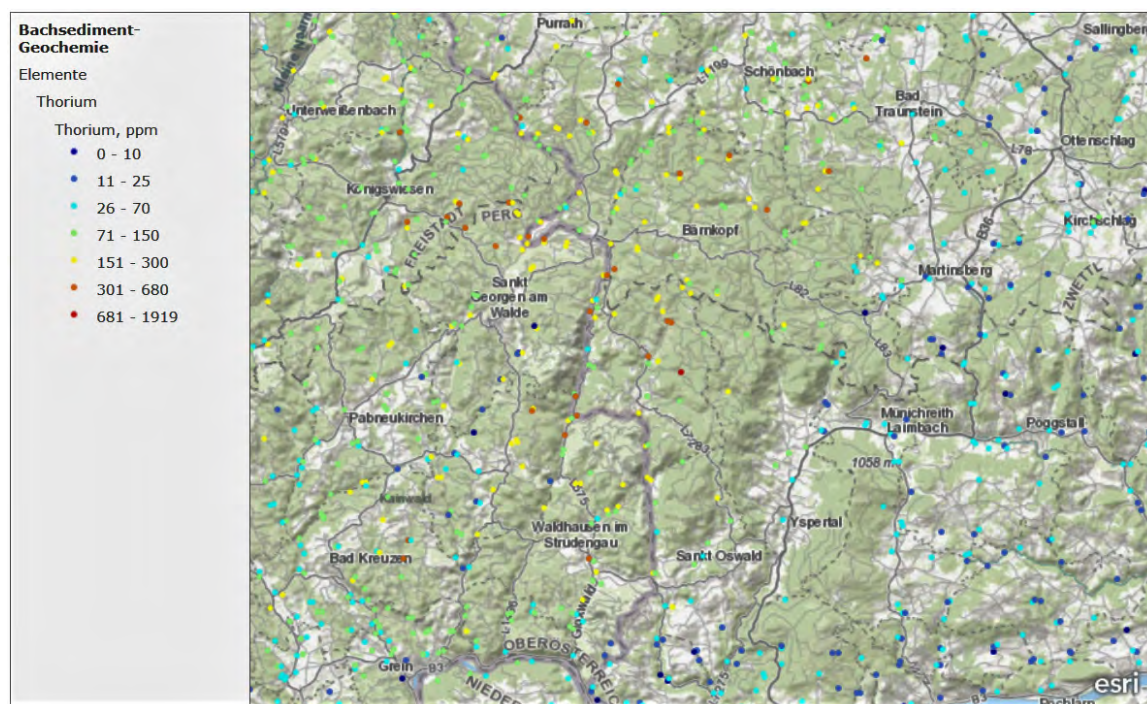
Figure 6.1.: Map of thorium concentration in the ground around Bärnkopf (Lipiarski 2017).

	Location name	Date	GPS coordinates
1	Dorfstetten Teich	25.07.2017	48°19'55.5"N 14°59'04.7"E
2	Dorfstetten Wald	25.07.2017	48°20'33.2"N 15°00'19.1"E
3	Dorfstetten Wiese	27.07.2017	48°21'07.9"N 14°57'57.4"E
4	Dorfstetten Nord	06.09.2017	48°20'45.8"N 14°59'30.6"E
5	Dürnberg See	05.09.2017	48°24'57.4"N 14°59'38.4"E
6	Reitern	05.09.2017	48°26'17.8"N 15°01'04.4"E
7	Poggschlag	07.09.2017	48°21'24.6"N 15°08'04.0"E
8	Hörzenschlag	07.09.2017	48°25'46.6"N 14°52'58.3"E

Table 6.1.: GPS coordinates of the locations at which the soil gas measurements were taken.
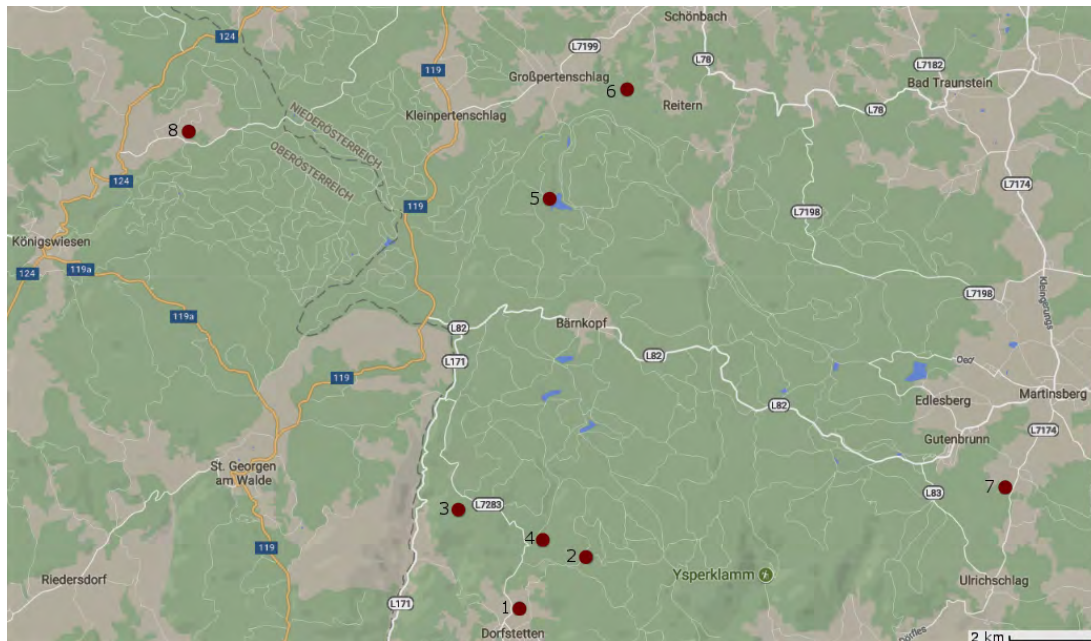
Figure 6.2.: Map showing the locations of the soil gas measurements (GoogleMaps 2017).

6.1. Measurement techniques

6.1.1. Radon and thoron activity concentration in soil gas

To measure the activity concentration of radon and thoron in soil gas, a steel probe of 1.2 m or 1.6 m length and 12 mm diameter is used. A metal tip is placed at the bottom of the probe, which is then hammered into the ground to the desired depth. A thin metal rod inserted into the probe is then used to hammer the tip 5 cm further into the ground. This allows the soil air to be drawn in from the top of the probe using either a syringe or a pump. A flexible rubber tube is mounted on the top of the probe in order to connect the syringe or pump to the probe. Before any measurements are made, a volume of 150 ml of soil gas is drawn in from the probe using a syringe and discarded. The probe is then sealed with a plug. This is done to avoid the mixing of the surrounding air with the soil gas in the probe.

Figure 6.3.: Taking a soil gas sample using a syringe.

The soil gas measurements in July 2017 (locations 1-3) were conducted by taking a volume of 100 ml of soil gas from the probe using a syringe (see figure 6.3) and inserting it into an AlphaGUARD. For this measurement technique, the AlphaGUARD is set to 10 min flow mode and its openings are closed after inserting the soil gas into the chamber. Since the AlphaGUARD has an active detector volume 0.56 l, but only 100 ml of soil gas are inserted into it, the displayed value is lower than the actual radon activity concentration in the soil gas sample. It therefore has to be multiplied by a previously determined calibration factor. The calibration factor is calculated by inserting 100 ml of gas with a known radon activity concentration into the AlphaGUARD and dividing the known radon activity concentration by the displayed value. The calibration factor for the AG BEV is 8.07 ± 0.01 (Gruber 2004). For the other AlphaGUARDs it is assumed to be $8 \pm 10\%$. At least four measurements are taken - the first one is discarded and the rest are used to calculate a mean value. This eliminates the effect of thoron on the radon measurement, as it will have decayed almost completely after the first 10 min measurement due to its short half-life of 55.6 s. However, this also means that this method can only be used to measure

64

the radon activity concentration and is not suitable to determine the thoron activity concentration.

To simultaneously measure the activity concentrations of radon and thoron in soil gas, the setup shown in figures 6.4 and 6.5 was used. Two AlphaPumps connected in series and set to 1 l/min suck air from the soil and blow it into the AlphaGUARDs. The first AlphaGUARD is set to 1 l RnTn mode and controls the AlphaPumps via a remote control cable. This means that the cycle consists of 3 min pumping followed by 7 min resting. The second AlphaGUARD is set to 10 min flow mode. AlphaG-UARD 1 measures the activity concentrations of both radon and thoron, whereas AlphaGUARD 2 only measures the radon activity concentration.

Figure 6.4.: Photograph of the setup to measure the activity concentration of radon and thoron in soil gas.

By comparing the measurements of these two AlphaGUARDs, it is possible to determine the influence of thoron on the radon measurement. This measurement technique was used for the soil gas measurements in September 2017 (locations 4-8). Measurements were taken for at least 40 min and one measurement was taken over night.
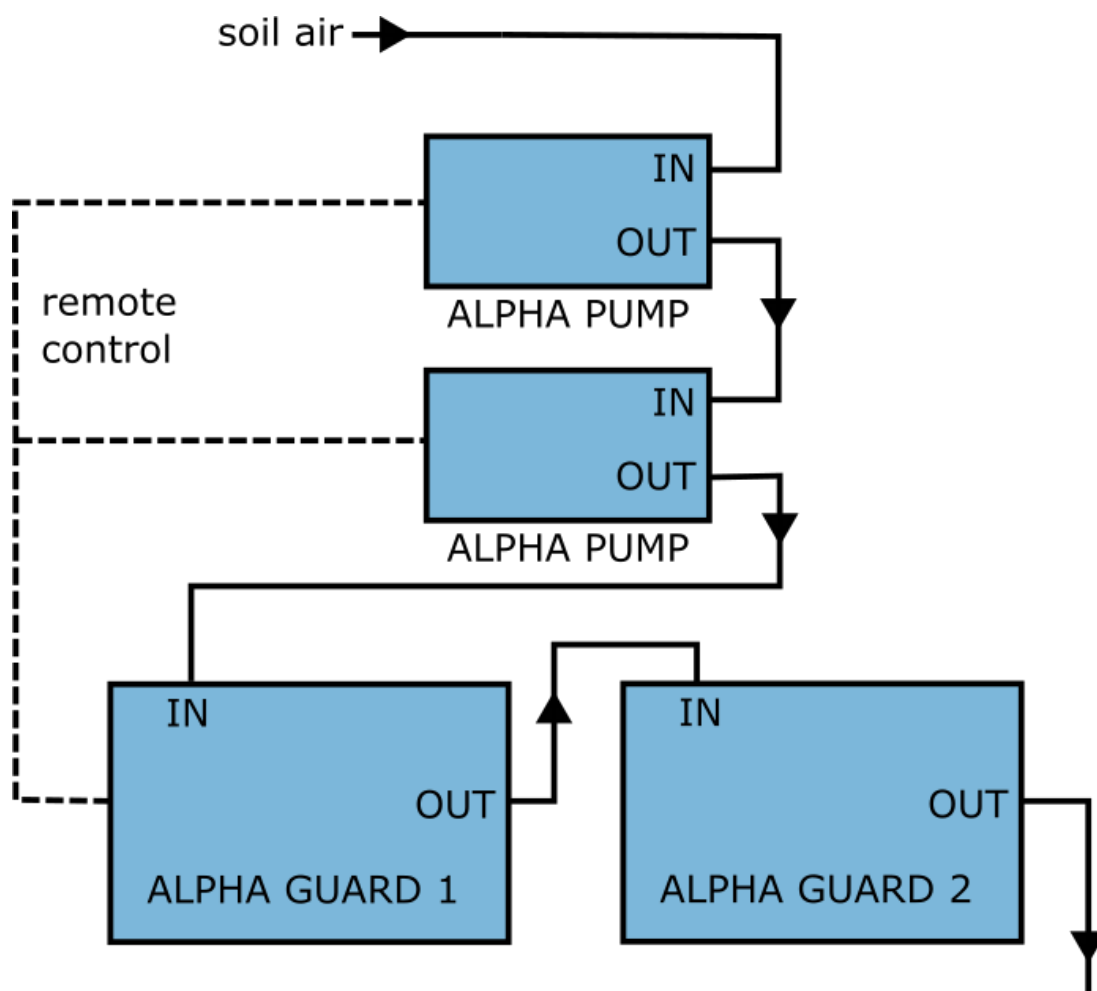
Figure 6.5.: Setup to measure the activity concentration of radon and thoron in soil gas. AlphaGUARD 1 is running in 1 L RnTn mode and controls the pumps, while AlphaGUARD 2 is running in 10 min flow mode. The pumps are set to 1 l/min.

6.1.2. Soil permeability

Permeability refers to the ability of the soil to allow fluids and gases to pass through it. Figures 6.6 and 6.7 show the setup used to measure the soil permeability. An AlphaPump set to 1 l/min sucks in soil gas through the probe. A manometer and a flowmeter are connected to measure the pressure and flow rate of the soil gas. The permeability of the soil can then be calculated using the following formula (Damkjaer and Korsbech 1992).

$$Q = \frac{Fkp}{\mu} \qquad (6.1)$$

Q ... Flow rate $(\mathrm{m^3/s})$

k ... Permeability $(\mathrm{m^2})$

p ... Pressure (Pa)

μ ... Viscosity of air $(1.75 \times 10^{-5}\,\mathrm{Pa\,s})$

F ... Form factor (m)

$$F = \frac{2\pi l}{\ln\left(\frac{2l}{d}\sqrt{\frac{4D-l}{4D+l}}\right)} \qquad (6.2)$$

l ... Length of the effective probe volume (m)

d ... Diameter of the effective probe volume (m)

D ... Lower depth of the effective probe volume underneath the surface (m)

For typical values of $l = 5\,\mathrm{cm}$, $d = 12\,\mathrm{mm}$ and $D = 1.05\,\mathrm{m}$, the value of the form factor is $F = 0.1490\,\mathrm{m}$.

Figure 6.6.: Photograph of the setup to measure the soil permeability.
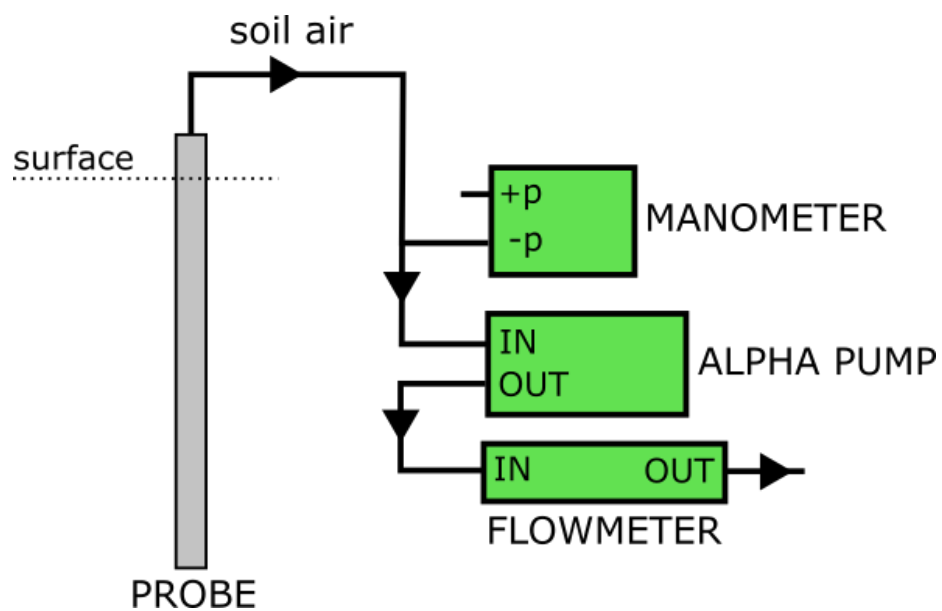
Figure 6.7.: Setup to measure the soil permeability. The AlphaPump is set to 1 l/min.

6.1.3. Gamma spectrometry of soil samples

At each measurement location soil samples were taken to determine the concentration of some of the radionuclides via low-level gamma spectrometry. The samples were weighed before and after drying at $80\,°C$ for a few days in order to determine their humidity. They were then filled into suitable air-tight containers of $11\,mm$ height and $64\,mm$ diameter, as shown in figure 6.8.
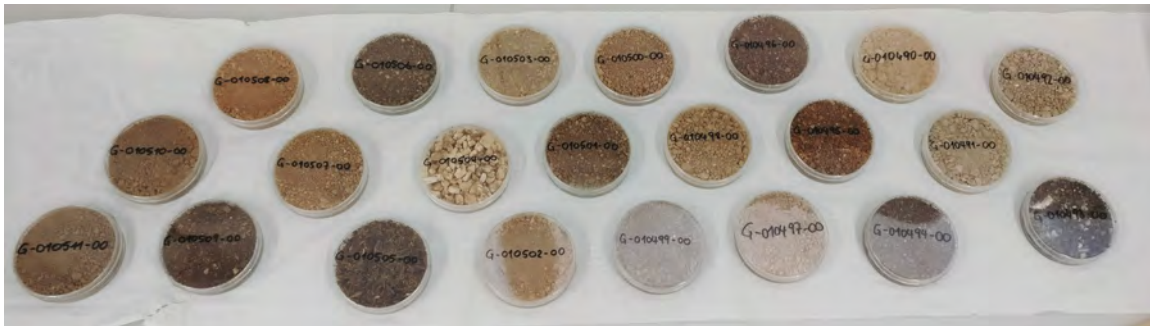
Figure 6.8.: Soil samples for gamma spectrometry.

A waiting period of at least three weeks before starting the measurement ensures that the Ra-226 in the samples is in secular equilibrium with its daughter nuclides. This is done so that the γ-lines of Pb-214 and Bi-214 can be used for the measurement of the Ra-226 activity concentration. The activity concentrations of Ra-228 and Th-228 in the soil samples are determined by the γ-lines of Ac-228 and Bi-212, respectively.

The gamma spectrometry measurements were carried out in cooperation with Dr. Michael Stietka at the University of Natural Resources and Life Sciences (BOKU) using the P-type high purity germanium semiconductor detector shown in figure 6.9. It is cooled with liquid nitrogen and makes use of a fully automated sample changer. The measurement time for each sample was between one and one and a half days.

Figure 6.9.: Photograph of the gamma spectrometry setup.

6.2. Measurement setup

At each location two to four probes were set up at a distance of 1–3 m from each other. Figure 6.10 illustrates a possible arrangement of the probes.
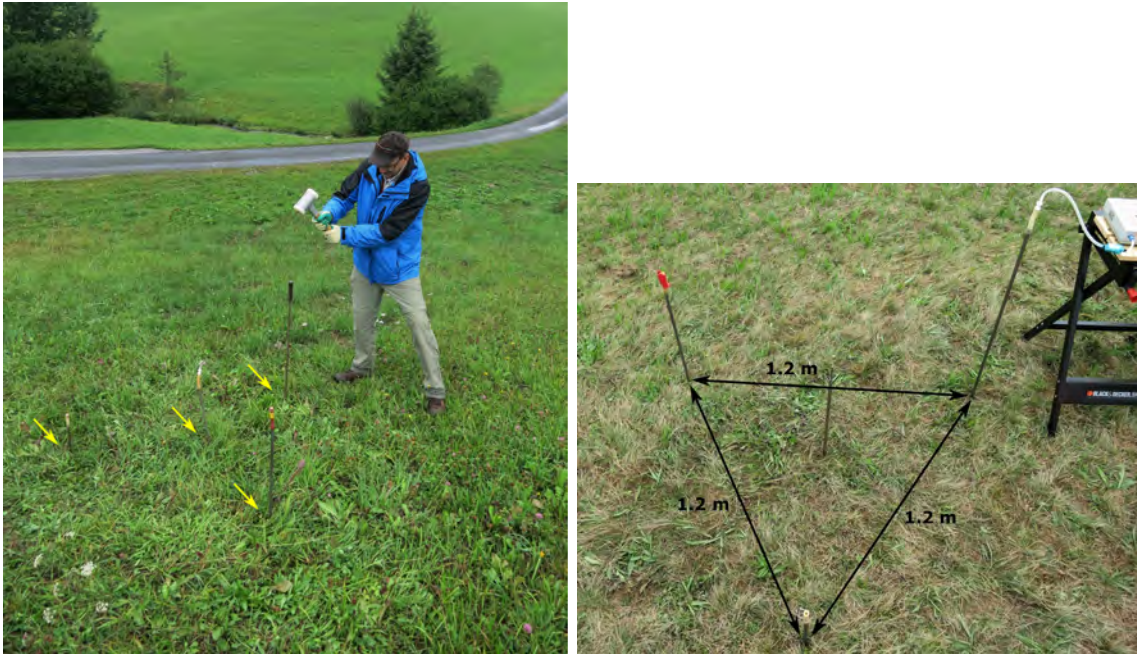
Figure 6.10.: Possible arrangement of soil gas probes. Three probes are set up in a triangle with a fourth probe in the center.

The soil samples for gamma spectrometry measurements were taken between or near the probes. At least two soil samples were taken at each location, one close to the surface (0–10 cm below the surface) and one deeper underground (30–50 cm below the surface).

Additionally, the dose rate was calculated at each location. The measuring instrument was placed on the workbench (at a height of approximately 80 cm) close to the probes and the measurement was carried out over a time period of about an hour. Two different measuring instruments[1] were used for the measurements in July 2017

---

[1]July: UMo Universeller Monitor für Strahlenschutz, EG&G Berthold. Type LB1236, SNr. 1513. September: NBR-Detector FHZ672E, ESM Eberline. Z.-Nr. 42540/61, F.-Nr. 0137.

and September 2017, but in both cases the measured quantity was the photon dose equivalent rate H_x.

Figure 6.11 shows the setup at a typical measurement location. The blue instrument on the workbench measures the gamma dose rate. The AlphaGUARDs are set up to measure the radon and thoron activity concentrations of the soil gas.

Figure 6.11.: Photograph of a measurement location (Dürnberg, Lower Austria. 05/09/2017).

6.3. Results

6.3.1. Soil gas measurements

The radon activity concentrations measured from individual soil gas probes lie between 22 kBq/m^3 and 246 kBq/m^3. Thoron activity concentrations lie between 44 kBq/m^3 and 310 kBq/m^3. Figure 6.12 shows the average radon and thoron activity concentrations at each of the measurement locations. The radon activity concentrations have been corrected to a depth of 1 m.

Figure 6.12.: Map of average radon and thoron activity concentrations (25/07/2017-07/09/2017). The radon activity concentrations have been corrected to a depth of 1 m.

The high uncertainty in the radon activity concentration at location 1 is due to the high variance in the activity concentrations obtained by the individual soil gas probes.

Figure 6.13.: Radon and thoron activity concentrations over time (Hörzenschlag, 07/09/2017-08/09/2017). Measuring instrument: AG BEV.
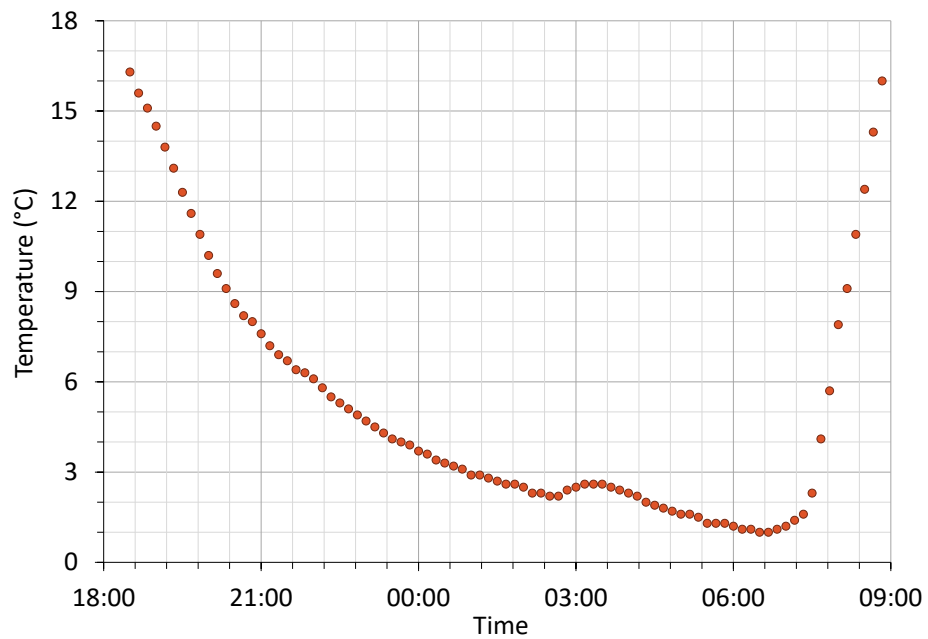
Figure 6.14.: Ambient air temperature over time (Hörzenschlag, 07/09/2017-08/09/2017). Measuring instrument: AG BEV.

Figure 6.13 shows the activity concentrations of radon and thoron in soil gas over one night (Hörzenschlag, 07/09/2017-08/09/2017). While the radon activity concentration clearly increases with time, the thoron activity concentration does not show such a trend. Figure 6.14 shows the ambient air temperature over the same time period (Hörzenschlag, 07/09/2017-08/09/2017).

Figure 6.15 clearly shows an inverse relationship between the radon activity concentration and the ambient air temperature. However, no such correlation was found between the temperature and the thoron activity concentration.
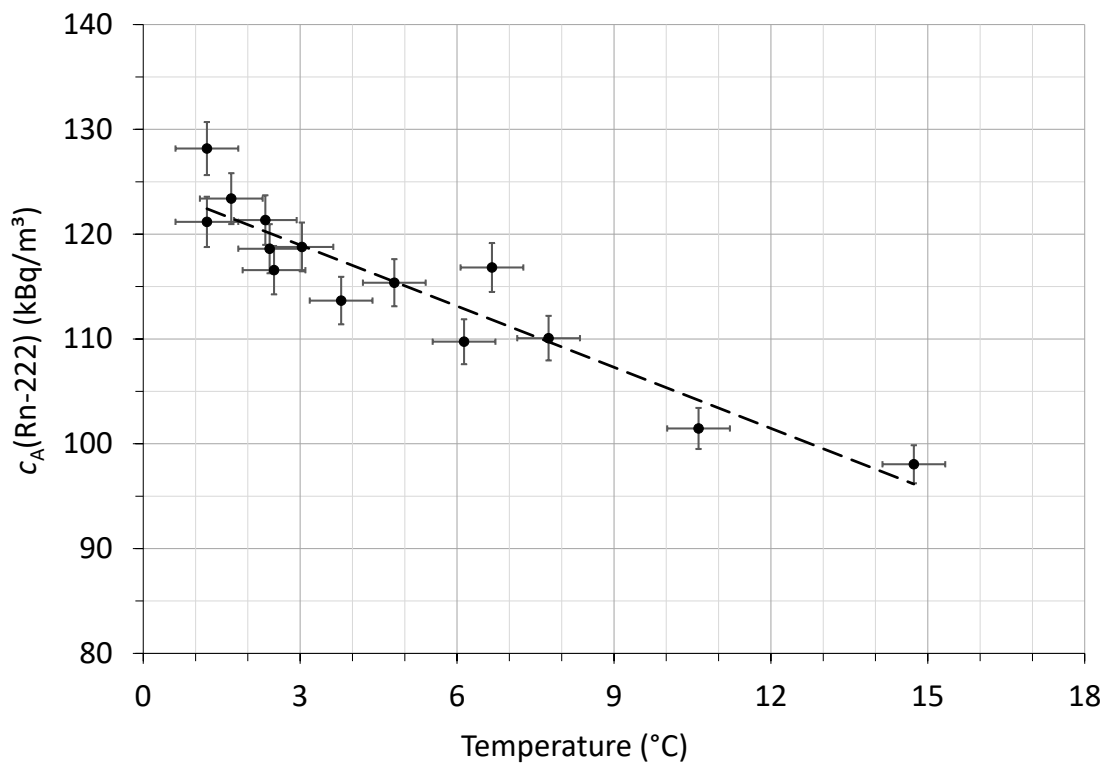
Figure 6.15.: Relationship between radon activity concentration and ambient temperature (Hörzenschlag, 07/09/2017-08/09/2017). Measuring instrument: AG BEV.

6.3.2. Radon potential

The maximum radon activity concentration and the average permeability were used to determine the radon potential at each measurement location according to the classification matrix introduced by Kemski, Siehl et al. (see chapter 4.5). The results are shown in table 6.2.

Location (see table 6.1)	Rn-222		Average Permeability (m^2)	Radon potential
	Activity concentration (max.)	Uncertainty		
	kBq/m^3			
1	246	63	2E-10	5
2	116	27	1E-09	5
3	126	17	7E-10	5
5	92	7	2E-10	4
6	58	2	2E-09	4
4	61	1	7E-10	4
8	108	14	1E-09	5
7	62	1	1E-09	4

Table 6.2.: Radon potential according to Kemski, Siehl et al. (25/07/2017-07/09/2017).

The geogenic radon potential can be a good indicator of possible indoor radon activity concentrations (Chen and Ford 2017). However, the actual indoor radon activity concentrations depend not only on the availability of radon in the soil, but also on the construction and usage of the individual buildings. In areas of high radon potential, indoor measurements are recommended in existing homes to assess the radon exposure of the inhabitants. Furthermore, protective measures against radon should be installed when building new homes in order to prevent the radon activity concentration exceeding the reference levels.

6.3.3. Radionuclides in the soil

Table 6.3 shows the activity concentrations of Ra-226, Th-228, U-238 and K-40 in the soil samples measured by low-level gamma spectrometry. The high levels of thorium are typical for the geology of the area.

Location (see table 6.1)	Mean depth (cm)	Ra-226		Th-228		U-238		K-40	
		Activity conc. (mean)	Uncertainty	Activity conc. (mean)	Uncertainty	Activity conc. (mean)	Uncertainty	Activity conc. (mean)	Uncertainty
		Bq/kg		Bq/kg		Bq/kg		Bq/kg	
1	45	61.8	1.8	203	8	71.6	3.7	1122	34
2	29	52.6	1.6	125	4	69.5	3.6	1022	31
3	16	54.0	2.3	233	15	49.4	2.5	961	29
5	20	44.7	1.9	176	7	47.2	2.4	966	29
6	60	65.2	2.8	183	7	51.5	2.6	942	28
4	28	42.7	1.8	133	5	54.7	2.7	945	29
8	25	80.2	3.4	153	6	53.1	2.6	964	29
7	25	56.7	2.2	59	2	51.4	2.6	1029	31

Table 6.3.: Activity concentrations of Ra-226, Th-228, U-238 and K-40 in the soil samples (25/07/2017-07/09/2017).

Figure 6.16 shows the relationship between the average Ra-226 activity concentration in the soil and the average radon activity concentration in the soil gas at the different measurement locations. High radium activity concentrations in the soil should lead to high radon activity concentrations in soil gas. The reason for the low correlation is that in addition to the Ra-226 activity concentration, the radon activity concentration in soil gas depends on many other geological and meteorological factors, such as the radon emanation coefficient, the density, porosity and moisture of the soil, as well as temperature, air pressure and wind (Gruber 2004). Furthermore, the variation of the Ra-226 activity concentrations at the measured locations is quite low, increasing the importance of the other factors mentioned previously. Figure 6.17 shows the relationship between the average Th-228 activity concentration in the soil and the average thoron concentration in the soil gas at the different measurement locations.

Figure 6.16.: Relationship between Ra-226 activity concentration and Rn-222 activity concentration (25/07/2017-07/09/2017). The Rn-222 activity concentrations have been corrected to a depth of 1 m. The data point labels indicate the measurement locations (see table 6.1).

Figure 6.17.: Relationship between Th-228 activity concentration and Rn-220 activity concentration (05/09/2017-07/09/2017). The data point labels indicate the measurement locations (see table 6.1).

6.3.4. Dose rate measurements

The detected gamma dose rates lie between $81\,\mathrm{nSv/h}$ and $225\,\mathrm{nSv/h}$. Figure 6.18 shows the relationship between the radon activity concentration in soil gas and the gamma dose rate. The gamma activity of radon progeny in the ground contributes to the dose rate above ground, which is why the dose rate increases with increased radon activity concentration. Information about the correlation between these two quantities is very useful, as gamma dose rate measurements are faster and easier to carry out than soil gas measurements. Dose rate measurements could therefore be used as an alternative way to examine the radon characteristics of an area (Smetsers and Blaauboer 1994).
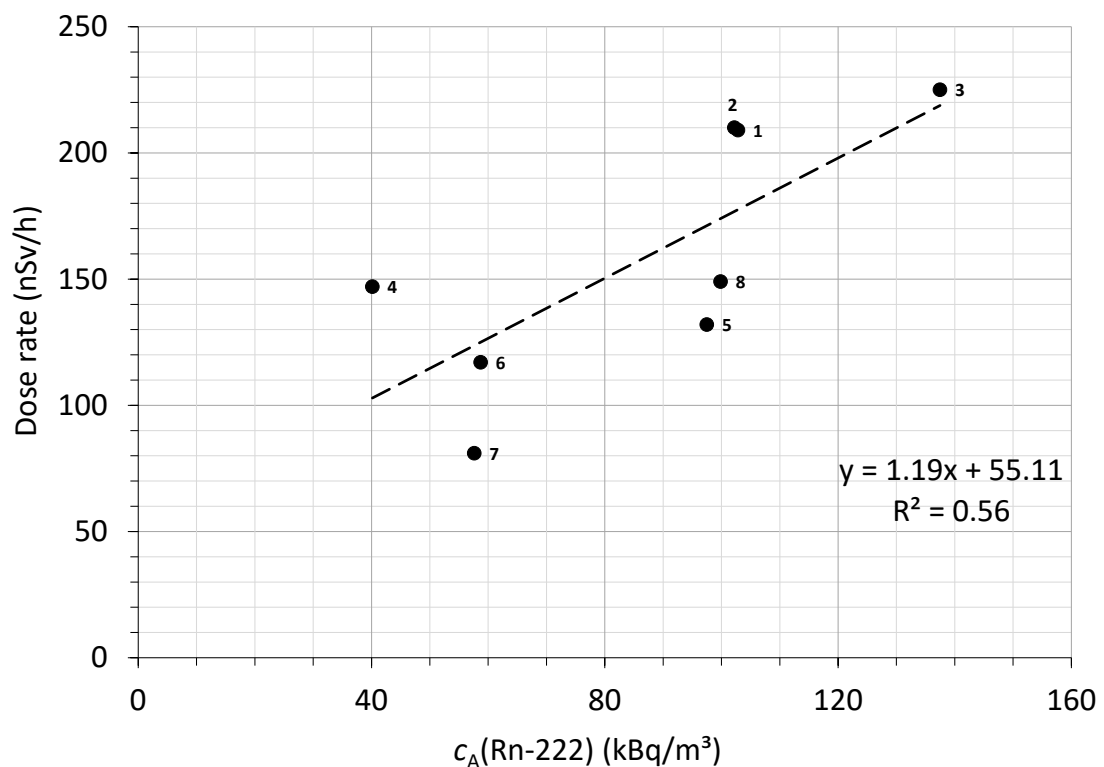
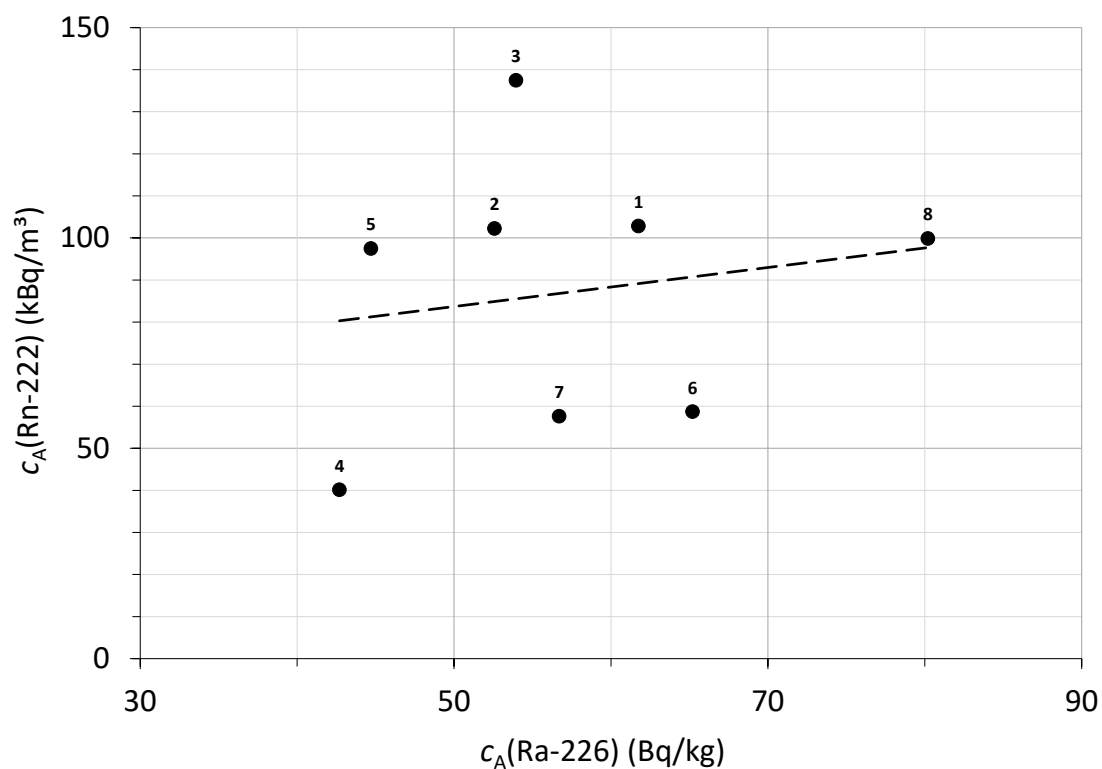**Figure 6.18.:** Relationship between Rn-222 activity concentration and gamma dose rate (25/07/2017-07/09/2017). The Rn-222 activity concentrations have been corrected to a depth of $1\,\mathrm{m}$. The data point labels indicate the measurement locations (see table 6.1).
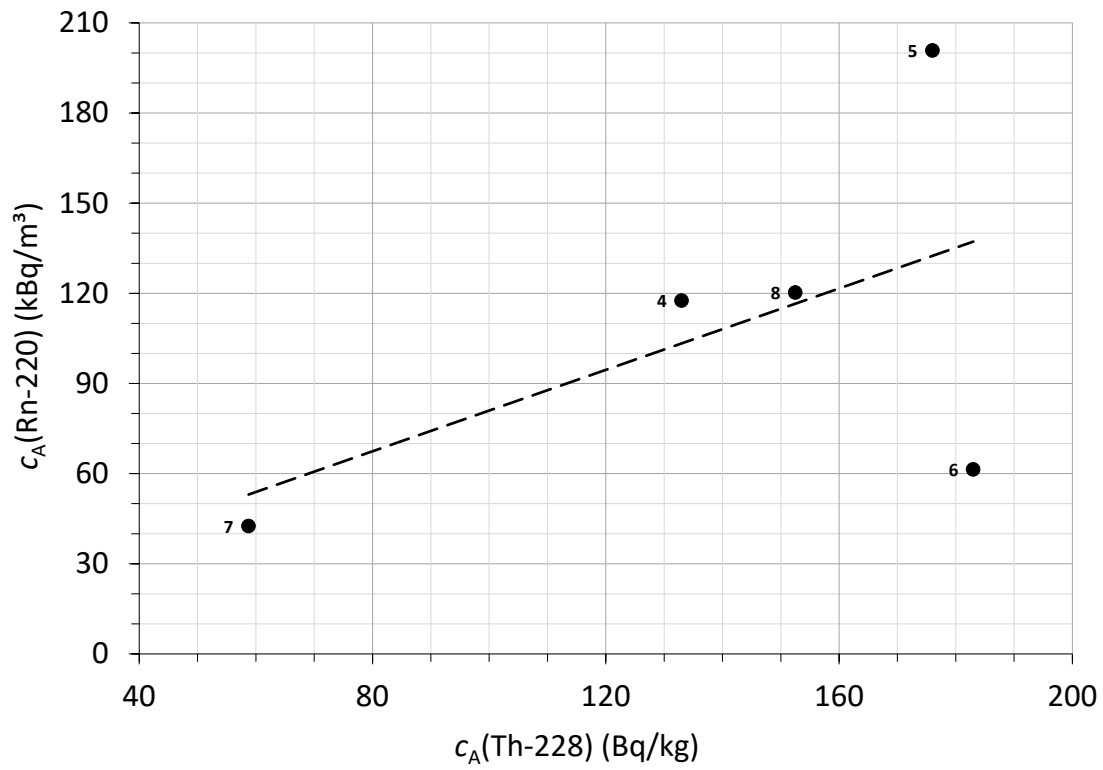
80
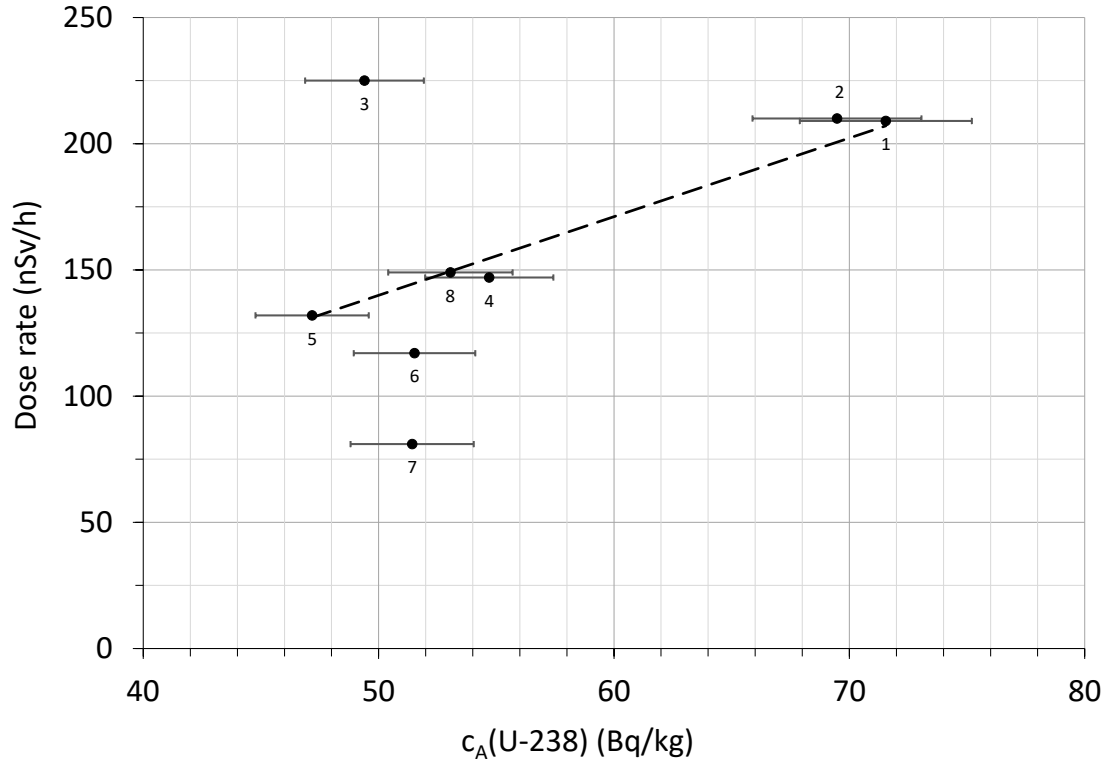
Figure 6.19.: Relationship between U-238 activity concentration and gamma dose rate (25/07/2017-07/09/2017). The data point labels indicate the measurement locations (see table 6.1).

Figure 6.19 shows the relationship between U-238 activity concentration and gamma dose rate. The weak correlation is due to the fact that the gamma dose rate depends on activity concentrations of radionuclides in the uranium series and the thorium series, as well as K-40 (Baumgartner et al. n.d.). Additionally, there is also a contribution from cosmic radiation.

The contribution from potassium, uranium and thorium in the ground to the gamma dose rate E 1 m above the ground can be estimated by equation 6.3 (Grasty et al. 1984).

$$E(\text{nSv/h}) = 14.04\text{K}(\%) + 5.83\text{U}(\text{ppm}) + 2.89\text{Th}(\text{ppm}) \tag{6.3}$$
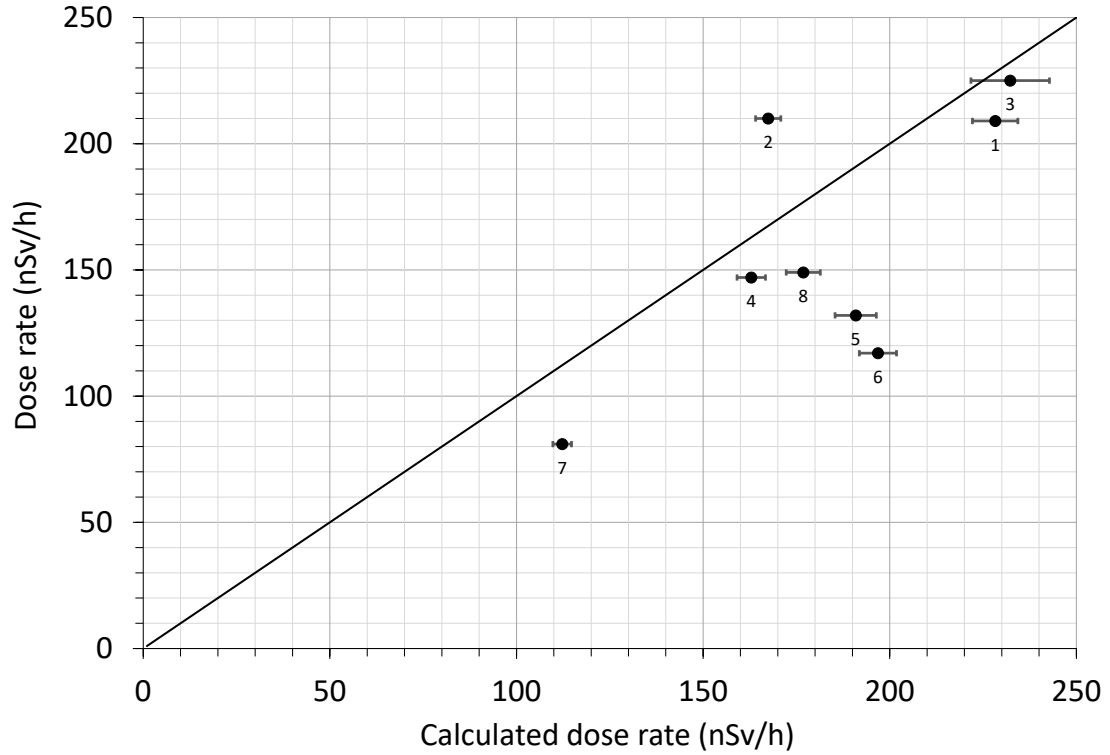
Figure 6.20.: Relationship between calculated dose rate and measured gamma dose rate (25/07/2017-07/09/2017). The solid line represents where the measured dose rate is equal to the calculated dose rate. The data point labels indicate the measurement locations (see table 6.1).

Figure 6.20 shows the measured gamma dose rates plotted against the values of the gamma dose rates calculated using equation 6.3. All but one of the measured dose rates are smaller than the calculated values. This is because the concentrations of uranium, thorium and potassium were determined from dried soil samples, while the dose rate was measured over soils with a certain water content. The gamma dose rate decreases with an increased soil moisture content due to the attenuation of gamma radiation by Compton scattering in water (Grasty et al. 1984). Nevertheless, equation 6.3 provides a reasonable estimate of the gamma dose rate based on the concentrations of potassium, uranium and thorium in the soil.

82

6.3.5. The influence of thoron on radon measurements

The radon activity concentrations measured by AlphaGUARDs in flow mode were up to 38 % higher than those measured by the AlphaGUARDs in radon/thoron mode. Figure 6.21 shows the deviation of the measured radon activity concentration by instruments in flow mode from instruments in radon/thoron mode plotted against the ratio of thoron activity concentration to radon activity concentration.

Figure 6.21.: The deviation of the measured radon activity concentration by instruments in flow mode from instruments in radon/thoron mode plotted against the ratio of thoron activity concentration to radon activity concentration (05/09/2017-07/09/2017).

The radon deviation is calculated as follows,

$$c_A(\text{Rn-222}) \text{ deviation } (\%) = 100\,\% \cdot \frac{c_A^*(\text{Rn-222}) - c_A(\text{Rn-222})}{c_A(\text{Rn-222})} \tag{6.4}$$
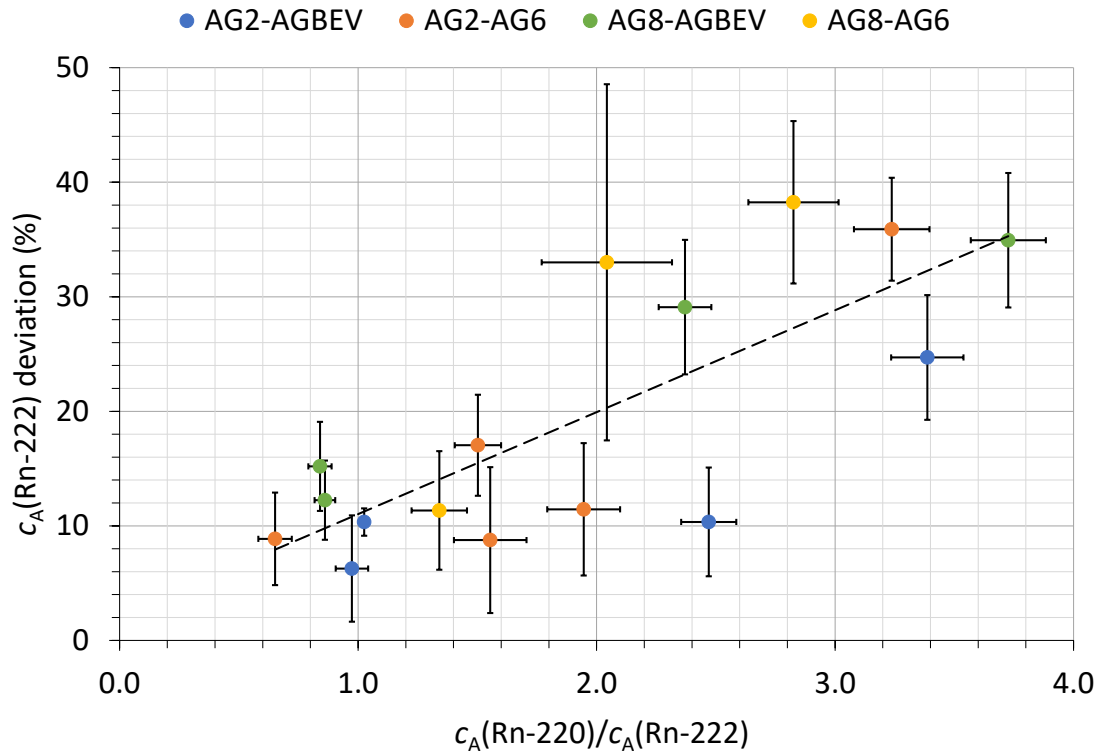
where $c_A^*(\text{Rn-222})$ is the radon activity concentration measured by the AlphaGUARD in flow mode and $c_A(\text{Rn-222})$ is the radon activity concentration measured by the AlphaGUARD in radon/thoron mode.

The deviation in radon activity concentration between the two modes of measurement increases with the ratio of thoron to radon activity concentration. This shows that the presence of thoron in soil gas affects the measurement of the radon activity concentration by AlphaGUARDs in flow mode. A possible explanation for the effect of thoron on the radon activity concentration measurement is that the measuring instrument counts some of the decays of thoron and its progeny as radon. The radon activity concentration by AlphaGUARDs in flow mode would therefore be given by

$$c_A^*(\text{Rn-222}) = c_A(\text{Rn-222}) + \alpha c_A(\text{Rn-220}) \tag{6.5}$$

where α is the fraction of thoron that the measuring instrument counts as radon. Figure 6.22 shows the difference of the measured radon activity concentration between instruments in flow mode and instruments in radon/thoron mode plotted against the thoron activity concentration. The linear fit through the data gives a value of $\alpha = 0.1$. This means that on average, $10\,\%$ of the thoron activity concentration in the soil gas is counted by the AlphaGUARD in flow mode as radon activity concentration.

Figures 6.23 and 6.24 show the same graphs using data from measurements taken over one night (07/09/2017-08/09/2017) at location 8.

84
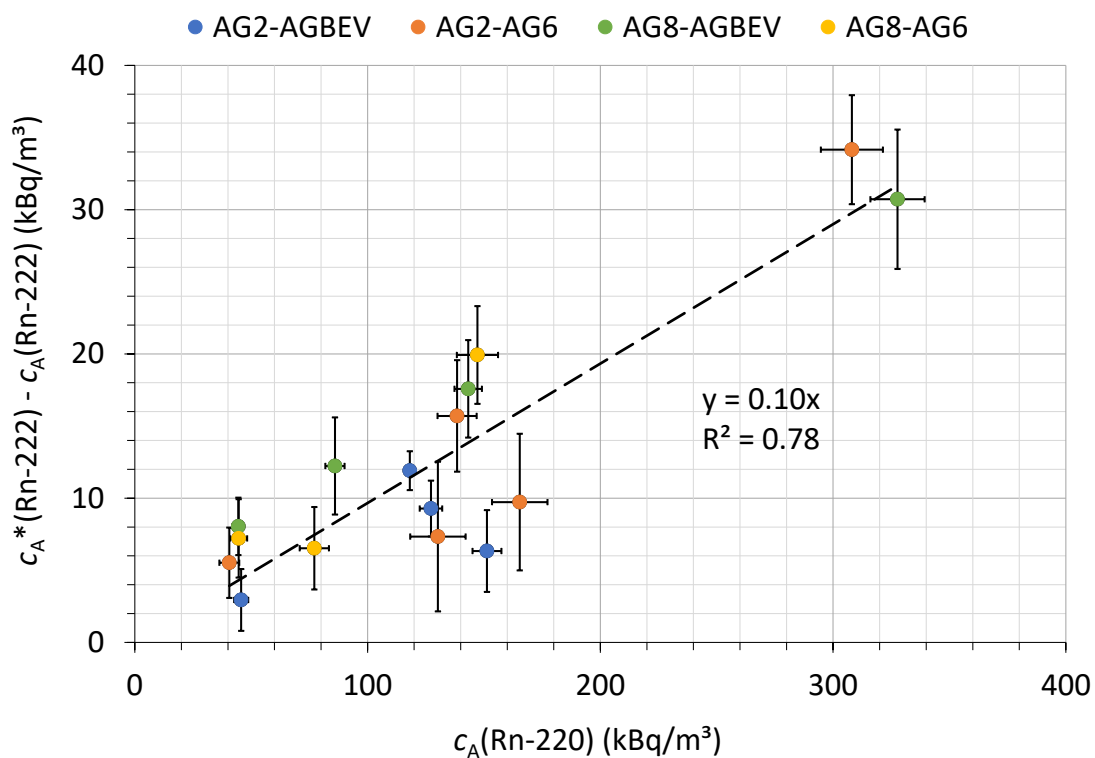
Figure 6.22.: The difference of the measured radon activity concentration between instruments in flow mode and instruments in radon/thoron mode plotted against thoron activity concentration (05/09/2017-07/09/2017).

Figure 6.23.: The deviation of the measured radon activity concentration by the AG2 (flow mode) from the AG BEV (radon/thoron mode) plotted against the ratio of thoron activity concentration to radon activity concentration. The measurements were taken overnight from the same soil gas probe at location 8 (Hörzenschlag, 07/09/2017-08/09/2017).
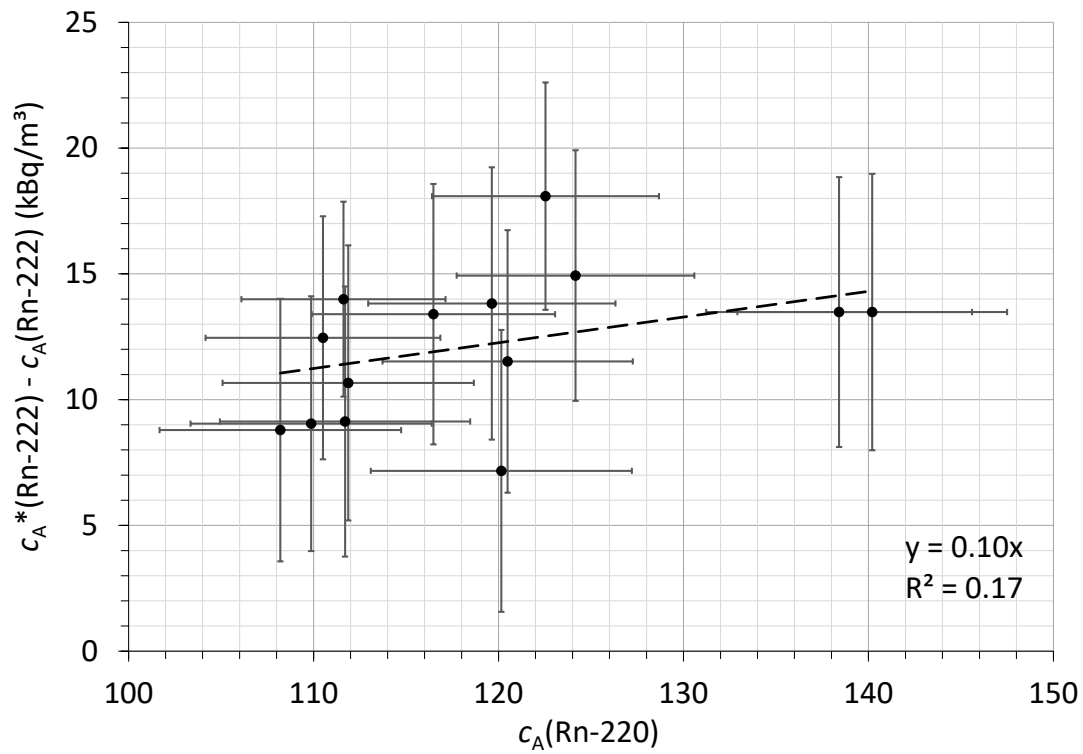
Figure 6.24.: The difference of the measured radon activity concentration between the AG2 (flow mode) and the AG BEV (radon/thoron mode) plotted against thoron activity concentration. The measurements were taken overnight from the same soil gas probe at location 8 (Hörzenschlag, 07/09/2017-08/09/2017).

Thoron progeny

When operated in radon/thoron mode, the AlphaGUARD measures the activity concentration of the thoron progeny Po-212 and corrects the results of the radon and thoron activity concentrations accordingly (Saphymo GmBH 2014). In modes that measure only the radon activity concentration, the Po-212 activity concentration is not measured and no such correction takes place. Therefore, it is possible that the build-up of Po-212 in the detector due to the thoron in the soil gas causes the overestimation of the radon activity concentration in the AlphaGUARDs operated in flow mode.

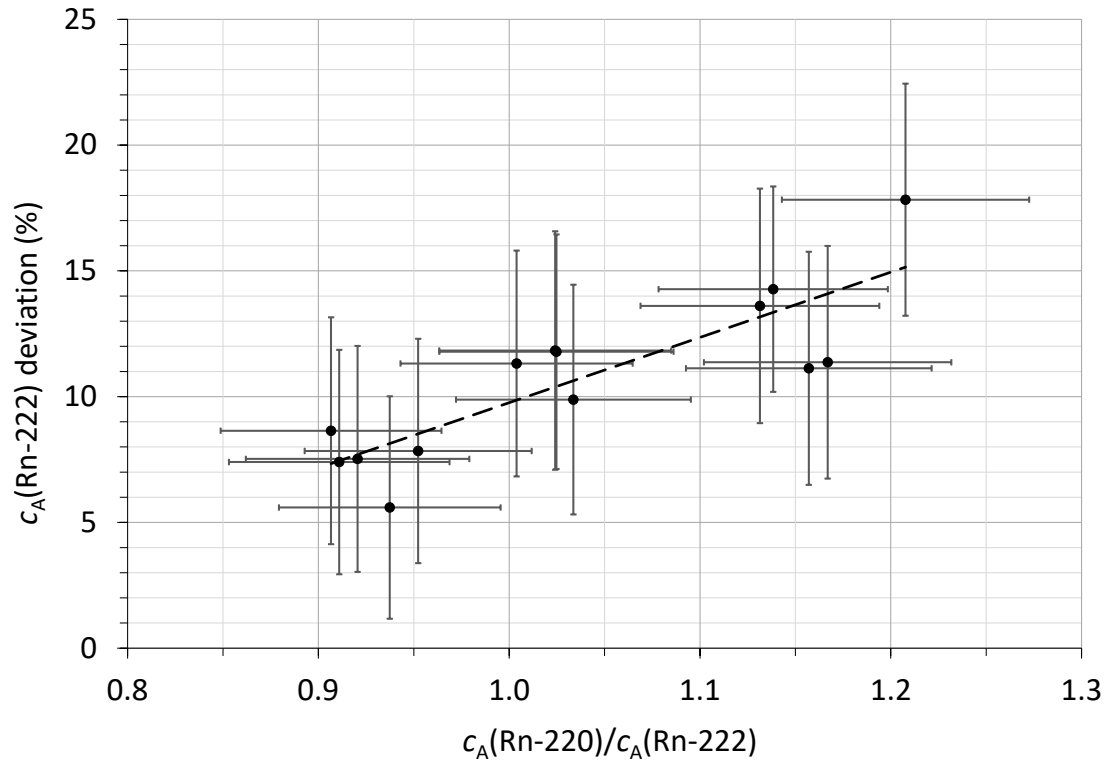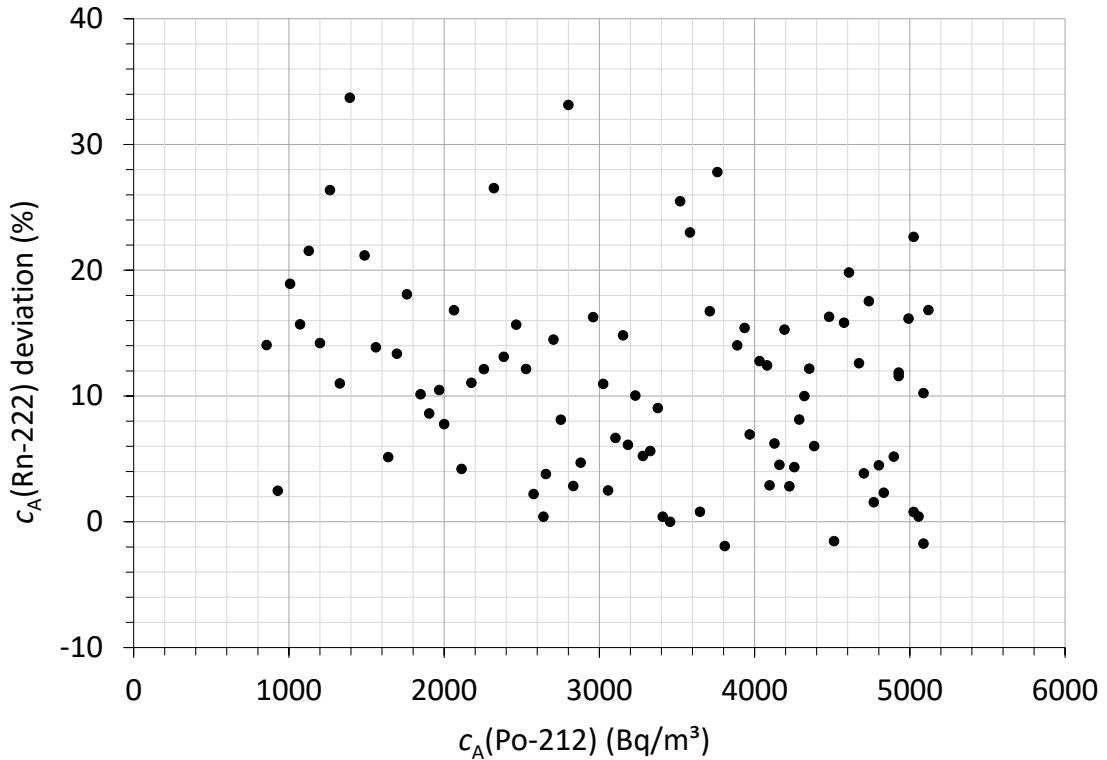**Figure 6.25.:** The deviation of the measured radon activity concentration by the AG2 (flow mode) from the AG BEV (radon/thoron mode) plotted against the Po-212 activity concentration. The measurements were taken overnight from the same soil gas probe at location 8 (Hörzenschlag, 07/09/2017-08/09/2017).

However, the overnight soil gas measurements (figure 6.25) show no correlation between the radon deviation and the activity concentration of Po-212. This is likely because the activity concentration of Po-212 is too low compared to that of radon and thoron to show any noticeable influence. The indoor measurements (see chapter 7) yielded an average radon activity concentration of $671 \pm 30\,\mathrm{Bq/m^3}$ measured by the ThoronScout and $875 \pm 26\,\mathrm{Bq/m^3}$ measured by the AG8 in diffusion mode. This difference is due to the remaining Po-212 activity concentration in the measurement chamber of the AG8. Michielsen and Bondiguel showed that, after being exposed to a thoron activity concentration of about $14\,\mathrm{kBq/m^3}$ for 5 days, the radon measuring instruments needed $40\,\mathrm{h}$ to regain their baseline (Michielsen and Bondiguel 2015).

6.4. Measurement uncertainties

6.4.1. Radon and thoron activity concentrations

The uncertainty of the individual soil gas measurements is given by the statistical standard uncertainty of the measuring instrument. The uncertainty of the average radon and thoron activity concentrations over multiple measurements by the same measuring instrument is calculated by the propagation of the uncertainties of the individual measurements. When soil gas measurements were taken by different measuring instruments at the same probe, the uncertainty of the average is made up of the propagated uncertainty as well as the standard deviation of the measurements multiplied by the Student factor. This same procedure is applied to determine the uncertainty of the average radon and thoron activity concentrations at one location.

The propagated uncertainty is calculated using equation 6.6,

$$u_y = \sqrt{\left(\frac{\partial y}{\partial x_1} \cdot u_1\right)^2 + \left(\frac{\partial y}{\partial x_2} \cdot u_2\right)^2 + \dots} \qquad (6.6)$$

where y is a function of the variables $(x_1, x_2, \dots, x_i, \dots, x_n)$, u_i is the uncertainty of the variable x_i and u_y is the uncertainty of the function y. When y is the average value of the individual measurements $x_1, x_2, \dots, x_i, \dots, x_n$ then its uncertainty u_y is given by $u_y = \frac{\sqrt{\sum u_i^2}}{n}$.

The standard deviation is a measure of the deviation of the individual values from the mean. For a small sample size, the sample mean follows the Student's t-distribution instead of the Gaussian normal distribution. To account for the small sample size, the standard deviation is multiplied by the Student factor, which describes the difference between those two distributions. The values of the Student factor are 1.84 for $n = 2$,

90

1.32 for $n = 3$ and 1.20 for $n = 4$.

Depth correction

Due to the vertical distribution of radon activity concentration in the soil (see section 4.3), a depth correction is necessary in order to compare radon activity concentrations between probes of different depths. Equation 4.1 was used to correct the radon activity concentrations to a depth of $1\,\text{m}$. A diffusion length of $155\,\text{cm}$ was used because it is a medium value that covers both moist clays and loams as well as dry sands and gravels (Baumgartner et al. n.d.). Any error in the depth correction due to a deviation of the real diffusion length from the assumed diffusion length increases with the distance between the real probe depth from the one that is corrected to. Therefore the probes at a depth of $30\,\text{cm}$ were not used in the calculation of the average radon activity concentration at each measurement location. The depth correction was only applied when directly comparing radon activity concentration measurements to each other or correlating them with another variable (Ra-226 activity concentration and dose rate). No depth correction was applied to thoron measurements as its concentration should be constant due to its short diffusion length.

Environmental factors

The radon activity concentration in soil gas depends on many factors, including soil moisture, rainfall, temperature, air pressure and wind. These conditions can change from one day to the next, and therefore the measured radon activity concentrations are only momentary values. Long-term measurements are needed to determine the fluctuations and long-term average radon activity concentrations. Nevertheless, the momentary values can give a rough indication of the radon and thoron activity con-

centrations in the area. Furthermore, momentary values are all that is needed for the determination of thoron on radon measurements.

6.4.2. Permeability

The permeability measurements were carried out with simple measuring instruments with high uncertainties. Therefore, the used measurement setup only allows the determination of the order of magnitude of the permeability. However, this is adequate for the determination of the radon potential and therefore the chosen measurement technique is a reasonable choice for the purposes of this work.

6.5. Comparison of measurement techniques

Soil air measurements were carried out using two different techniques to determine the radon and thoron activity concentrations, as described in section 6.1.

In July 2017, a syringe was used to draw 100 ml of soil gas from the probes and insert it into the AlphaGUARDs. As explained previously, this method eliminates the influence of thoron on the radon measurement. This is an advantage if one is only interested in the radon activity concentration, but clearly a disadvantage if the thoron activity concentration is also of interest. Another disadvantage of this method is that it is not suitable for long-term measurements. A possible source of errors is leakage during the withdrawal of soil gas from the probe and during its insertion into the AlphaGUARD. Therefore, the procedure has to be carried out carefully and the tightness of the syringe should be confirmed periodically. Because only 100 ml of soil gas are used for the measurement, any leakage or mixture of soil gas with ambient air can lead to a significant error in the measured radon activity concentration.

In September 2017, the soil gas was pumped into two AlphaGUARDs in series, one in radon/thoron mode and one in flow mode. This way, accurate measurements of both the radon and thoron activity concentrations of the soil gas can be performed. The AlphaGUARD in flow mode allows for the investigation of the influence of thoron on radon measurements. Because the pumps are operated automatically by the Alpha-GUARD, it is possible to carry out continuous measurements over a few days using this method. Limiting factors are the batteries of the measuring instruments and pumps, as well as the weather (rain). The permeability measurements indicated high soil gas permeabilities in all measurement locations, allowing for easy withdrawal of soil gas from the probes. However, low soil gas permeabilities may lead to difficulties if the pump is not able to maintain its set pump rate.

7. Radon and thoron in indoor air and water

In addition to the soil gas measurements, indoor radon and thoron measurements were carried out in a home in Königswiesen, Upper Austria as well as in the waterworks in Bärenkopf, Lower Austria. Furthermore, the radon content of selected water samples was determined.

7.1. Methods

7.1.1. Indoor air measurement

Due to the high daily and seasonal variations in indoor radon activity concentrations, long-term measurements are essential to determine the average annual radon activity concentration in a home. For the reliable estimation of the average annual radon activity concentration, the measurement has to fulfil certain requirements (Gräser et al. 2011). The measurement has to has to be carried out over a time period of at least three months, with at least half of that time between October and April. The radon activity concentration has to be measured in at least two separate and frequently occupied rooms, preferably with ground contact. Passive measuring devices are used

because they are cheap and convenient. The measuring instrument should not be moved during measurement and it should be placed:

- approximately at breathing level

- away from doors and windows

- at a distance of least $10\,cm$ from the walls

- away from direct heating

- somewhere without condensed humidity

- somewhere inaccessible by children and pets

Short-term measurements over a few days or weeks can be carried out to estimate the potential radon hazard in a home. Activity concentration measurements of radon and thoron were carried out over one night in a home in the municipality of Königswiesen, Upper Austria. The measurement was carried out with the ThoronScout, which was placed in the kitchen at a height of about $1\,m$.

7.1.2. Radon in water

Water samples were collected from a house in Königswiesen, Upper Austria (07/09/2017), the waterworks in Bärnkopf, Lower Austria (06/09/2017) and from a spa in Bad Zell, Upper Austria (08/09/2017). All samples were collected using commercially available $1\,L$ glass bottles.

The radon content in the water samples was determined using an ionization chamber with a volume of $9.3\,L$ and an applied voltage of $260\,V$. The experimental setup is shown in figure 7.1.

First, air is pumped out of the ionization chamber to reduce the pressure. Then,

Figure 7.1.: Photograph of the setup to measure the radon activity concentration in a water sample.

the cap of the bottle containing the water sample is removed and replaced by a plug with two tubes connected to it (figure 7.2). When connecting one of those tubes to the ionization chamber, the reduced pressure causes air to be sucked into the chamber through the water bottle. The resulting bubbles cause the emanation of radon from the water. After an amount of air three times the volume of the water has passed through the bottle, virtually all the radon will have emanated from the water (Friedmann 1977).

An electrometer was used to measure the charge collected over a time interval. By dividing the collected charge by the time interval, the current of the ions produced in the chamber can be calculated. The radon activity A in the ionization chamber is directly proportional to the produced current I and is given by

$$A(\text{Bq}) = 19.24 \cdot I(\text{pA}) \tag{7.1}$$
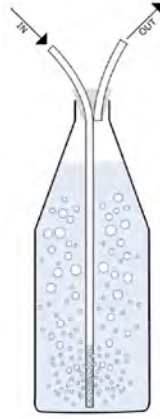
Figure 7.2.: Emanation of radon from the water bottle (Karner 2017).

At least five measurements were taken from each water sample, about half an hour after the radon had finished transferring from the bottle to the ionization chamber. However, equation 7.1 is only valid when the radon in the ionization chamber is in equilibrium with its daughter products, which happens after about three hours. Figure 7.3 shows the development of the total activity in the ionization chamber after the insertion of radon.
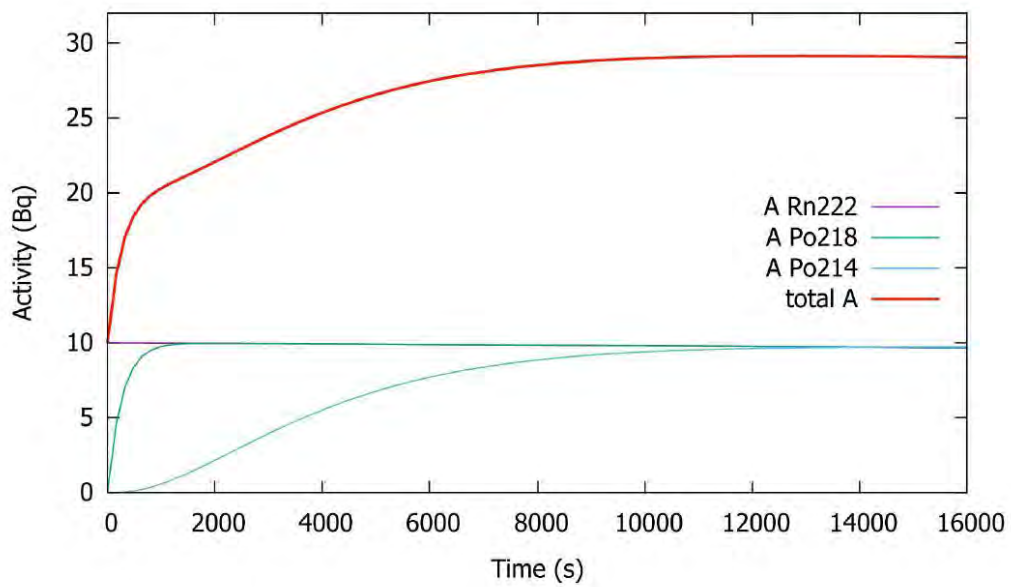
Figure 7.3.: Development of total activity after the insertion of radon in the ionization chamber (Lotter 2017).

98

Because the measurements were taken before equilibrium was reached, they were multiplied by a factor of 1.3 ± 0.1. Furthermore, because the measurements took place a few days after the collection of the samples, the results were corrected to account for the radioactive decay of radon between the sampling time and the measurement time.

The uncertainties of the radon activity concentrations were calculated by multiplying the standard deviation of the measurements by the Student factor.

7.2. Results

The average radon and thoron activity concentrations measured over one night in a house in the municipality of Königswiesen, Upper Austria were $671 \pm 30 \, \mathrm{Bq/m^3}$ and $48 \pm 6 \, \mathrm{Bq/m^3}$, respectively. Figures 7.4 and 7.5 show how the activity concentrations vary over time. During the night, windows and doors remain closed, which leads to a decreased ventilation rate allowing the build-up of the radon activity concentration. Furthermore, the lower temperatures during the night lead to a stronger stack effect (see chapter 4.4). The fall in radon activity concentration between 6 a.m. and 7 a.m. is due to the increased ventilation of the room from opening the windows in the morning. This shows that the rate of ventilation has a significant influence on the indoor radon activity concentration. The thoron activity concentration also increases during the night. Although there is also a fall in thoron activity concentration after 6 a.m., it is not as big as the decrease in radon activity concentration at the same time. This is likely because the thoron decay constant $(45 \, \mathrm{h}^{-1})$ is higher than typical ventilation rates $(1 \, \mathrm{h}^{-1})$, and therefore changes in the ventilation rate should not significantly affect the indoor thoron activity concentration (Steinhäusler 1996).

Figure 7.4.: Radon activity concentration during one night in the kitchen of a home in Hörzenschlag, Upper Austria (07/09/2017-08/09/2017). The higher values of the AG8 are due to the remaining Po-212 activity concentration (see section 6.3.5).
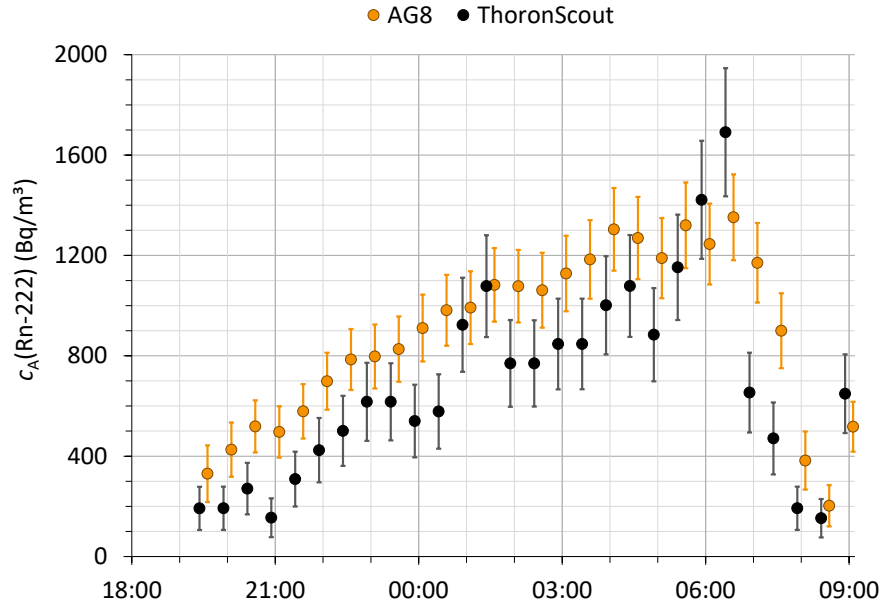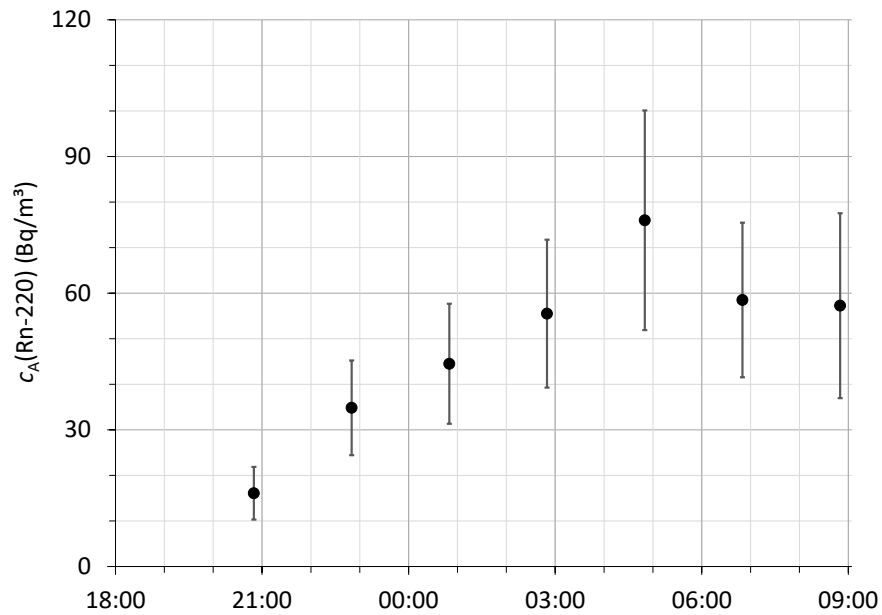

Figure 7.5.: Thoron activity concentration during one night in the kitchen of a home in Hörzenschlag, Upper Austria (07/09/2017-08/09/2017).

A short measurement of the radon activity concentration inside the waterworks of Bärenkopf, Lower Austria yielded a value of $19 \pm 5\,\mathrm{kBq/m^3}$. The main source of radon in this case is likely the emanation of radon from water, although a significant contribution of radon from soil gas is also plausible. Another reason for the extremely high radon activity concentration is the lack of ventilation: for sanitary reasons, the windows are kept closed to avoid bugs entering the water basin.

The results of measurements of the radon content in water samples are summarised in table 7.1.

Sample name	Sampling date	Rn-222	
		Activity concentration	Uncertainty
		Bq/l	
Alter Brunnen 1	07.09.2017 18:15	60	9
Alter Brunnen 2	07.09.2017 18:18	59	9
Unterer (neuer) Brunnen 1	07.09.2017 18:25	87	10
Unterer (neuer) Brunnen 2	07.09.2017 18:27	98	24
Bärnkopf Wasserwerk Dreiblöchelberg Quelle	06.09.2017 14:35	118	11
Bärnkopf Wasserwerk Q2	06.09.2017 14:40	45	19
Bärnkopf Wasserwerk Q3 2	06.09.2017 14:30	42	8
Bad Zell Radonarium	08.09.2017 10:50	102	17

Table 7.1.: Radon activity concentrations of water samples.

Alter Brunnen (old well) and Unterer (neuer) Brunnen (lower (new) well) refer to the water supply of the house in Königswiesen in which the indoor radon and thoron measurements were carried out. Dreiblöchelberg Quelle, Q2 and Q3 are the names of the sources from the waterworks in Bärnkopf. Bad Zell Radonarium refers to the spa in Bad Zell, where the water sample was taken from a water fountain in the lobby.

Figure 7.6 is a photograph of the basin at the waterworks. As the water from the different sources pours into the basin, the movement can cause significant radon emanation, leading to a high radon activity concentration in the air.

Figure 7.6.: Basin of the Bärnkopf waterworks (06/09/2017). The dimensions of the basin are approximately $1.5\,\mathrm{m} \times 2.5\,\mathrm{m}$.

8. Conclusion

As part of this thesis, measurements of radon and thoron in soil gas and indoors were taken in the Austrian Wald- and Mühlviertel and in the radioactivity laboratory of the Federal Office for Metrology and Surveying (BEV) in Seibersdorf. Additionally, above-ground dose rates were measured, radon concentrations in water samples were determined using an ionization chamber and the activity concentrations of radionuclides of the uranium and the thorium decay chains in soil samples were measured using low-level gamma spectrometry.

Radon activity concentrations of up to $246\,\text{kBq/m}^3$ and thoron activity concentrations of up to $310\,\text{kBq/m}^3$ were measured at individual soil gas probes.

An innovative measurement setup using two AlphaGUARDs was introduced for the investigation of the influence of thoron on radon activity concentration measurements. The results showed that measuring instruments that did not account for the presence of thoron overestimated the radon activity concentration in soil gas by up to $38\,\%$. This deviation increased with the ratio of thoron to radon activity concentration, as on average, $10\,\%$ of the thoron activity concentration in the soil gas was recorded by the measuring instrument as radon activity concentration. Due to the thoron progeny Pb-212, an influence on the radon measurement can also be observed after the exposition to thoron.

Correlations between the radon activity concentrations in soil gas, the activity concentrations of Ra-226, U-238, Th-228 and K-40 in the soil and the above-ground gamma dose rates were investigated. The results show a linear relationship between the radon activity concentration in soil gas and the gamma dose rate above the ground, indicating that dose rate measurements could be another way to examine the radon characteristics of an area. Furthermore, is was confirmed that the gamma dose rate can be estimated from the activity concentrations of potassium, uranium and thorium in the soil.

Indoor measurements showed the development of the radon and thoron activity concentrations over night and the effect of ventilation. Radon activity concentrations of up to $118 \pm 11 \, \text{Bq/l}$ were found in the collected water samples.

In the course of the laboratory measurements, a thoron source was developed using natural monazite sand. Furthermore, experimental setups were proposed in which the thoron source can be used calibrate radon and thoron measuring instruments as well as check radon monitors for sensitivity to thoron.

8.1. Outlook

This thesis provides a basis for the understanding of how thoron influences radon activity concentration measurements by AlphaGUARDs. In future research the developed thoron source can be used to further investigate the influence of thoron on different radon measuring instruments in greater detail under more controlled conditions. Furthermore, in the scope of the metroRADON project, different filters, foils and membranes that may serve as thoron barriers are to be studied with the aim of developing practical techniques to reduce the influence of thoron on radon measurements.

Bibliography

Alvarez, J. L. (1990). *Radon Analysis Methods. A Comparative Study.* Air Chek, Inc. URL: `http://www.radon.com/radon_analysis/` (visited on 16/01/2018).

Baumgartner, A. et al. (n.d.). *Radonvollerhebung in den Gemeinden Reichenau, Haibach und Ottenschlag i.M.* Bundesministerium für Land- und Forstwirtschaft, Umwelt und Wasserwirtschaft.

Bé, M.-M., V. Chisté, C. Dulieu, E. Browne, V. Chechev, N. Kuzmenko, R. Helmer et al. (2004). *Table of Radionuclides.* Vol. 2. Monographie BIPM-5. Bureau International des Poids et Mesures. ISBN: 92-822-2207-1. URL: `http://www.bipm.org/utils/common/pdf/monographieRI/Monographie_BIPM-5_Tables_Vol2.pdf`.

Bé, M.-M., V. Chisté, C. Dulieu, E. Browne, V. Chechev, N. Kuzmenko, F. Kondev et al. (2008). *Table of Radionuclides.* Vol. 4. Monographie BIPM-5. Bureau International des Poids et Mesures. ISBN: 92-822-2230-6. URL: `http://www.bipm.org/utils/common/pdf/monographieRI/Monographie_BIPM-5_Tables_Vol4.pdf`.

Bruno, R. C. (1983). "Sources of Indoor Radon in Houses: A Review". *Journal of the Air Pollution Control Association* 33.2, pp. 105–109.

Bundesministerium für Nachhaltigkeit und Tourismus (2018). *Radon in Österreich.* URL: `https://www.bmnt.gv.at/umwelt/strahlen-atom/radon/radonpotenzial.html` (visited on 15/02/2018).

Cable, M. (2005). *Calibration: A Technician's Guide.* ISA - Instrumentation, Systems, and Automation Society. ISBN: 1-55617-912-X.

Cetnar, J. (2006). "General solution of Bateman equations for nuclear transmutations". *Annals of Nuclear Energy* 33.7, pp. 640–645.

Chen, J. and K. L. Ford (2017). "A study on the correlation between soil radon potential and average indoor radon potential in Canadian cities". *Journal of Environmental Radioactivity* 166, pp. 152–156.

Cinelli, G. et al. (2015). "Radiological risk from thoron, a case study: The particularly radon-prone area of Bolsena, and the lesson learned". *Radiation Physics and Chemistry* 116.Supplement C, pp. 381–385.

Damkjaer, A. and U. Korsbech (1992). "A Small-Diameter Probe for In Situ Measurements of Gas Permeability of Soils". *Radiation Protection Dosimetry* 45.1-4, pp. 85–89.

Darby, S. et al. (2005). "Radon in homes and risk of lung cancer: collaborative analysis of individual data from 13 European case-control studies". *BMJ* 330.7485, p. 223.

Ditto, M. et al. (2013). *Radioaktivität und Strahlung in Österreich 2011 und 2012. Daten und Bewertung.* Bundesministerium für Gesundheit.

Friedmann, H. et al. (2007). *Das österreichische nationale Radonprojekt - ÖNRAP. Projekt Endbericht.* Wien: Bundesministerium für Land- und Forstwirtschaft, Um-

welt und Wasserwirtschaft und Bundesministerium für Gesundheit, Familie und Jugend.

Friedmann, H. (1977). "Modell für die Entemanierung radioaktiver Lösungen". *Anzeiger der mathematisch naturwissenschaftlichen Klasse der österreichischen Akademie der Wissenschaften* 114.7.

Geiger, H. and J. M. Nuttall (1911). "LVII. The ranges of the α particles from various radioactive substances and a relation between range and period of transformation". *The London, Edinburgh, and Dublin Philosophical Magazine and Journal of Science.* 6th ser. 22.130, pp. 613–621.

Genitron Instruments GmbH, ed. (1995). *Emanation- and Calibration Container.* Technical Description. Frankfurt/Main, Germany.

Gierl, S. et al. (2014). "Thoron and thoron progeny measurements in German clay houses". *Radiation Protection Dosimetry* 160.1-3, pp. 160–163.

GoogleMaps (2017). URL: https://goo.gl/maps/2rXt26CmdiL2 (visited on 14/11/2017).

Gräser, J. et al. (2011). *Radon Messung und Bewertung.*

Grasty, R. L. et al. (1984). *Natural background radiation in Canada.* Bulletin. Geological Survey of Canada.

Gruber, V. (2004). "Untersuchung und Evaluierung der geogenen Radon-Aktivitätskonzentration in eiszeitlich-glazialen Ablagerungen in Oberösterreich". Diplomarbeit. Vienna University of Technology.

Hykes, J. (2011). *Absorption coefficient of aluminium.* Wikimedia Commons, licensed under CC BY-SA 3.0. URL: `https://commons.wikimedia.org/wiki/File:Al-gamma-xs.svg` (visited on 23/12/2017).

ICRP (2007). "The 2007 Recommendations of the International Commission on Radiological Protection. ICRP Publication 103". *Ann. ICRP* 37.2-4.

ICRP (2010). "Lung Cancer Risk from Radon and Progeny and Statement on Radon. ICRP Publication 115". *Ann. ICRP* 40.1.

Interaction of Gamma Radiation with Matter (2017). Nuclear Power for Everybody. URL: `http://www.nuclear-power.net/nuclear-power/reactor-physics/interaction-radiation-matter/interaction-gamma-radiation-matter/` (visited on 23/12/2017).

Kalsi, P. C., A. Ramaswami and V. K. Manchanda (2005). "Solid state nuclear track detectors and their applications". *Bhabha Atomic Research Center Newsletter* 257, p. 6.

Kanse, S. D. et al. (2016). "A study of thoron exhalation from monazite-rich beach sands of High Background Radiation Areas of Kerala and Odisha, India". *Environmental Earth Sciences* 75.23, p. 1465.

Karner, P. (2017). "Methodical study of the radon-222 activity concentration in drinking Water". Bachelor thesis. Vienna University of Technology.

Kemski, J., K. R and A. Siehl (1996). "Das geogene Radon-Potential". In: *Umweltradioaktivität*. Berlin: Ernst & Sohn, pp. 179–222.

Kemski, J., A. Siehl et al. (2001). "Mapping the geogenic radon potential in Germany". *Science of The Total Environment* 272.1, pp. 217–230.

Knoll, G. F. (1999). *Radiation Detection and Measurement*. 3rd ed. Wiley. ISBN: 978-0-471-07338-3.

Kotrappa, P. (2002). "Review of Electret ion chamber technology for measuring technologically enhanced natural radioactivity". *Technologically enhanced natural radiation (TENR II)*, p. 45.

Kukk, E. (2011). *Radiation and particle detectors*. Lecture Notes. URL: `http://www.physics.ohio-state.edu/~klaus/s12-780/references/turku_lecturenotes.pdf` (visited on 11/01/2018).

Lagarde, F. et al. (2001). "Residential Radon and Lung Cancer among Never-Smokers in Sweden". *Epidemiology* 12.4, pp. 369–404.

L'Annunziata, M. F. (2012). *Handbook of Radioactivity Analysis*. Elsevier, AP. ISBN: 9780123848734.

Lipiarski, P. (2017). *IRIS online. Interaktives Rohstoff-Informationssystem*. URL: `http://arcg.is/11aKPC` (visited on 14/11/2017).

Lotter, K. (2017). "Evaluation of different Techniques for Measurement of Radon in Water Samples". Projektarbeit. Vienna University of Technology.

Maringer, F. J. and A. Ramer (1999). *Konzeption, Durchführung und mathematisch-statistische Auswertung eines Ringvergleichs für Radondetektoren und Radonmeßgeräte österreichischer Meßstellen im Radonkalibrierlabor des ÖFPZ Arsenal*. Endbericht. Österreichisches Forschungs- und Prüfzentrum Arsenal GmbH.

"Maß- und Eichgesetz" (1950). *BGBl.* Nr. 152/1950.

MetroRADON (2018). URL: http://metroradon.eu/ (visited on 23/02/2018).

Michielsen, N. and S. Bondiguel (2015). "The influence of thoron on instruments measuring radon activity concentration". *Radiation Protection Dosimetry* 167.1-3, pp. 289–292.

Pawel, D. J. and J. S. Puskin (2003). *EPA Assessment of Risks from Radon in Homes.* U.S. Environmental Protection Agency.

Qwerty123uiop (2013). *Schematic view of a photomultiplier coupled to a scintillator, illustrating detection of gamma rays.* Wikimedia Commons, licensed under CC BY-SA 3.0. URL: https://commons.wikimedia.org/wiki/File:PhotoMultiplierTu beAndScintillator.svg (visited on 16/01/2018).

Saphymo GmBH, ed. (2014). *AlphaGuard Portable Radon Monitor.* User Manual. Frankfurt/Main, Germany.

SARAD GmBH, ed. (2015). *Thoron-Scout.* Handbook. Dresden, Germany.

Sim, D. (2012). *Practical gaseous ionization detection regions.* Wikimedia Commons, licensed under CC BY-SA 3.0. URL: https://commons.wikimedia.org/wiki/File:Detector_regions.gif (visited on 07/01/2018).

Sjlegg (2009). *Graph of isotopes by type of nuclear decay.* Wikimedia Commons, licensed under CC BY-SA 3.0. URL: https://commons.wikimedia.org/wiki/File:Table_isotopes_en.svg (visited on 20/12/2017).

Smetsers, R. C. G. M. and R. O. Blaauboer (1994). "Time-Resolved Monitoring of Outdoor Radiation Levels in the Netherlands". *Radiation Protection Dosimetry* 55.3, pp. 173–181.

Steinhäusler, F. (1996). "Environmental ^{220}Rn: A review". *Environment International* 22.Supplement 1, S1111–S1123.

Tokonami, S. (2010). "Why is ^{220}Rn (thoron) measurement important?" *Radiation Protection Dosimetry* 141.4, pp. 335–339.

Tosaka (2008a). *Decay chain 4n, Thorium series*. Wikimedia Commons, licensed under CC BY-SA 3.0. URL: `https://commons.wikimedia.org/wiki/File:Decay_chain(4n,Thorium_series).PNG` (visited on 11/01/2018).

Tosaka (2008b). *Decay chain 4n+2, Uranium series*. Wikimedia Commons, licensed under CC BY-SA 3.0. URL: `https://commons.wikimedia.org/wiki/File:Decay_chain(4n%5C%2B2,_Uranium_series).PNG` (visited on 11/01/2018).

UNSCEAR (2008). *Sources and effects of ionizing radiation*. Vol. 1. New York: United Nations.

van Velzen, L. et al., eds. (2010). *Radon detectors and measurement techniques*. EURSSEM. URL: `http://eurssem.eu/pages/c-4-4-radon-detectors-and-measurement-techniques` (visited on 06/01/2018).

Wang, N. et al. (2016). "The characteristics of radon and thoron concentration from soil gas in Shenzhen City of Southern China". *Nukleonika* 61 (3), pp. 315–319.

WHO (2016). *Radon and health*. Fact sheet. URL: `http://www.who.int/mediacentre/factsheets/fs291/en/` (visited on 17/02/2018).

Zeeb, H. and F. Shannoun, eds. (2009). *WHO handbook on indoor radon: a public health perspective*. World Health Organization. ISBN: 978 92 4 154767 3.

List of Figures

114

116

Appendices

Corentium Pro datasheet

Corentium Pro
by Airthings

DOWNLOADS
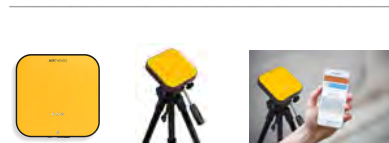
Corentium Pro, a favorite among home inspectors and professionals. Fully AARST-NRPP certified for the North American market and beyond, this professional radon detector will be a reliable workhorse for decades.

SPECIFICATIONS

Radon sampling: passive diffusion chamber
Detection method: alpha spectrometry
Detector: 4 silicon photodiodes in 4 distinct radon chambers
Diffusion time constant: 25 min
Measurement range: 0 - 50 000 Bq/m^3
Sensitivity: ~100 cph at 1000 Bq/m^3
Sampling rate: 1 hour
Operation environment

- 4°C to 40°C
- 5% RH to 85% RH non-condensing
- 50 kPa to 110 kPa

ENVIRONMENTAL SENSORS

Temperature: 0.2°C resolution, ± 1°C accuracy
Humidity: 0.5% RH resolution, ± 4.5% accuracy
Barometric pressure: 0.002 kPa resolution, ± 1 kPa accuracy

MEMORY

Internal memory stores 5 years of data
Capacity: ~ 1900 days of measurement

- 5 data sets of one year length
- 177 data sets of 1-week length
- 325 data sets of 2-days length

Memory type: non-volatile flash memory

LONG BATTERY LIFE

Approximately 1.5 year of continuous monitoring
Comes with replaceable AA batteries

DATA & ACCURACY

Data accessible via Android or iOS app
Free reporting and analysis software for PC
After 24 hours: σ < 7 % ± 5 Bq/m³
After 7 days: σ < 5 % ± 2 Bq/m³

ADDITIONAL INFORMATION

PACKAGE CONTENTS

Radon detector
3 x alkaline batteries type AA (LR06)
2x quick start guides (CRA and Detector)
Memory Stick w/software
1x USB-cable (mini-B Plug to Type-A plug)
Torx6 Key L shape
Calibration certificate
Protective casing

PACKAGE

Weight: 1500g
Dimension: 307x255x105 mm

PRODUCT CODES

EAN: 7090031102364
SKU: 236
GLN: 7080003872449

DETECTOR

Dimensions: 140x140x30 mm
Weight: 325g (with batteries)
Housing: ABS plastic

OTHER

Tampering detection (moving device)
Factory calibrated
Control: 1 push-button re-start

SigmaPlot nonlinear regression report

```
Nonlinear Regression                  Donnerstag, Jänner 18, 2018, 16:28:27

Data Source: AG BEV in 10.-23.8.2017_60minDiff_Rn222
Equation: Exponential Decay; Single, 2 Parameter
f = a*exp(-b*x)


R      Rsqr  Adj Rsqr    Standard Error of Estimate

0.9996     0.9993      0.9993              153.9213


      Coefficient Std. Error t      P

a     22556.5661 27.8346    810.3799   <0.0001
b     0.1839     0.0003     528.3262   <0.0001


Analysis of Variance:

      DF    SS    MS
Regression 2    33155647472.9202 16577823736.4601
Residual   306  7249679.0798      23691.7617
Total 308   33162897152.0000 107671744.0000


Corrected for the mean of the observations:
      DF    SS    MS    F      P
Regression 1    9878192677.2838  9878192677.2838  416946.3125 <0.0001
Residual   306  7249679.0798      23691.7617
Total 307   9885442356.3636  32200137.9686


Statistical Tests:

Normality Test (Shapiro-Wilk)    Failed     (P = <0.0001)
      W Statistic= 0.9416   Significance Level = 0.0500


Constant Variance Test       Failed     (P = <0.0001)


Fit Equation Description:
[Variables]
x = col(2)
y = col(5)
reciprocal_y = 1/abs(y)
reciprocal_ysquare = 1/y^2
reciprocal_x = 1/abs(x)
reciprocal_xsquare = 1/x^2
reciprocal_pred = 1/abs(f)
reciprocal_predsqr = 1/f^2
weight_Cauchy = 1/(1+4*(y-f)^2)
'Automatic Initial Parameter Estimate Functions
F(q) = if(size(x)>1; if(total(abs(y))>0; ape(x;log(abs(y));1;0;1); -306);
0)
asign(q) = if(mean(q)>=0;1;-1)
[Parameters]
a = if(F(0)[1]< 307; if(F(0)[1]>-307; asign(y)*10^F(0)[1]; asign(y)*10^(-
307)); asign(y)*10^307) ''Auto
{{previous: 22556.6}} {{MinRange: -3}} {{MaxRange: 9}}
b = if(x50(x;y)-min(x)=0; 1;  -ln(.5)/(x50(x;y)-min(x)))  ''Auto
{{previous: 0.18391}} {{MinRange: 0}}
{{MaxRange: 1}}
```

Monazite sand gamma spectrometry results

Universität für Bodenkultur Wien

Prüflabor für Umweltradioaktivität und Strahlenschutz

Gammaspektrometrie - Aktivitätsmessergebnisse

Probe

G4832   4 | Monazitsand |

BOSSEW200 **27.06.2000**   11:00

Spektrum	Meßdatum	PeakNr	Nuklid	Aktivität *(zum Probennahmezeitpunkt)*				Erkennungsgrenze
SP9883	28.06.2000		*K-40*	**1,38E4**	±	1,12E3	Bq/kg	*1,25E1*
SP9883	28.06.2000		*La-138*		<	2,01E0	Bq/kg	*2,01E0*
S21708	26.05.2000		*Pb-210*		<	3,93E0	Bq/kg	*3,93E0*
SP9883	28.06.2000		*Ra-223*		<	7,32E1	Bq/kg	*7,32E1*
SP9883	28.06.2000		*Ra-226*	**2,08E4**	±	1,15E3	Bq/kg	*2,79E0*
SP9883	28.06.2000		*Ra-228*	**1,89E5**	±	1,54E4	Bq/kg	*5,07E0*
SP9883	28.06.2000		*Th-227*	**9,43E2**	±	2,76E2	Bq/kg	*1,49E1*
SP9883	28.06.2000		*Th-228*	**1,85E5**	±	1,06E4	Bq/kg	*4,00E0*
S21708	26.05.2000		*Th-232*	**1,87E5**	±	1,47E4	Bq/kg	*0,00E0*
SP9883	28.06.2000		*U-235*	**3,53E3**	±	5,87E2	Bq/kg	*1,76E1*

Results tables

Date	Location	Probe no.	Depth (cm)	Rn-222				Rn-220		Permeability (m²)
				Activity concentration (measured)	Uncertainty	Activity concentration (depth corrected)	Uncertainty	Activity concentration	Uncertainty	
				kBq/m³		kBq/m³		kBq/m³		
25.07.2017	1	1	30	43	3	117	7			6E-10
		2	60	45	3	67	4			< 3E-13
		3	90	23	1	25	1			< 3E-13
		4	120	246	63	217	55			> 6E-10
25.07.2017	2	1	120	116	27	102	24			1E-09
27.07.2017	3	1	30	97	10	262	26			2E-11
		2	60	117	7	173	10			5E-10
		3	90	119	9	128	9			1E-11
		4	120	126	17	111	15			3E-09
05.09.2017	5	1	80	92	7	108	8	318	20	1E-10
		2	80	73	23	86	27	154	21	7E-11
		3	80	84	3	99	3	130	12	4E-10
05.09.2017	6	1	80	47	1	55	1	46	3	3E-09
		2	90	58	2	62	2	77	6	1E-09
06.09.2017	4	1	100	38	1	38	1	127	5	3E-10
		2	100	22	2	22	2	45	4	4E-12
		3	100	61	1	61	1	151	6	5E-10
		4	150	52	2	40	1	147	9	2E-09
07.09.2017	8	1	100	92	2	92	2	138	8	2E-10
		2	100	108	14	108	14	102	30	3E-09
07.09.2017	7	1	100	62	1	62	1	41	4	2E-09
		2	100	53	1	53	1	44	2	5E-11

Location	Mean depth (cm)	Rn-222				Rn-220				Max. permeability (m²)	Dose rate (nSv/h)	Relative air humidity (%)	Ambient temperature (°C)
		Activity concentration (mean)	Uncertainty	Activity concentration (max.)	Uncertainty	Activity concentration (mean)	Uncertainty	Activity concentration (max.)	Uncertainty				
		kBq/m³				kBq/m³							
1	75	89	110	246	63					> 6E-10	209	52	20
2	120	116	27	116	27					1E-09	210	75	16
3	75	115	14	126	17					3E-09	225	71	19
5	80	83	13	92	7	201	111	318	20	4E-10	132	44	24
6	85	52	10	58	2	61	29	77	6	3E-09	117	46	23
4	112.5	43	18	61	1	118	52	151	6	2E-09	147	78	18
8	100	100	16	108	14	120	37	138	8	3E-09	149	60	15
7	100	58	9	62	1	43	4	44	2	2E-09	81	54	18

Measurement time	Rn-222 (RnTn mode)		Rn-220 (RnTn mode)		Rn-222 (flow mode)		c$_A$(Po-212) (Bq/m³)	Thoron/radon ratio	uncertainty thoron/radon ratio	Radon deviation (%)	uncertainty radon deviation (abs. %)	Relative air humidity (%)	Temperature (°C)
	Activity concentration	Uncertainty	Activity concentration	Uncertainty	Activity concentration	Uncertainty							
	Bq/m³		Bq/m³		Bq/m³								
07.09.2017 18:30	98,304	4,320	114,176	12,928	112,128	7,648	856	1.16	0.14	14	9	55.8	16.3
07.09.2017 18:40	103,936	4,576	110,080	13,888	106,496	7,712	928	1.06	0.14	2	9	57.8	15.6
07.09.2017 18:50	94,720	4,288	126,976	13,568	112,640	8,320	1008	1.34	0.16	19	10	62.3	15.1
07.09.2017 19:00	97,792	4,512	109,056	13,824	113,152	8,640	1072	1.12	0.15	16	10	64.0	14.5
07.09.2017 19:10	92,672	4,352	90,624	12,480	112,640	8,768	1128	0.98	0.14	22	11	64.5	13.8
07.09.2017 19:20	100,864	4,608	118,784	14,336	115,200	9,152	1200	1.18	0.15	14	10	66.0	13.1
07.09.2017 19:30	93,184	4,384	108,032	13,568	117,760	9,536	1264	1.16	0.16	26	12	67.5	12.3
07.09.2017 19:40	107,008	5,024	103,936	14,016	118,784	9,856	1328	0.97	0.14	11	11	68.5	11.6
07.09.2017 19:50	88,064	4,224	116,736	14,336	117,760	9,792	1392	1.33	0.17	34	13	69.5	10.9
07.09.2017 20:00	103,936	4,832	148,480	16,064	125,952	10,432	1488	1.43	0.17	21	12	71.0	10.2
07.09.2017 20:10	107,008	5,088	129,024	16,640	121,856	10,304	1560	1.21	0.17	14	11	71.5	9.6
07.09.2017 20:20	109,568	5,152	129,024	15,296	115,200	9,920	1640	1.18	0.15	5	10	72.5	9.1
07.09.2017 20:30	111,104	5,248	104,960	15,488	125,952	10,816	1696	0.94	0.15	13	11	73.5	8.6
07.09.2017 20:40	101,888	4,896	117,760	16,064	120,320	10,432	1760	1.16	0.17	18	12	75.0	8.2
07.09.2017 20:50	111,104	5,248	139,264	16,512	122,368	10,560	1848	1.25	0.16	10	11	76.0	8.0
07.09.2017 21:00	107,008	4,992	107,520	15,296	116,224	10,240	1904	1.00	0.15	9	11	77.0	7.6
07.09.2017 21:10	117,248	5,472	116,736	15,936	129,536	11,072	1968	1.00	0.14	10	11	77.0	7.2
07.09.2017 21:20	112,128	5,376	76,800	13,888	120,832	10,624	2000	0.68	0.13	8	11	78.5	6.9
07.09.2017 21:30	106,496	5,120	133,120	15,808	124,416	10,944	2064	1.25	0.16	17	12	80.0	6.7
07.09.2017 21:40	121,856	5,728	92,160	15,744	126,976	11,008	2112	0.76	0.13	4	10	79.5	6.4
07.09.2017 21:50	111,104	5,312	125,440	15,936	123,392	11,072	2176	1.13	0.15	11	11	80.0	6.3
07.09.2017 22:00	105,472	5,120	136,192	15,744	118,272	10,560	2256	1.29	0.16	12	11	81.0	6.1
07.09.2017 22:10	100,352	4,864	125,952	14,912	126,976	11,200	2320	1.26	0.16	27	13	81.0	5.8
07.09.2017 22:20	113,152	5,312	132,096	16,256	128,000	11,328	2384	1.17	0.15	13	11	82.5	5.5
07.09.2017 22:30	111,104	5,312	145,408	17,280	128,512	11,136	2464	1.31	0.17	16	11	83.0	5.3
07.09.2017 22:40	109,568	5,216	108,544	14,848	122,880	11,072	2528	0.99	0.14	12	11	83.0	5.1
07.09.2017 22:50	116,224	5,600	122,880	16,768	118,784	10,752	2576	1.06	0.15	2	10	83.5	4.9

07.09.2017 23:00	124,416	5,952	118,784	17,152	124,928	11,200	2640	0.95	0.15	0	10	83.5	4.7
07.09.2017 23:10	121,344	5,664	58,112	14,016	125,952	11,264	2656	0.48	0.12	4	10	83.5	4.5
07.09.2017 23:20	109,568	5,280	105,472	15,488	125,440	11,264	2704	0.96	0.15	14	12	84.0	4.3
07.09.2017 23:30	119,808	5,728	103,424	16,384	129,536	11,520	2752	0.86	0.14	8	11	84.5	4.1
07.09.2017 23:40	94,208	4,832	111,104	15,424	125,440	11,328	2800	1.18	0.17	33	14	84.5	4.0
07.09.2017 23:50	125,952	5,984	88,064	15,296	129,536	11,584	2832	0.70	0.13	3	10	85.5	3.9
08.09.2017 00:00	119,808	5,792	108,032	16,192	125,440	11,328	2880	0.90	0.14	5	11	85.5	3.7
08.09.2017 00:10	110,080	5,408	161,792	17,536	128,000	11,520	2960	1.47	0.17	16	12	86.0	3.6
08.09.2017 00:20	112,128	5,472	126,464	15,744	124,416	11,136	3024	1.13	0.15	11	11	86.0	3.4
08.09.2017 00:30	122,880	5,792	85,504	14,976	125,952	11,264	3056	0.70	0.13	3	10	86.5	3.3
08.09.2017 00:40	122,880	5,920	131,072	17,024	131,072	11,520	3104	1.07	0.15	7	11	87.0	3.2
08.09.2017 00:50	107,008	5,216	105,984	15,872	122,880	11,264	3152	0.99	0.16	15	12	87.0	3.1
08.09.2017 01:00	125,440	5,952	88,064	14,976	133,120	11,904	3184	0.70	0.12	6	11	87.0	2.9
08.09.2017 01:10	117,248	5,664	116,224	16,512	129,024	11,584	3232	0.99	0.15	10	11	87.5	2.9
08.09.2017 01:20	117,248	5,600	122,368	16,512	123,392	11,136	3280	1.04	0.15	5	11	87.5	2.8
08.09.2017 01:30	118,272	5,760	115,712	15,872	124,928	11,136	3328	0.98	0.14	6	11	88.0	2.7
08.09.2017 01:40	113,152	5,408	121,856	16,512	123,392	11,072	3376	1.08	0.15	9	11	90.0	2.6
08.09.2017 01:50	127,488	6,016	88,576	15,424	128,000	11,520	3408	0.69	0.13	0	10	88.0	2.6
08.09.2017 02:00	126,976	6,176	109,056	17,920	126,976	11,584	3456	0.86	0.15	0	10	89.0	2.5
08.09.2017 02:10	104,448	5,216	143,360	17,408	131,072	11,584	3520	1.37	0.18	25	13	88.5	2.3
08.09.2017 02:20	109,056	5,248	144,384	16,192	134,144	11,904	3584	1.32	0.16	23	12	89.0	2.3
08.09.2017 02:30	127,488	6,112	140,288	17,920	128,512	11,520	3648	1.10	0.15	1	10	89.0	2.2
08.09.2017 02:40	113,152	5,504	142,336	17,408	132,096	11,840	3712	1.26	0.17	17	12	88.5	2.2
08.09.2017 02:50	104,960	5,152	120,832	16,064	134,144	11,840	3760	1.15	0.16	28	13	91.0	2.4
08.09.2017 03:00	133,120	6,336	139,264	18,304	130,560	11,712	3808	1.05	0.15	-2	10	90.0	2.5
08.09.2017 03:10	116,736	5,632	147,456	18,432	133,120	11,840	3888	1.26	0.17	14	12	92.0	2.6
08.09.2017 03:20	116,224	5,632	140,288	17,408	134,144	12,160	3936	1.21	0.16	15	12	91.0	2.6
08.09.2017 03:30	125,440	5,792	110,592	16,768	134,144	12,096	3968	0.88	0.14	7	11	90.5	2.6
08.09.2017 03:40	116,224	5,632	127,488	16,512	131,072	11,904	4032	1.10	0.15	13	12	90.5	2.5
08.09.2017 03:50	115,200	5,536	145,408	18,816	129,536	11,904	4080	1.26	0.17	12	12	91.0	2.4
08.09.2017 04:00	123,392	5,856	105,984	15,936	126,976	11,648	4096	0.86	0.14	3	11	91.0	2.3
08.09.2017 04:10	123,392	5,920	83,968	15,552	131,072	11,648	4128	0.68	0.13	6	11	91.0	2.2
08.09.2017 04:20	124,416	6,016	96,768	15,616	130,048	11,648	4160	0.78	0.13	5	11	91.0	2.0

08.09.2017 04:30	117,248	5,568	110,080	16,064	135,168	12,096	4192	0.94	0.14	15	12	91.0	1.9
08.09.2017 04:40	126,976	6,112	115,200	16,512	130,560	11,712	4224	0.91	0.14	3	10	91.0	1.8
08.09.2017 04:50	129,536	6,176	104,960	17,280	135,168	12,096	4256	0.81	0.14	4	11	91.5	1.7
08.09.2017 05:00	125,952	6,080	99,328	15,872	136,192	12,224	4288	0.79	0.13	8	11	91.0	1.6
08.09.2017 05:10	122,880	6,016	106,496	17,536	135,168	12,032	4320	0.87	0.15	10	11	91.0	1.6
08.09.2017 05:20	117,760	5,728	135,168	16,512	132,096	11,840	4352	1.15	0.15	12	11	91.0	1.5
08.09.2017 05:30	127,488	6,176	115,712	16,768	135,168	12,096	4384	0.91	0.14	6	11	91.0	1.3
08.09.2017 05:40	116,224	5,632	181,248	19,584	135,168	12,224	4480	1.56	0.18	16	12	91.0	1.3
08.09.2017 05:50	133,120	6,304	130,048	18,304	131,072	11,776	4512	0.98	0.15	-2	10	91.0	1.3
08.09.2017 06:00	122,880	5,856	129,536	17,920	142,336	12,544	4576	1.05	0.15	16	12	91.0	1.2
08.09.2017 06:10	113,664	5,600	144,384	17,664	136,192	12,160	4608	1.27	0.17	20	12	91.5	1.1
08.09.2017 06:20	113,664	5,632	140,288	16,768	128,000	11,840	4672	1.23	0.16	13	12	91.0	1.1
08.09.2017 06:30	133,120	6,272	111,616	17,024	138,240	12,416	4704	0.84	0.13	4	11	91.5	1.0
08.09.2017 06:40	116,736	5,824	122,368	16,896	137,216	12,352	4736	1.05	0.15	18	12	91.5	1.0
08.09.2017 06:50	132,096	6,336	125,440	17,280	134,144	12,096	4768	0.95	0.14	2	10	91.5	1.1
08.09.2017 07:00	125,440	6,112	113,664	16,320	131,072	12,096	4800	0.91	0.14	4	11	91.5	1.2
08.09.2017 07:10	133,120	6,400	127,488	18,944	136,192	12,160	4832	0.96	0.15	2	10	91.5	1.4
08.09.2017 07:20	128,512	6,240	120,320	17,152	135,168	12,352	4896	0.94	0.14	5	11	92.0	1.6
08.09.2017 07:30	119,296	5,856	128,000	17,024	133,120	12,032	4928	1.07	0.15	12	11	97.0	2.3
08.09.2017 07:40	120,832	5,952	101,376	16,064	135,168	12,224	4928	0.84	0.14	12	12	95.5	4.1
08.09.2017 07:50	117,248	5,696	131,072	17,536	136,192	12,480	4992	1.12	0.16	16	12	98.0	5.7
08.09.2017 08:00	103,936	5,184	131,072	15,552	127,488	11,840	5024	1.26	0.16	23	13	96.5	7.9
08.09.2017 08:10	129,536	6,240	96,256	15,680	130,560	11,776	5024	0.74	0.13	1	10	91.5	9.1
08.09.2017 08:20	110,080	5,344	130,048	16,320	121,344	11,392	5088	1.18	0.16	10	12	90.0	10.9
08.09.2017 08:30	123,392	5,952	67,584	15,104	123,904	11,264	5056	0.55	0.13	0	10	86.0	12.4
08.09.2017 08:40	118,272	5,696	113,664	16,512	116,224	10,944	5088	0.96	0.15	-2	10	82.5	14.3
08.09.2017 08:50	103,424	5,088	102,912	15,680	120,832	11,072	5120	1.00	0.16	17	12	81.0	16.0

Sample number	Date	Location	Depth (cm)	Ra-226 Activity concentration Bq/kg	Ra-226 Uncertainty	Th-228 Activity concentration Bq/kg	Th-228 Uncertainty	U-238 Activity concentration Bq/kg	U-238 Uncertainty	K-40 Activity concentration Bq/kg	K-40 Uncertainty
GAM1-00757	25.07.2017	1	95	72.2	4.3	269	27	60.8	5.5	1260	76
GAM1-00758	25.07.2017	1	55	85.0	4.3	253	13	127	11.4	1200	72
GAM1-00759	25.07.2017	1	25	50.4	3.0	171	9	56.1	5.6	1080	65
GAM1-00760	25.07.2017	1	5	39.4	2.4	117	7	42.3	4.7	947	57
GAM1-00761	25.07.2017	2	5	53.0	3.2	126	6	52.5	4.7	860	52
GAM1-00762	25.07.2017	2	35	46.3	2.8	105	6	46.7	5.1	956	57
GAM1-00795	25.07.2017	2	15	50.6	3.0	126	8	47.2	4.7	1100	66
GAM1-00796	25.07.2017	2	62.5	60.4	3.6	142	9	59.7	6.0	851	51
GAM1-00797	27.07.2017	3	27.5	60.8	3.6	274	22	65.2	5.9	874	52
GAM1-00798	27.07.2017	3	5	47.1	2.8	192	19	40.1	4.4	1030	62
GAM1-00799	05.09.2017	5	35	43.9	2.6	160	13	40.7	4.5	1360	82
GAM1-00800	05.09.2017	5	5	45.5	2.7	147	7	48.9	5.9	1330	80
GAM1-00801	05.09.2017	6	30	58.7	3.5	154	8	46.7	4.2	948	57
GAM1-00802	05.09.2017	6	90	71.7	4.3	212	11	60.1	4.8	153	14
GAM1-00807	06.09.2017	4	5	42.0	2.5	139	7	40.4	4.8	1210	73
GAM1-00808	06.09.2017	4	50	43.4	2.6	127	6	47.3	4.7	1190	71
GAM1-00809	07.09.2017	8	45	82.5	5.0	162	8	70.2	6.3	1060	64
GAM1-00810	07.09.2017	8	5	77.9	4.7	143	9	70.2	5.6	951	57
GAM1-00811	07.09.2017	7	45	55.8	3.3	62.0	4	46.7	3.7	749	45
GAM1-00812	07.09.2017	7	5	57.6	2.9	55.5	3	47.1	3.3	647	39

Rn-222 (RnTn mode)		Rn-220 (RnTn mode)		Rn-222 (flow mode)		Thoron/radon ratio	Uncertainty thoron/radon ratio	Radon deviation (%)	Uncertainty radon deviation (abs. %)
Activity concentration	Uncertainty	Activity concentration	Uncertainty	Activity concentration	Uncertainty				
kBq/m³		kBq/m³		kBq/m³					
95.2	2.2	308	13	129	3	3.24	0.16	36	4
60.4	1.3	143	6	78.0	3.1	2.37	0.11	29	6
85.0	2.6	165	12	94.7	3.9	1.95	0.15	11	6
87.9	2.0	328	12	119	4	3.73	0.16	35	6
83.8	2.9	130	12	91.1	4.3	1.55	0.15	9	6
46.9	1.1	45.7	3.0	49.9	1.9	0.97	0.07	6	5
57.5	1.7	77.1	6.3	64.1	2.3	1.34	0.12	11	5
37.6	0.9	127	5	46.8	1.7	3.39	0.15	25	5
21.8	2.3	44.6	3.6	29.1	1.4	2.04	0.27	33	16
61.2	1.4	151	6	67.6	2.5	2.47	0.12	10	5
52.1	1.5	147	9	72.0	3.0	2.83	0.19	38	7
92.2	2.1	138	8	108	3	1.50	0.10	17	4
99.9	1.5	86.0	4.1	112	3	0.86	0.04	12	3
115	1	118	2	127	1	1.03	0.02	10	1
62.3	1.4	40.6	4.3	67.8	2.0	0.65	0.07	9	4
53.0	0.9	44.5	2.5	61.0	1.8	0.84	0.05	15	4

Curriculum Vitae

Katharina Newrkla · 31 May 1992
Neustiftgasse 12/3/39 · 1070 Vienna, Austria
katharina.newrkla@gmail.com · +43 676 4951410

EDUCATION AND QUALIFICATIONS

2015 – 2018	MSc in Technical Physics Vienna University of Technology

Master's thesis:
- *Investigation of the influence of thoron on radon monitors and development of innovative measurement techniques*

Research projects:
- *Semiclassical quantization of particle-like scattering states in a cavity*
- *Surface Analysis of Ultrathin Zirconia Films on Zirconium (0001)*

01/2016 – 06/2016	Erasmus exchange programme University of Zaragoza, Spain
2010 – 2014	BSc in Technical Physics Vienna University of Technology
2008 – 2010	International Baccalaureate Diploma Vienna International School

SKILLS AND INTERESTS

Languages	German: Native English: Fluent Spanish: Intermediate
IT skills	Programming: Python, MATLAB, Mathematica, Fortran, C Microsoft Office (Word, Excel, PowerPoint)
Personal interests	Member of the Austrian Association for Radiation Protection Chess: **Austrian women's chess champion 2015. Member of the Austrian national team since 2007.** Travel: exploring new places and cultures.